UNIVERSITY OF CALIFORNIA
RIVERSIDE

Methodology Development for Understanding Interactions at the Nano-bio Interface

A Dissertation submitted in partial satisfaction
of the requirements for the degree of

Doctor of Philosophy

in

Chemistry

by

Shang Zeng

August 2014

Dissertation Committee:
Dr. Wenwan Zhong, Chairperson
Dr. Cindy Larive
Dr. Huiwang Ai

The Dissertation of Shang Zeng is approved:

_____

_____

_____

Committee Chairperson

University of California, Riverside

ACKNOWLEDGEMENTS

My life has been changed a lot since I came to UCR to pursue advanced education. I made a few new friends, experienced different cultures, broadened perspective, and obtained advanced degree. Here, I would like to express my sincere gratitude to those people, without whose support and help this dissertation would not have become possible.

I am indebted to my advisor, Dr. Wenwan Zhong, for all her financial support and research guidance in the past five years. She encouraged me to explore new research fields, multi-task on various projects and solve problems. Every time when I met difficulties, she was always ready to provide advice and inspiration. I feel lucky to be one of her students.

Many thanks go to Dr. Cindy Larive, Dr. Huiwang Ai, Dr. Yinsheng Wang, Dr. Yadong Yin and Dr. Eric Chronister for being on my SYRE, oral exam or thesis committee. Their valuable comments and constructive suggestions on my research work during my PhD studies were sincerely appreciated.

I wish to acknowledge Dr. Chia-en A. Chang and her student Dr. Yu-ming Mindy Huang for the help in computer simulations and valuable suggestions on setting up our computer

clusters. My grateful thanks also go to Dr. Berlin Jacob and Ethan White at City of Hope for proving novel single wall carbon nanotube samples and inspiring discussions on our collaboration project. Collaborating with their research groups greatly broadened my perspective and inspired my research interests in new fields.

I would like to thank Dr. Ryan R. Julian, and his lab members for all the help and kindness they have given to me. I am grateful to Dr. Le He for using his nanomaterials in good quality and his generosity of sharing synthesis skills. I also would like to thank Dr. Yongsheng Xiao, Lei Guo, Lijuan Fu, Qian Cai and Dr. Changjun You. Thank them all for their thoughtful discussions on my projects and sharing technical experience with me. My thanks should also go to Dr. Huiwang Ai and his lab members Zhijie Chen, Yichong Fan and Wei Ren for letting me use their UV-Vis and fluorescence spectrophotometer.

My thanks also need go to Dr. Songqin Pan, Dr. Dan Borchardt, Dr. Richard Kondrat and Dr. Ronald New. I acquired new knowledge and developed new skills from the facility trainings they conducted, which benefited a lot when I was pursing my career goal in industry setting.

I would like to express my sincere thanks to my colleges Dr. Ni Li, Dr. Lei Ren, Dr. Jonathan Tyrone Ashby, Jimmy Vo, for their great help both in my work and my life. Without them, my life in the US would not have been so colorful. I also would like to thank all my group members and friends for the life we spent together here at UCR.

Last but certainly not least, my thanks must go to my dearest family members and my best childhood friends for their unconditional love, continuous encouragement and solid support.

My apologies if I missed anyone. Best wishes to all.

COPYRIGHT ACKNOWLEDGEMENTS

The text and figures in Chapter 2, in part or full, are a reprint of the material as it appears in Analytical Chemistry 2010, 82:7460-7466. The coauthor (Dr. Wenwan Zhong) listed in that publication directed and supervised the research that forms the basis of this chapter.

The text and figures in Chapter 3, in part or full, are a reprint of the material as it appears in Analyst 2014, 139:1364-1371. The coauthor (Dr. Wenwan Zhong) listed in that publication directed and supervised the research that forms the basis of this chapter.

The text and figures in Chapter 4, in part or full, are a reprint of the material as it appears in Analytical Chemistry 2011, 83:6929-6934. The coauthor (Dr. Wenwan Zhong) listed in that publication directed and supervised the research that forms the basis of this chapter.

ABSTRACT OF THE DISSERTATION

Methodology Development for Understanding Interactions at the Nano-bio Interface

by

Shang Zeng

Doctor of Philosophy, Graduate Program in Chemistry
University of California, Riverside, August 2014
Dr. Wenwan Zhong, Chairperson

Nanoparticles have attracted huge attention due to their unique size-dependent properties. The fabrication of nanoparticles and exploration of their potential use has become a strong interest in numerous areas including biomedicine and information technology. These highly potential applications of nanoparticles lead to the concern for the design of safe nano-biomaterials and promoted the study of nanotoxicology, and safety assessment research in parallel to development of applications.

Protein adsorption is believed to be the primary event when nanoparticles enter a living system. In this dissertation, focus was placed on method development for evaluating the nanoparticle interactions with either a single protein or a cellular proteome. For the nanoparticle-single protein interaction, a novel method was developed for quantitative measurement on nanoparticle-protein interaction using capillary electrophoresis. With this method, we screened the affinity of polyacrylic acid-coated nanoparticles towards a selected list of proteins and found that protein adsorption was so sensitive to the surface properties of particles that it can reveal even small variations in the structure of a nanoparticle surface ligand. The binding site of nanoparticles on protein was also revealed by cross-linking chemistry coupled with mass spectrometry. The peptides located at protein-nanoparticle interface were cross-linked to nanoparticle surface, cleaved off after trypsin digestion and identified by mass spectrometry.

For the nanoparticle-proteome interaction, we believe for nanoparticles to work effectively in a biological system, an appropriate protein corona is needed for their cell internalization and cellular response. CpG-conjugated single wall carbon nanotubes were found to have superior anti-tumor efficacy than free CpG in glioma-bearing mice. Therefore we analyzed the protein corona composition of CpG-conjugated single wall carbon nanotubes in mouse macrophage cells. The CpG-conjugated single wall carbon nanotubes were incubated with cell lysate or live cells, then isolated and processed with protease. The resulted peptides were analyzed with liquid chromatography-mass

spectrometry. The abundance of proteins was determined by calculating their exponentially modified protein abundance index. We found 35 proteins were specifically selected and enriched by CpG motifs. Their confirmation change or function inhibition may potentially contribute to the excellent anti-tumor efficacy of CpG functionalized single wall carbon nanotubes.

TABLE OF CONTENTS

Chapter 2 Probing nanoparticle-protein interaction by capillary electrophoresis

Chapter 3 Protein binding for detection of small changes on a nanoparticle surface

LIST OF FIGURES

LIST OF TABLES

Chapter 1

General Overview

1.1 Introduction

Nanoparticles are defined as particles with at least one dimension less than 100 nm in size. In the past few decades, nanoparticles have attracted huge attention due to their unique mechanical, electrical, optical, or magnetic properties, which are different from the properties of their bulk counterparts. The fabrication of functional nanoparticles and exploration of their potential use is now a strong interest of scientists in numerous areas including biomedicine, energy and information technology.[1]

From the perspective of biomedical applications, the primary interest of nanoparticles arises from their small size, which means they could interact with cellular machinery, and potentially reach previously inaccessible targets such as passing through the blood-brain barrier.[2] Their comparable size to bio-molecules also makes them excellent systems for biomimetic chemistry, such as modeling protein surface, because they can be readily fabricated with desirable dimensions and functionalized with tailored surface coating.[3] Conjugation of inorganic nanoparticles to bio-molecules generates hybrid materials, which combines the properties and functionality of both materials and can be used to specifically target nanoparticles to biological systems via molecular recognition.[4]

These highly potential applications of nanoparticles in biomedical areas lead to the concern for the design of safe nano-biomaterials. Meanwhile, the large scale usage of nanoparticles may cause unintentional exposure to living matters and environments, which has promoted the study of nanotoxicology, and safety assessment research in parallel to development of applications.[5-7]

1.2 Nanoparticles

1.2.1 Properties and Biomedical Applications of Magnetic Nanoparticles

Among various types of promising nanoparticles developed so far, magnetic nanoparticles (MNPs, e.g. FePt, Fe_3O_4, Fe_2O_3, and $CoFe_2O_4$) have demonstrated their great potential in diagnostic and therapeutic applications.[8-12] First, the size and properties of the MNPs can be readily tailored to meet the interest of study or application purpose. Second, when the size of MNPs is sufficiently small, such as below 20 nm, these MNPs are often in a superparamagnetic state at room temperature. It means an external magnetic field is able to magnetize the nanoparticles, similarly to a paramagnet. But in the absence of external magnetic field, their average magnetization appears to be zero due to thermal agitation. Therefore, an external magnetic force is able to control MNPs remotely and easily, which provides superior advantages comparing to other non-magnetic NPs. Third, the magnetic moment of a MNP enhances the signal of nearby protons, which allows MNPs to be used as MRI contrast agents.[13, 14] In addition, these

MNPs can also be heated by an alternating magnetic field, which offers a promising therapeutic solution through magnetic fluid hyperthermia.[15,16]

It is now a well-established procedure to separate a target protein from protein matrix using the magnetic force of MNPs.[17] One of the earliest successes is using nickel-nitrilotriacetic acid (Ni-NTA) modified MNPs to separate histidine-tagged proteins from cell lysate. Xu and co-workers reported using FePt MNP, which was covered by Ni–NTA through a simple mercaptoalkanoic acid as the anchor, to separate the over-expressed his-tagged green fluorescence protein from *E. coli* cell lysate.[18] This work has demonstrated the advantage of MNPs, such as high protein binding capacity, fast separation under external magnetic field, and elimination of extensive washing.

Park and co-workers developed another kind of silica-coated MNPs with different alkyl groups on the surface[19]. Under various pH, these alkyl chains will form hydrophobic pockets with various size on the silica-coated MNPs. Utilizing the hydrophobic interaction between protein and these hydrophobic pockets, they successfully separated BSA with high efficiency. Even though the orientation and activity of the bound proteins in hydrophobic pocket still need to be further evaluated, these hydrophobic chains could be potentially used for mimicking the cell membrane units for protein manipulation.

Besides organic molecules, large bio-molecules such as antibodies can also be conjugated onto MNPs surface to enable detection that requires high affinity. Kriz and co-workers

demonstrated a MNPs-based system for detection of C reaction protein (CRP) by conjugating the monoclonal anti-CRP onto iron oxide MNPs.[20] This immunoassay offers a rapid (11.5 min) procedure with a low detection limit (0.2 mg/L) and high accuracy. With the same basic concept presented by Kriz et al., Ouyang et al. functionalized MNPs with hemoglobin and applied them for the enrichment of human serum amyloid P component, vitamin D-binding protein, and serine peptidase inhibitor.[21]

Core/shell MNPs with metal or metal oxide coating (e.g. Au and TiO_2) have also been adopted for affinity purification. Chen and co-workers has demonstrated a novel strategy using TiO_2 coated MNPs as both capture probe and effective matrix for matrix-assisted laser desorption/ionization mass spectrometry (MALDI-MS).[22] They synthesized the Fe_3O_4/TiO_2 core/shell MNPs and applied them into the protein digests to enrich phosphopeptides based on the affinity between phosphates and TiO_2. After using a magnetic field to isolate the MNPs, they directly treated the Fe_3O_4/TiO_2 core/shell MNPs as the matrix for MALDI-MS and achieved the detection of the phosphopeptides with upper detectable mass limit at about 24 kDa and the sensitivity in the low-femtomole range.

A number of studies have demonstrated the advantages of using MNPs for magnetically guided drug delivery. MNPs conjugated with methotrexate (MTX), a therapeutic drug, can target cancer cells that overexpress folate receptors.[23,24] The internalization of the

MTX-MNPs is higher in cancer cells than healthy cells. The low-pH environment and the intracellular enzymes inside the cancer cells can induce the release of MTX from the NPs and trigger apoptosis of cancer cells.

Hollow Fe_3O_4 NPs were also demonstrated to be an efficient carrier for targeted delivery and controlled release of *cis*-platin. The porous structure allowed *cis*-platin in and out by diffusion.[25] The *cis*-platin-loaded hollow NPs with Herceptin as targeting molecule provided efficient delivery of *cis*-platin to HER2-positive breast cancer cells (SK- BR-3).

More recently, various novel MNPs have been designed for simultaneous magnetically-guided drug delivery and cancer-targeted MRI. For example, a lipophilic near infrared (NIR) dye and an anticancer drug (Taxol) were incorporated into the polymeric matrix of PAA-coated MNPs for combined optical imaging/MRI detection and targeted cancer therapy.[26]

1.2.2 Properties and Biomedical Applications of Carbon Nanotubes

Carbon nanotubes (CNT) are another major category of nanomaterials that is widely studied and developed for potential applications in the electronics, aerospace, biomedicine and other industries.[27-30] There are two forms of CNT, single-wall (SWCNT) and multi-wall (MWCNT). An individual SWCNT is a very thin fiber with diameter at approximately 1~5 nm and length at least a few μm. It appears like a rolled-up seamless single layer of graphene or graphite sheet formed by bonded carbon atoms

arranged in a hexagonal pattern. MWCNTs are composed of multiple concentric layers of rolled graphene with various diameters and lengths.

In 1991, Sumio Iijima discovered that MWCNTs could be deposited at the graphite anode in a graphite arc process.[31] In 1993, Iijima successfully synthesized SWCNTs in the presence of metal catalyst and found the presence of a small amount of metal catalyst helps to align the nanotubes.[32] In 1996, Richard Smalley and co-workers succeeded in producing SWCNT with a much higher yield and greater purity by adapting the laser ablation process instead of the arc process. [33]

Since the time CNTs were discovered, enormous research efforts have been devoted to explore their applications in biomedical areas. However, pristine carbon nanotubes are not soluble in aqueous solvents and likewise in biological environments because they aggregate due to hydrophobic interactions. Therefore, surface modification on the carbon nanotube is essential for dispersing the carbon nanotubes. Surfactants like sodium dodecyl sulfate or sodium cholate have been used to help dispersing carbon nanotubes. [34] However, such surfactants are not suitable for biological applications because the stability of surfactant micelles requires the presence of excess amount of surfactant monomer. Moreover, these surfactants may interfere with the protein interactions, especially molecule recognitions, due to the protein denaturation under these conditions.

The strategies for surface modification of carbon nanotubes to enhance their water solubility and biocompatibility can be categorized into two types: covalent and non-

covalent. Oxidation, halogenation, radical reaction and addition chemistry are the most common ways to covalently modify the surface of carbon nanotubes. The advantage for covalent modification is that it is more stable and can be orientated to specific sites. However, the introducing of new chemical bonds on carbon atoms may potentially alter the optical or electrochemical properties of the carbon nanotubes.

Non-covalent modification includes the wrapping of polymers (such as polyethylene glycol, polyacrylic acid) or the grafting of biomolecules like DNA, lipids or proteins. The adsorption of these molecules on CNT surface is mediated by hydrophobic interaction or π-π stacking. Evidence has shown the biocompatible molecules on CNT surface may increase the biocompatibility of CNT in biological systems.[35] The non-covalent modification does not disturb the carbon backbone of CNTs. Therefore, the original optical and electrochemical properties of CNT are well preserved.

Both theoretical calculations and experimental results show that MWCNTs are more difficult to characterize and study than SWCNTs due to their higher heterogeneity.[36-38] Moreover, SWCNTs have demonstrated more favorable and controllable mechanical, electrical and chemical properties.[39,40] Therefore, the following review is mainly focused on the biomedical applications of SWCNTs.

SWCNT can quench fluorescence in solution.[41] Based on this concept, Yang and co-workers developed a SWCNT-based bio-sensing system for detecting complementary

oligonucleotide-sequences in solution.[42] The fluorescent dye-labeled DNA sequence was pre-loaded onto the SWCNT surface where the fluorescence of the dye was quenched. When a complementary strand was present in the solution, the dye-labeled DNA sequence was released due to its hybridization with the complementary strands, thus the fluorescence was recovered. With this approach, oligonucleotides could be detected at nanomolar range.

SWCNT has also been demonstrated to be useful for optical imaging thanks to their intrinsic near-infrared fluorescence emission.[43] The main difficulties of optical imaging in living objects are poor penetration and strong light scattering.[44] The intrinsic near-infrared fluorescence emission of SWCNT provides opportunities for optical image in deep tissues. Clear spectra could be obtained because the absorbance of all biomolecules in the near-infrared range is negligible.[45] It was recently reported that antibody conjugated-SWCNTs were used as near-infrared fluorescence tags for probing the receptors on cell surface.[46] The near-infrared fluorescence microscopy was utilized to timely monitor the binding of SWCNT to the cell receptor.

SWCNT has attracted significant attention as drug delivery nanocarriers because they can pass through the cell membrane, transporting molecules into cytoplasm without inducing toxic effect.[47-49] Moreover, the half-lives of their blood circulation is as long as a few hours. [50] The proposed mechanism of SWCNT-mediated drug delivery includes (1)

loading of drugs within the mesh of SWCNT; (2) covalently or non-covalently conjugate drugs onto the exterior wall of SWCNT; (3) trapping of drugs inside the SWCNT channel.

Misra and co-workers recently reported a novel folate-decorated, carbon nanotube-mediated drug delivery system.[51] Doxorubicin, an anti-cancer drug, was pre-adsorbed onto SWCNT via π–π stacking interaction, followed by encapsulation of the drug-loaded SWCNTs with folic acid-conjugated chitosan. The non-covalent π–π stacking interaction between drug and SWCNT allowed the controlled drug release. Encapsulation of SWCNTs by chitosan enhanced the stability and biocompatibility of SWCNT in biological medium. The incorporation of folate in the system enabled the targeting drug delivery since folate receptors were often over-expressed on cancer cells. They successfully demonstrated both targeted and controlled in vitro drug release with this SWCNT-based drug carrier.

1.2.3 Other Nanoparticles

Besides the magnetic nanoparticles and carbon nanotubes reviewed above, many other types of nanomaterials, such as gold nanoparticles and quantum dots, are also highly potential for biomedical applications. For instance, the ability of gold nanoparticles to absorb energy in the near-infrared wavelength spectrum has been adapted to induce hyperthermia and kill tumor cells upon laser irradiation.[52] This concept is called "thermal scalpel". Quantum dots have unique size- and composition-tunable fluorescence emission from visible to infrared wavelengths, large absorption coefficients across a wide

spectral range and very high levels of brightness and photostability. Because of their broad excitation profiles and narrow, symmetric emission spectra, high-quality quantum dots are well suited to encode genes, proteins and small-molecule for ultrasensitive bioassays and diagnostics by combining multiple colors and intensities.[53,54]

1.3 Protein-Nanoparticle Interaction

It is now widely believed that protein adsorption is the primary event when nanoparticles enter a living system. When protein adsorbs onto nanoparticles, the cells actually see and response to this dynamic layer of proteins, so-called protein corona, instead of the bare nanoparticle surface. Therefore, this protein corona would affect the behaviors of nanoparticles in biological environment, as well as their biodistribution such as translocation, accumulation in the body.[55] Upon binding to NP surface, the conformation and function of protein could also be disturbed, which might further interfere the downstream interactions of proteins.[56, 57] Therefore, an understanding of interactions at the nano-bio interface is needed in order to ensure safe implementation of nanomaterials and increase efficacy of nano-medicines.

Nanoparticle–protein interactions can be categorized into two situations: interaction with single proteins or with the whole proteome. For the single-protein interaction, investigations are mainly focused on measuring binding affinity and binding ratio, determining protein conformational changes induced by nanoparticle binding, and exploring the binding mechanism. For the proteome interaction, the main goal is to

separate and identify the proteins bound to these nanoparticles, which is known as the nanoparticle-protein corona.

1.3.1 Analytical Techniques for Probing Single Protein-Nanoparticle Interaction

When protein binds to a nanoparticle, a few changes occur at the same time, such as the size and shape change, the spectroscopic shift, or other alterations on both partners. Therefore, by monitoring these alterations, the binding affinity or binding ratio of NP–protein interaction can be determined. For instance, dynamic light scattering and transmission electron microscopy have been used to show the evidence of protein adsorption on nanoparticle by determining the size increase of nanoparticle after incubation with protein.[58,59] During protein-nanoparticle interaction, the absorbance or fluorescence spectra of either or both parties may be altered. UV/Vis and fluorescence spectroscopy could be used to quantitatively determine the spectroscopic change as a function of the component concentration.[60,61] Further information on the binding affinity and binding ratio could be obtained by fitting the function into appropriate interaction model.

Proteins may undergo structure and stability changes upon adsorption onto a nanoparticle's surface. These changes are closely related to the properties of the adsorbed proteins and the physicochemical parameters of the nanoparticle surface. Reports have shown the higher degree of surface curvature of nanoparticles has a more significant

influence on governing protein structure and function comparing to a macroscopic flat surface.[62]

A few analytical techniques have been adapted for analyzing these conformational changes of protein upon binding to a nanoparticle. For example, circular dichroism, a widely used technique for determining the secondary structure of protein, was used to monitor the conformational change in the secondary structure of NP-bound protein. Since the nanoparticle does not have characteristic spectra in circular dichroism, the interference from the nanoparticle itself is negligible.[63,64] Fourier transform infrared spectroscopy and Raman spectroscopy can be used to monitor the chemical bond perturbation in protein upon nanoparticle binding.[65-67] Besides these methods, NMR should be able to provide atom-level information about the coupled H and N atoms in a protein. X-Ray crystallography attempts to provide global 3-D structure information on protein-NP complex. [68,69]

Even though no efficient analytical methods have been proved for directly determining the mechanism of NP–protein interactions, the studies on binding site, interaction force, and binding constant can provide mechanism-related information. The strategies for such studies include isothermal titration calorimetry, fluorescence spectroscopy, X-ray crystallography, and Förster resonance energy transfer.[70-72] However, the elucidation

of the binding mechanism is difficult and the exploration is still not enough. More analytical methods need to be developed for further research in this area.

1.3.2 Analytical Techniques for Probing Proteome-Nanoparticle Interaction

The proteome, commonly plasma proteins or cellular proteins, contains hundreds of proteins. When nanoparticles interact with proteome, the biological activities of many proteins could be affected. The protein corona identity also influences the following consequence of the nanoparticle in the biological environment. Hence, identifying the NP-bound proteins is a prerequisite for predicting the behavior of nanoparticles.

The most common approaches for separation of NP-bound proteins are chromatography and electrophoresis. It has been reported to use size exclusion chromatography to separate silica NPs-bound proteins on the basis of size.[73,74] Reverse phase chromatography was used to separate copper NP-bound proteins from hemolysate based on the different retention times on stationary phase. Ion exchange chromatography was applied to separate gold nanoparticles (AuNPs) with various peptide capping based on their net charge.[75]

Capillary electrophoresis and gel electrophoresis are also widely used for analyzing NP-protein complex. CE is able to directly quantify NP-bound proteins with UV or fluorescent detector.[76] CE was used to study the adsorption of the major plasma protein, albumin, onto poly(methoxypolyethyleneglycol cyanoacrylate- co-

hexadecylcyanoacrylate) (PEG-PHDCA) NPs.[77] However, the drawback of CE is the protein adsorption onto the inner capillary wall.

1-D Gel electrophoresis separates proteins based on their molecular weight. For example, six different polystyrene NPs were incubated with human plasma proteins and bound different proteins, suggesting the importance of the surface property and the size of NPs.[78] 2-D gel electrophoresis separates proteins based on their molecular weight and isoelectric point which is more suitable for complicate biological samples. Plasma and serum proteins bound to poly(D,L-lactic acid) (PLA) NPs were analyzed by 2-D PAGE.[79]

Mass spectrometry is the most straightforward and widely used method for determining the identity of the NP-bound proteins. Proteins are either released from NP or kept in the purified NP-protein complex, followed by digestion with a selected protease. The protein digests are analyzed by mass spectrometry. The obtained peptide masses are searched in databases to identify proteins. However, mass spectrometry is not a good quantitative method for protein analysis. Western blots can be used to analyze proteins of interest for quantitative analysis.[80-83]

1.4 Scope of the Dissertation

In chapter 2, we examined the effectiveness of CE in measuring the affinity between NPs and proteins with an appropriate interaction model. Interactions of bovine serum albumin

(BSA) with the gold and superparamagnetic Fe_3O_4 NPs, which have shown great potential in biomedical applications, were investigated. Depending on the complex dissociation rate, binding situations could be studied with two CE operation modes: capillary zone electrophoresis (CZE) and affinity capillary electrophoresis (ACE). The response curves of peak area ratios in CZE or electrophoretic mobility shifts in ACE versus protein concentrations were fitted with the Hill equation, and the dissociation constants (K_D) and the Hill coefficients (*n*) were obtained. Our study demonstrates the great power of CE in studying NP-protein interaction and paves the way for future investigation on the multicomponent interaction systems to probe the binding of substrate, cargo molecules, ligands, receptors, etc. to proteins adsorbed on the NP surface.

In chapter 3, we investigated whether protein adsorption could reveal small changes in the surface ligand of NPs. Highly stable iron oxide NPs were coated with polyacrylic acid (PAA). Up to 20-fold difference in the dissociation constant of the protein–NP complex was detected on the NPs synthesized at different heating durations. Investigation of the PAA structures by NMR and MS confirmed that the heating duration could affect the head group of PAA. Computational work also verified that the subtle difference in the head-group structure was sufficient to alter the binding energy to a target protein. Our results support the finding that protein adsorption could be a quick and simple way to evaluate particle surfaces and assess small variations in surface ligands, before detailed characterization was performed by more sophisticated techniques. Such assessments are

highly important for particles intended for biomedical applications or with biosafety concerns.

In chapter 4, we revealed the possible binding site of nanoparticles on protein by cross-linking chemistry coupled with mass spectrometry. The peptides located very close to the poly(acrylic acid) (PAA)-coated Fe3O4 nanoparticles (NPs) during interaction with human serum albumin (HSA) were cross-linked to the surface of NPs. Following protease digestion, the attached peptides were cleaved off the particle surface and identified by matrix-assisted laser desorption/ionization time-of-flight mass spectrometry (MALDI-TOF-MS). The peptides were found to be part of the so-called drug binding site 2 of HSA; and the competitive binding to HSA between the corresponding drug, ibuprofen, and the NPs was observed. Our results demonstrated that cross-linking chemistry coupled with MS was a quick and simple method for locating the possible binding sites of NPs on protein. Information on NP-protein binding interface will benefit the study of how the interactions are governed by the physicochemical properties of NPs, for guiding the design of functional bionano constructs. It can also help to predict the biological consequence of protein adsorption on NPs, for obtaining more knowledge on nanotoxicity.

In chapter 5, we demonstrated the identification of protein corona on CpG-conjugated SWCNT in the mouse macrophage cells. The SWCNT-CpG tended to tolerate less protein adsorption than the SWCNT-NH_2. When there was protein corona present, the

stability of CpG ligand on SWCNT surface was improved significantly. In the protein corona composition analysis, we found 35 proteins were specifically enriched by CpG motif *in vitro*. These proteins did not show obvious trend in their isoelectrical point values, but more of them were cytoplasm and membrane proteins, nucleotides-binding proteins, and enzymatic proteins. When using formaldehyde to crosslink the CpG-interacting protein network in live cells, we found the protein corona composition of the SWCNT-CpG was almost identical to that of free CpG ligand indicating the CpG was the main factor determining the protein corona composition *in vivo*. AP-2 complex, protein disulfide isomerase and heat shock protein 90 were deeply involved in the transport or functioning of SWCNT-CpG. Further characterization of their function inhibition or conformational change upon binding to SWCNT-CpG needs to be carried out continuously.

1.5 References

[1] Cedervall, T, Lynch, I, Lindman, S, Berggard, T, Thulin, E, Nilsson, H, Dawson, K. A, Linse, S. *Proc. Natl. Acad. Sci. U.S.A.* **2007**, *104*, 2050.

[2] Nel, A. E, Ma¨dler, L.; Velegol, D, Xia, T.; Hoek, E. M. V, Somasundaran, P, Klaessig, F, Castranova, V, Thompson, M. *Nat. Mater.* **2009**, *8*, 543.

[5] D. W. Grainger and D. G. Castner, *Adv. Mater.*, **2008**, *20*, 867.

[6] K. Riehemann, S. W. Schneider, T. A. Luger, B. Godin, M. Ferrari and H. Fuchs, *Angew. Chem., Int. Ed.*, **2009**, *48*, 872.

[7] W. R. Sanhai, J. H. Sakamoto, R. Canady and M. Ferrari, *Nat. Nanotechnol.*, **2008**, *3*, 242.

[8] B. Bonnemain, *J. Drug Target.* **1998**, *6*, 167.

[9] I. Brigger, C. Dubernet, P. Couvreur, *Adv. Drug Delivery Rev.* **2002**, *54*, 631.

[10] K. Shamsi, T. Balzer, S. Saini, P. R. Ros, R. C. Nelson, E. C. Carter, S. Tollerfield, H. P. Niendorf, *Radiology* **1998**, *206*, 365.

[11] A. Ito, M. Shinkai, H. Honda, T. Kobayashi, *J. Biosci. Bioeng.* **2005**, *100*, 1.

[12] Q. A. Pankhurst, J. Connolly, S. K. Jones, J. Dobson, *J. Phys. D: Appl. Phys.* **2003**, *36*, R167.

[13] L. E. Jennings, N. J. Long, *Chem. Commun.* **2009**, 3511.

[14] J. W. M. Bulte, D. L. Kraitchman, *NMR Biomed.* **2004**, *17*, 484.

[15] L. A. Thomas, L. Dekker, M. Kallumadil, P. Southern, M. Wilson, S. P. Nair, Q. A. Pankhurst, I. P. Parkin, *J. Mater. Chem.* **2009**, *19*, 6529.

[16] M. Jeun, S. Bae, A. Tomitaka, Y. Takemura, K. H. Park, S. H. Paek, K. W. Chung, *Appl. Phys. Lett.* **2009**, *95*, 082501.

[17] I. Safarik and M. Safarikova, BioMagn. *Res. Technol*., **2004**, *2*, 7.

[18] C. J. Xu, K. M. Xu, H. W. Gu, X. F. Zhong, Z. H. Guo, R. K. Zheng, X. X. Zhang and B. Xu, *J. Am. Chem. Soc.*, **2004**, *126*, 3392.

[19] J. H. Chang, J. Lee, Y. Jeong, J. H. Lee, I. J. Kim and S. E. Park, *Anal. Biochem.*, **2010**, *405*, 135

[20] K. Kriz, F. Ibraimi, M. Lu, L. O. Hansson and D. Kriz, *Anal. Chem*., **2005**, *77*, 5920.

[21] B. Sun, L. Huang, N. Na, D. He and J. Ouyang, *Electrophoresis*, **2011**, *32*, 2091.

[22] C. T. Chen and Y. C. Chen, *Anal. Chem*., **2005**, *77*, 5912.

[23] M. Vallet-Regi, F. Balas, D. Arcos, *Angew. Chem. Int. Ed.* **2007**, *46*, 7548.

[24] S. T. Selvan, P. K. Patra, C. Y. Ang, J. Y. Ying, *Angew. Chem. Int. Ed.* **2007**, *46*, 2448

[25] K. Cheng, S. Peng, C. J. Xu, S. Sun, *J. Am. Chem. Soc.* **2009**, *131*, 10637.

[26] S. Santra, C. Kaittanis, J. Grimm, J. M. Perez, *Small*, **2009**, *5*, 1862.

[27] Qiu X, Freitag M, Perebeinos V, Avouris P, *Nano Lett*, **2005**, *5*, 749.

[28] Ferrari M, *Nat Rev Cancer*, **2005**, *5*, 161.

[29] Ferriera L, Karp JM, Nobre L, Langer R, *Cell Stem Cell*, **2008**, *3*, 136

[30] Rivera GP, Oberdörster G, Elder A, Puntes V, Parak WJ, *ACS Nano*, **2010**, *4*, 5527

[31] S. Iijima, *Nature*, **1991**, *354*, 586.

[32] S. Iijima, T. Ichihashi, *Nature*, **1993**, *363*, 603.

[33]A. Thess, R. Lee, P. Nikolaev, H. Dai, P. Petit, J. Robert, C. Xu, Y. H. Lee, S. G. Kim, A. G. Rinzler, D. T. Colbert, G. E. Scuseria, D. Tománek, J. E. Fischer, R. E. Smalley, *Science*, **1996**, *273*, 483

[34] V.C. Moore, M.S. Strano, E.H. Haroz, R.H. Hauge, R.E. Smalley, J. Schmidt, Y. Talmon, *Nano Lett.* **2003**, *10*, 1379.

[35] M. Zheng, A. Jagota, E.D. Semke, B.A. Diner, R.S. McLean, S.R. Lustig, R.E. Richardson, N.G. Tassi, *Nat. Mater*. **2003**, *5*, 338

[36] Edgington AJ, Roberts AP, Taylor LM, Alloy MM, Reppert J, Rao AM, *Environ Toxicol Chem* **2010**, *29*, 2511.

[37] Roberts AP, Mount AS, Seda B, Souther J, Qiao R, Lin S, *Environ Sci Technol*, **2007**, *41*, 3025.

[38] Petersen EJ, Akkanen J, Kukkonen J, Weber WJ Jr, *Environ Sci Technol*, **2009**, *43*, 2969.

[39] Petersen E. J, Pinto R. A, Mai D. J, Landrum P. F, Weber W. J Jr, *Environ Sci Technol*, **2011**, *45*, 1133

[40] Zhu X, Zhu L, Chen Y, Tian S, *J Nanopart Res*, **2009**, *11*, 67.

[41] Z. Zhu, R. Yang, M. You, X. Zhang, Y. Wu, W. Tan, *Anal. Bioanal. Chem*. **2010**, *396*, 73.

[42] R. Yang, J. Jin, Y. Chen, N. Shao, H. Kang, Z. Xiao, Z. Tang, Y. Wu, Z. Zhu, W. Tan, *J. Am. Chem. Soc.* **2008**, *130*, 8351.

[43] W. F. Cheong, S. A. Prahl, A. J. Welch, *IEEE J*. **1990**, *26*, 2166.

[44] J. V. Frangioni, *Curr. Opin. Chem. Biol*., **2003**, *7*, 626.

[45] P. Cherukuri, S.M. Bachilo, S.H. Litovsky, R.B. Weisman, *J. Am. Chem. Soc.*, **2004**, *126*, 5638.

[46] K. Welsher, Z. Liu, D. Daranciang, H. Dai, *Nano Lett.* **2008**, *8*, 586

[47] M. Prato, K. Kostarelos, A. Bianco, *Accounts of Chemical Research*, **2008**, *41*, 60.

[48] D. Pantarotto, J. P. Briand, M. Prato, A. Bianco, *Chemical Communication*, **2004**, 16.

[49] N. W. Kam, T. C. Jessop, P. A. Wender, H. Dai, *J. Am. Chem. Soc*, **2004**, *126*, 6850.

[50] Z. Liu, C. Davis,W. Cai, L. He, X. Chen, H. Dai, *Proc. Natl. Acad. Sci. U.S.A.* **2008**, *105*, 1410.

[51] H. Huang, Q. Yuan, J.S. Shah, R. D. K. Misra, *Advanced Drug Delivery Reviews*, **2011**, *63*, 1332.

[52] Rosi, N. L., Mirkin, C. A., *Chem. Rev.* **2005**, *105*, 1547.

[53] Gao, X.H. & Nie, S.M., *J. Phys. Chem. B.* **107**, 11575–11578 (2003).

[54] Gao, X.H., Nie, S.M., *Anal. Chem.* **2004**, *76*, 2406.

[55] A. Nel, T. Xia, L. Madler, N. Li, *Science*, **2006**, *311*, 622.

[56] M. L. Schipper, N. Nakayama-Ratchford, C. R. Davis, N. W. S. Kam, P. Chu, Z. Liu, X. M. Sun, H. J. Daiand, S. S. Gambhir, *Nat. Nanotechnol*., **2008**, *3*, 216.

[57] T. Cedervall, I. Lynch, S. Lindman, T. Berggard, E. Thulin, H. Nilsson, K. A. Dawson and S. Linse, *Proc. Natl. Acad. Sci. U. S. A.*, **2007**, *104*, 2050.

[58] B. I. Ipe, A. Shukla, H. C. Lu, B. Zou, H. Rehage, C. M. Niemeyer, *Chem Phys Chem*, **2006**, *7*, 1112.

[59] C. C. You, M. De and V. M. Rotello, *Curr. Opin. Chem. Biol.*, **2005**, *9*, 639.

[60] V. Zorbas, A. L. Smith, H. Xie, A. Ortiz-Acevedo, A. B. Dalton, G. R. Dieckmann, R. K. Draper, R. H. Baughman, I. H. Musselman, *J. Am. Chem. Soc.*, **2005**, *127*, 12323.

[61] B. Belgorodsky, L. Fadeev, V. Ittah, H. Benyamini, S. Zelner, D. Huppert, A. B. Kotlyar, M. Gozin, *Bioconjugate Chem.*, **2005**, *16*, 1058.

[62] H. S. Mandal and H. B. Kraatz, *J. Am. Chem. Soc*., **2007**, *129*, 6356.

[63] N. Wangoo, C. R. Suri and G. Shekhawat, *Appl. Phys. Lett.*, **2008**, *92*, 133104.

[64] Q. Xiao, S. Huang, Z. D. Qi, B. Zhou, Z. K. He and Y. Liu, *Biochim. Biophys. Acta, Proteins Proteomics*, **2008**, *1784*, 1020.

[65] S. S. Karajanagi, A. A. Vertegel, R. S. Kane and J. S. Dordick, *Langmuir*, **2004**, *20*, 11594.

[66] H. S. Mandal and H. B. Kraatz, *J. Am. Chem. Soc*., **2007**, *129*, 6356.

[67] Z. G. Peng, K. Hidajat and M. S. Uddin, *J. Colloid Interface Sci.*, **2004**, *271*, 277.

[68] B. C. Braden, F. A. Goldbaum, B. X. Chen, A. N. Kirschner, S. R. Wilson and B. F. Erlanger, *Proc. Natl. Acad. Sci. U. S. A.*, **2000**, *97*, 12193.

[69] M. Lundqvist, I. Sethson and B. H. Jonsson, Langmuir, 2005, 21, 5974–5979.

[70] M. De, C. C. You, S. Srivastava and V. M. Rotello, *J. Am. Chem. Soc*., **2007**, *129*, 10747.

[71] S. Lindman, I. Lynch, E. Thulin, H. Nilsson, K. A. Dawson and S. Linse, *Nano Lett.*, **2007**, *7*, 914.

[72] S. P. Rozhkov, A. S. Goryunov, G. A. Sukhanova, A. G. Borisova, N. N. Rozhkova, G. V. Andrievsky, *Biochem. Biophys. Res. Commun*., **2003**, *303*, 562.

[73] M. Lundqvist, I. Sethson, B. H. Jonsson, *Langmuir*, **2004**, *20*, 10639.

[74] M. Karlsson and U. Carlsson, Biophys. J., **2005**, *88*, 3536.

[75] H. Kawasaki, T. Akira, T. Watanabe, K. Nozaki, T. Yonezawa, R. Arakawa, *Anal. Bioanal. Chem*., **2009**, *395*, 1423.

[76] H. R. Kim, K. Andrieux, C. Delomenie, H. Chacun, M. Appel, D. Desmaele, F. Taran, D. Georgin, P. Couvreur and M. Taverna, *Electrophoresis*, **2007**, *28*, 2252.

[77] H. R. Kim, K. Andrieux, S. Gil, M. Taverna, H. Chacun, D. Desmaele, F. Taran, D. Georgin, P. Couvreur, *Biomacromolecules*, **2007**, *8*, 793.

[78] M. Lundqvist, J. Stigler, G. Elia, I. Lynch, T. Cedervall, K. A. Dawson, *Proc. Natl. Acad. Sci. U. S. A.*, **2008**, *105*, 14265.

[79] E. Allemann, P. Gravel, J. C. Leroux, L. Balant, R. Gurny, *J. Biomed. Mater. Res.*, **1997**, *37*, 229.

[80] H. R. Kim, K. Andrieux, S. Gil, M. Taverna, H. Chacun, D. Desmaele, F. Taran, D. Georgin, P. Couvreur, *Biomacromolecules*, **2007**, *8*, 793.

[81] S. Nagayama, K. Ogawara, Y. Fukuoka, K. Higaki and T. Kimura, *Int. J. Pharm.*, **2007**, *342*, 215.

[82] S. Stolnik, B. Daudali, A. Arien, J. Whetstone, C. R. Heald, M. C. Garnett, S. S. Davis, L. Illum, *Biochim. Biophys. Acta, Biomembr*., **2001**, *1514*, 261.

[83] P. Aggarwal, J. B. Hall, C. B. McLeland, M. A. Dobrovolskaia, S. E. McNeil, *Adv. Drug Delivery Rev*., **2009**, *61*, 428.

Chapter 2

Probing nanoparticle-protein interaction by capillary electrophoresis

2.1 Introduction

Nanoparticles (NPs), with at least one dimension smaller than 100 nm, have been proposed to be revolutionary substances for drug delivery, disease diagnosis and treatment, in vivo biomedical imaging, etc. On the other hand, the rapidly increasing production of nanoparticles will unavoidably lead to their mounting accumulation in the environment and, thus, rising chances to be exposed to human beings. Both trends have raised great attention on how these materials with size scales comparable to biological components interact with the biological systems.[1] More understanding on the nano-bio interface will definitely promote their applications in biomedical technologies and at the same time help to reduce or prevent any possible nanotoxicity.

It has been reported that nanoparticles could adsorb many plasma proteins.[2] The resulted protein coat could increase the stability of NPs[3,4] or assist cell internalization, [5,6] beneficial for NPs functioning as diagnostic or therapeutic substances. However, adsorption onto NPs has been found to induce protein aggregation,[7] misfolding, and deactivation[8] and could also affect protein-protein interaction,[9] possibly resulting in protein malfunctioning and, thus, adverse biological effects. In order to impose better

control over both the advantageous and harmful outcomes of NPs being in the biological systems, driving forces for their interaction with proteins need to be identified. Many variables play roles in the interaction, including the noncovalent binding forces of electrostatic and hydrophobic interactions, hydrogen bonding, and π-π stacking, the solvation of NPs and the NP-protein complexes, as well as the surface curvature of the nanostructures.[10] To sort out how this many variables influence the interaction between NPs and proteins with diverse physicochemical properties, quantitative comparison of the interaction kinetics, affinity, and stoichiometry when systematically varying the types of protein or NPs is highly demanded.

Presently, techniques like circular dichroism (CD),[11] surface plasmon resonance (SPR),[12] isothermal titration calorimetry (ITC),[10] and fluorescence correlation or quenching microscopy[13,14] dominate the measurement of NP-protein interaction because of the high simplicity in direct measurement of the interaction mixture. However, low sensitivity, spectral interference from NPs in the background, requirement for protein or NP immobilization, and/or necessity for NPs to be luminescent or photoquenching prevent one from using the above techniques for studying NPs and proteins with wide ranges of physicochemical properties.[14] Moreover, it is difficult for these techniques to probe the interaction-induced changes in protein's binding capability to its ligands, substrates, or carrier molecules.[6,10,14-16]

Separation tools like size exclusion chromatrography (SEC), slab gel electrophoresis, and micellar electrokinetic chromatography have been applied to isolate proteins stably adsorbed onto NPs for downstream identification.[17,18] SEC could be used to estimate the binding rates between single proteins and NPs, but the exclusion resin seemed to adsorb the NP-protein complex and interfere with the estimation. On the contrary, capillary electrophoresis (CE) operates in an open-column format without any packing materials, imposing the least impact to the NP-protein complex. This feature, in addition to other advantages it offers, such as high resolution power and rapid separation speed, makes CE highly suitable for quantitative measurement of the affinity between individual proteins and NPs. Additionally, CE can handle nanomaterials very well.[19-21] Polymeric and inorganic NPs ranging from 20 nm to 1.5 μm in diameter have been used as the stationary or pseudostationary phase in capillary eletrochromatography[22,23] and have demonstrated good performance in electrophoretic separation of small molecules[24], DNA[25], and proteins.[26,27] Moreover, by adding the ligands to the running buffer, CE can conveniently study the transient complexes with fast association/dissociation rates.[28,29] Diverse separation modes have been developed to facilitate analysis of molecules with different characteristics in charge, size, and hydrophobicity, and multichannel CE on microchips can significantly enhance the analysis throughput, both adding extra values to the applicability of CE in studying NP-protein interaction.

In the present study, we examined the effectiveness of CE in measuring the affinity between NPs and proteins with an appropriate interaction model. Interactions of bovine serum albumin (BSA) with the gold and superparamagnetic Fe_3O_4 NPs, which have shown great potential in biomedical applications, were investigated. Depending on the complex dissociation rate, binding situations could be studied with two CE operation modes: capillary zone electrophoresis (CZE) and affinity capillary electrophoresis (ACE). The response curves of peak area ratios in CZE or electrophoretic mobility shifts in ACE versus protein concentrations were fitted with the Hill equation, and the dissociation constants (K_D) and the Hill coefficients (n) were obtained. Our study demonstrates the great power of CE in studying NP-protein interaction and paves the way for future investigation on the multicomponent interaction systems to probe the binding of substrate, cargo molecules, ligands, receptors, etc. to proteins adsorbed on the NP surface.

2.2 Experiment Section

2.2.1 Reagents and Materials

Gold colloid solutions (5 and 10 nm Au NPs) were from Sigma-Aldrich Corporation (St. Louis, MO), as well as all chemicals used for CE and superparamagnetic poly(acrylic acid) (PAA)-Fe_3O_4 NP synthesis. EMD OmniPur 10× PBS liquid concentrate (NaCl, 137 mM; KCl, 2.7 mM; phosphate buffer, 10 mM (Na_2HPO_4/KH_2PO_4, pH 7.4) on 10× dilution) and molecular biology grade dimethyl sulfoxide (DMSO) were obtained from

Fisher Scientific (Fairlawn, NJ). Solutions were prepared in the deionized water purified by the Milli·Q water purification system (Billerica, MA).

2.2.2 Synthesis and Characterization of NPs

Highly water-soluble PAA-coated Fe_3O_4 NPs (average sizes of 8 and 10 nm) were synthesized by hydrolyzing FeCl3 with NaOH/diethylene glycol (DEG) in the presence of PAA (Mw, 1800).30 A NaOH/ DEG stock solution was prepared by dissolving 50 mmol of NaOH in 20 mL of DEG. In a typical synthesis, a mixture of PAA (4 mmol), FeCl3 (2 mmol), and DEG (15 mL) was heated up to 220 °C in a nitrogen atmosphere with stirring. A NaOH/ DEG stock solution (4.5 mL) was then injected rapidly into the above hot mixture. The subsequent steps were different for the synthesis of PAA-Fe_3O_4 NPs with average diameters of 8 and 10 nm. The smaller NPs were obtained by continuously heating the resulting mixture for 12 h at 220 °C. The larger ones were achieved in several steps: heating the resulting mixture back to 220 °C, adding another 5 mL of 0.4 M $FeCl_3$ stock solution that dropped the solution temperature to around 200 °C, heating the solution back to 220 °C again, and injecting another 3 mL of 2.5 M NaOH/DEG and reacting for 10 min at 220 °C. An excess amount of PAA and other reagents in the reaction mixture were removed by centrifugation-assisted washing several times with a mixture of deionized water and ethanol. Finally, the PAA-Fe_3O_4 NPs were suspended in 10 mL of water to form the stock solutions.

A Philips Tecnai 12 transmission electron microscope (TEM) was used to investigate the morphology of NPs. TEM images of NPs are shown in the Supporting Information (Figure S2.1). Inductively coupled plasmas atomic emission spectroscopy (ICP-AES) tests were performed on a Perkin-Elmer Optima 2000 DV optical emission spectrometer to measure the concentration of Au or Fe element in NPs. With the size measured under TEM and the element content obtained from ICP-AES, molar concentration of the NPs stock solutions were obtained. Zeta potential and hydrodynamic size were measured with a ZetaPALS system (Brookhaven, Holtsville, NY) at 25 °C, which was equipped with a 660 nm laser and a build-in precision Peltier temperature controller.

2.2.3 Capillary Electrophoresis

A P/ACE MDQ capillary electrophoresis system equipped with a diode array detector (Beckman Coulter, Fullerton, CA) was used for all CE experiments. The 50 cm fused-silica capillary (75 μm id, 365 μm od; PolymicroTechnologies, Phoenix, AZ) with an effective length of 40 cm was sequentially rinsed at 30 psi with 0.1 M NaOH (2 min), deionized water (1 min), and the running buffer (6 min) prior to injection. All CE separations were done at 25 kV in room temperature. Peak area calculation was done by the 32Karat software provided by Beckman Coulter.

Capillary zone electrophoresis was performed in 10 mM borate buffer at pH 8.3. BSA at different concentrations (from 3.79 to 37.9 μM) was incubated with 194.8 nM 8 nm PAA-Fe_3O_4 at room temperature overnight before CZE analysis. For pH and salt effect

study, the 8 nm PAA-Fe_3O_4 and BSA (from 3.79 to 60.6 μM) were preincubated in 10 mM borate buffer at pH 8.3, 17.5 mM phosphate buffer at pH 7.5, or 1× PBS containing 150 mM NaCl.

In affinity capillary electrophoresis, NP was injected and different concentrations of proteins were included in the running buffer of 17.5 mM phosphate buffer (pH 7.5). The Au NPs (5.66 nM for the 10 nm Au NPs and 19.1 nM for the 5 nm Au NPs) were injected with 0.01% (v/v) DMSO.

2.3 Results and Discussion

2.3. 1 CE Modes and Affinity Calculation

Unlike the well-defined ligand-receptor system, NPs could be the ligands or the receptors in their interaction with proteins, and thus, our first step was to setup the appropriate roles for NPs and proteins. NPs have uniform distribution of the same type of functional groups on their surface, forming multiple and possibly similar binding pockets for proteins. They range from 5 nm up to 100 nm,[6,14,31] much larger than proteins and able to accommodate more than one protein molecule on the surface. Additionally, NPs entering the circulation systems are present at small doses and face highly abundant proteins. The characteristics of NPs and the interaction circumstance make it more logical to consider each NP as a receptor with multiple binding sites and the protein as the monovalent ligand (L) and present in excess. Moreover, this interaction model

determines that the migration behavior of the NPs would be measured but not of the proteins, which simplifies the analysis because NPs usually possess more prominent optical properties than proteins.

The process of using CE to measure the binding affinity between NPs and proteins is described in Figure 2.1. The dissociation equilibrium constant of the NP-protein complex can be calculated from the Hill equation[13,14,32,33] using the protein-bound NP fraction (θ) and the protein concentration:

$$\theta = [\text{protein}]n/(K\ n + [\text{protein}]n) \qquad (1)$$

In eq 1, K_D is microscopic dissociation constant, describing the affinity of each binding site to the protein ligand; and n represents the binding cooperativeness. The multivalent nature of the NP-protein interaction determines that competition or cooperation among the same protein molecules for the binding sites on the NP surface would occur, which would be accurately described by n. However, the Hill equation assumes each binding site is occupied by one ligand and cannot reveal the adsorption of multiple protein layers on the NP surface. This binding situation may happen when the protein concentration is very large or the protein tends to aggregate in the interaction buffer. It should be avoidedby controlling the protein concentration, and aggregation could be monitored from the migration behavior of the protein and NP-protein complexes in CE. Protein binding to the NP surface can bring in significant change to the charge and size of NPs

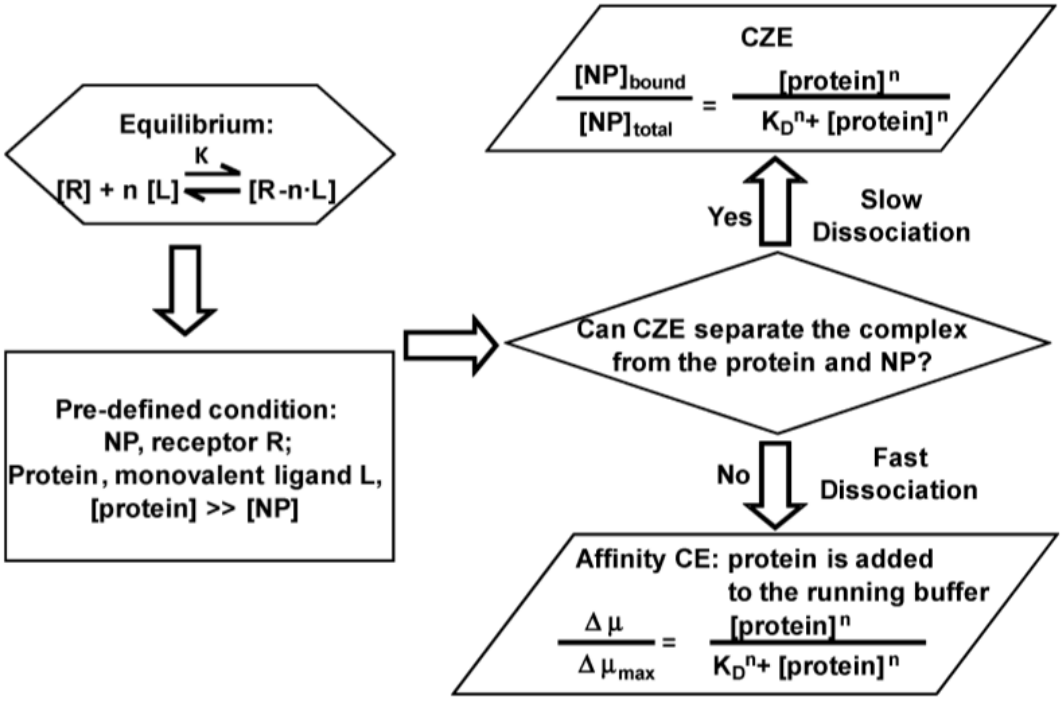

Figure 2.1 Flowchart of CE as a flexible probing platform for NP-protein interaction

remains stable during the separation and is resolved by CZE from the free ones. Then, θ is equal to the peak area ratio of the protein-bound and total NPs. For complexes formed and dissociated rapidly during CE, θ can be calculated from the apparent electrophoretic mobility (μ_{app}) of NP in ACE with different protein concentrations in the running buffer.

$$\mu_{app} = f_1 \cdot \mu_{max} + f_2 \cdot \mu_{free} \quad (2)$$

where f_1 and f_2 are the fractions of protein-bound and free NPs, and μ_{free} and μ_{max} are the mobility values when there is no protein and saturated protein in the running buffer, respectively. Thus, we have

$$\theta = NP_{bound}/NP_{total} = f_1 = (\mu - \mu_{free})/(\mu_{max}-\mu_{free}) \quad (3)$$

For the study of slow dissociation systems with CZE, NPs at a fixed concentration were incubated with different concentrations of BSA, and the equilibrium mixture was injected. The duration of incubation was determined by sampling the mixture at various times until no more change in the protein-bound NP peak was observed. Peak areas of the protein-bound and free NPs measured at the distinct wavelength of NPs with minimal interference from BSA were used to calculate the bound NP ratio. In the ACE mode, the mobility of NPs was monitored. Protein concentrations in the running buffer would be increased until the maximum mobility shift was observed. A neutral marker, DMSO, was used to adjust the change in the electroosmotic flow (EOF).

2.3.2 Slow Dissociation System

Interactions between BSA and the PAA-Fe_3O_4 (8 and 10 nm) NPs were typical slow dissociation systems. The interaction reached equilibrium after overnight incubation. The borate buffer (10 mM sodium borate, pH 8.3) provided the best separation of the bound- and free- NPs and, thus, was employed as the running buffer. We initially used water as the incubation buffer to promote BSA unfolding and facilitate its adsorption onto the NP surface. Both the protein and the NPs were negatively charged. Under the normal electric field, BSA migrated faster than the NPs and its adsorption onto the NP surface slightly sped up the apparent migration of NPs. This is probably due to the increase in NP size after being bound with BSA, because the total negative charges of NP or NP-protein complex should be majorly determined by the PAA which carried a large number of carboxyl groups. Hydration size and zeta potential measurement using the ZetaPALS confirmed this hypothesis. After mixing the 8 nm PAA-Fe_3O_4 NP with excess BSA in 10 mM borate buffer, a slight increment in the hydrodynamic size (from 47.5 to 49.1 nm) and a small decrease in the ζ potential (from -26.55 to -23.14 mV) were observed. This comparison demonstrates another advantage of the use of CE to study NP-protein interaction: the μ of NPs can be used to calculate the ζ potential of NPs before and after interaction with proteins. Since the hydrodynamic size of NP is larger than 10 nm, it is appropriate to assume the NP diameter is much larger than the electrical double layer thickness (κ^{-1}) and apply the simplified Smoluchowski model in the calculation[35]:

$$\zeta = \mu\eta/\varepsilon \quad (4)$$

in which ε is the dielectric constant and η is the solution viscosity. The ζ potentials obtained from CE data fitted to the simplified Smoluchowshki model were 10-15% higher than those measured from ZetaPALS, owing to the simplified calculation, but CE consumed much smaller volumes of samples.

The NP-BSA complex peak increased with the BSA concentration, while the NP peak area decreased gradually. The peak area of the protein-bound NP should be dominant from UV absorption of NPs. Therefore, we compared the electropherograms at different wavelengths. The electropherogram at 200 nm showed the largest signals for both the protein and the NPs (Figure S2.2, Supporting Information), suitable for monitoring of the separation process. The one obtained at 288 nm resulted in small signals from the protein at all concentrations used in our investigation and reasonable signals from the NPs. It was selected for the calculation of θ.

Moreover, our model employed high molar ratio of protein to NPs to validly approximate the equilibrium protein concentration using the initial concentration. The plot of θ (NP_{bound}/NP_{total}) vs BSA concentration fit to the Hill equation very well (Figure 2.2). By aligning the electropherograms (insets in Figure 2.2), we observed a small shift of the NP-BSA complex peak to the left with increasing protein concentration, which illustrated

that the number of BSA molecules per NP increased with protein concentration until no more protein could be accommodated due to space hindrance. The representative

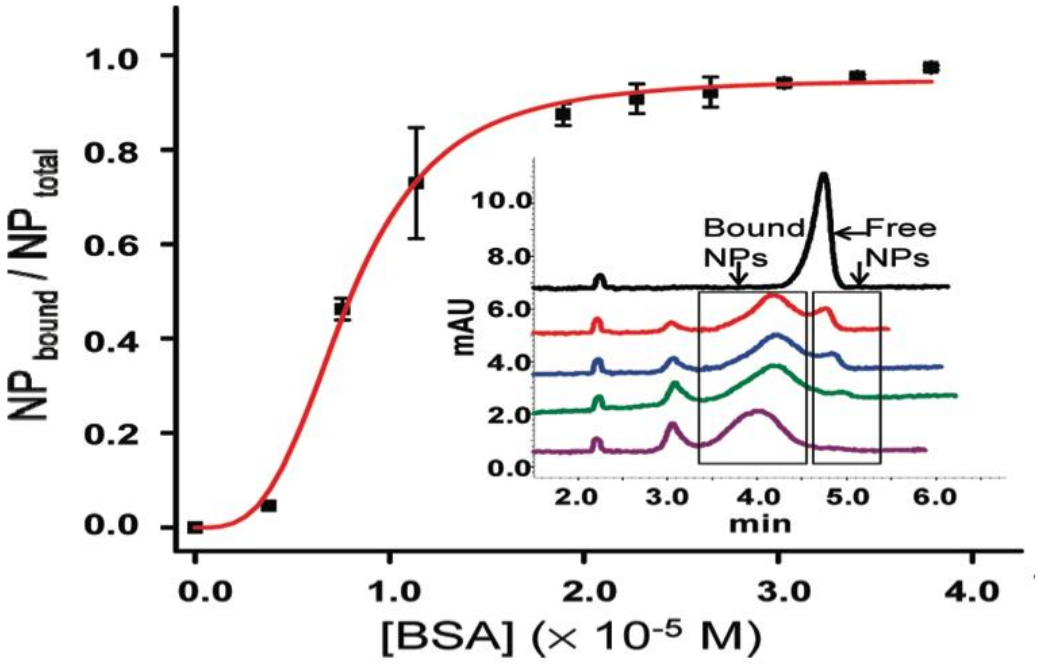

Figure 2.2. Representative electropherograms at 288 nm for an interaction study between BSA and 8 nm PAA-Fe_3O_4 NPs (1.94×10^{-7} M) by CZE and a model fitting curve (in triplicate). From top to bottom, traces were free 8 nm PAA-Fe_3O_4 NPs and mixtures of BSA and PAA-Fe_3O_4 NPs at molar ratios of 58.3:1, 97.2:1, 155.6:1, and 194.5:1. The peaks at around 2.2 min were from DMSO, and the peaks at around 3.0 min were for BSA.

electropherograms for the 10 nm PAA-Fe_3O_4 NPs can be found in Figure S2.3, Supporting Information.

2.3.3 Fast Dissociation System

Interaction between the Au NPs (5 nm and 10 nm) and BSA rendered only mobility shift but no separation of the complex and free NP peaks. The interaction was then investigated using ACE by adding BSA to the running buffer. Since no separation was involved, we employed the phosphate buffer (17.5 mM, pH 7.5) that more resembled the physiological conditions than the borate system. No additional NaCl was added to minimize band broadening from joule heating. Representative electropherograms and the curve fitting results for interaction of BSA with the 10 nm Au NP are shown in Figure 2.3, and those with the 5 nm Au NPs are displayed in Figure S2.4, Supporting Information. Again, association with BSA decreased the mobility of NPs and shortened their migration times inside the capillary, indicating the size of the NP was enlarged. The change in mobility shift became smaller and smaller until no longer observable at high BSA concentrations. Along with higher protein contents, several phenomena were observed. First is the decrease in EOF due to the adsorption of BSA onto the capillary wall, judged from the migration time of DMSO. Second, the reduced EOF also contributed to a broader Au NP peak at higher protein concentrations. Third, a negative peak before the Au NP peak appeared from the depletion of protein in the sample zone, though all these changes did not affect the mobility measurement as long as the current and baseline remained stable. High measurement reproducibility (relative standard deviations of

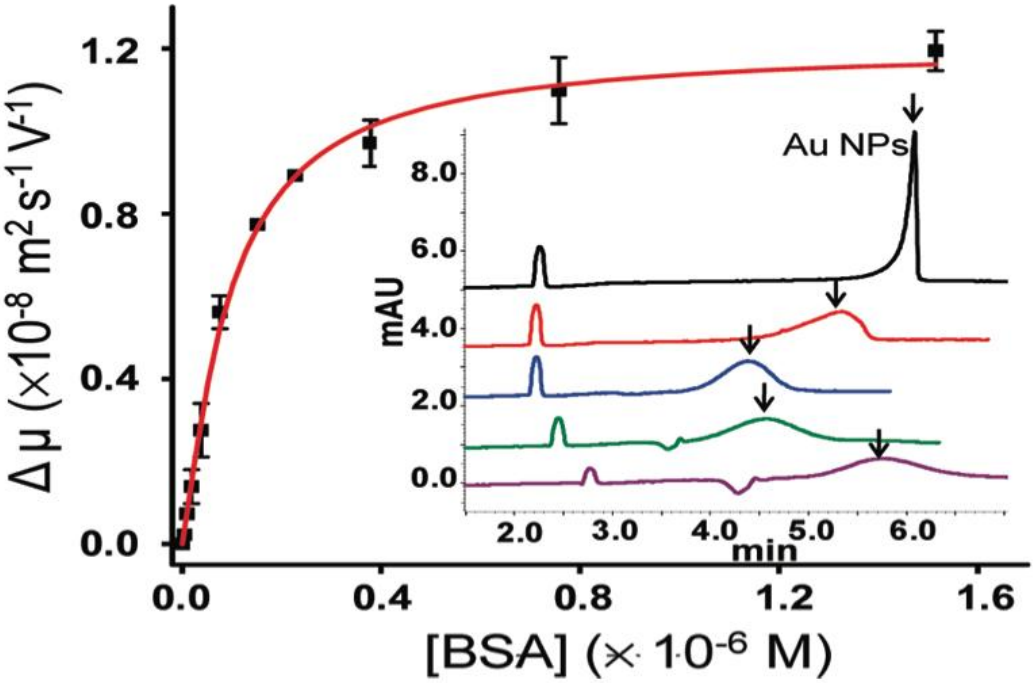

Figure 2.3. Representative electropherograms at 235 nm for an interaction study between BSA and 10 nm Au NPs (5.66×10^{-9} M) by ACE and a model fitting curve (in triplicate). From top to bottom, traces were an interaction study for BSA and 10 nm Au NPs at molar ratios of 0:1, 6.7:1, 26.8:1, 133.9:1, and 267.7:1.

mobility shifts were smaller than 10%) and correlation constants close to 0.99 in curve fittings were still obtained.

2.3.4 Impact on Affinity from Incubation Conditions

The pH and ionic strength of the interaction buffer would affect the double layer thickness and the ζ potential of both the protein and NPs and, therefore, could alter the interaction. In the above study, the interactions occurred in different environments, i.e., water vs the phosphate buffer. To explore how much difference in affinity would be caused by such changes, we measured the affinities between BSA and the 8 nm PAA-Fe_3O_4 NPs in different incubation buffers: 17.5 mM phosphate (pH 7.5), 10 mM sodium borate (pH 8.3), or 1× PBS. The results were shown in Figure 2.4. The affinity obtained with the 17.5 mM phosphate buffer decreased by 3-fold in comparison with that in water (values reported in Table 1). Interaction in 1× PBS showed almost the same Hill coefficient as and a 1.8-fold weaker affinity than that in the 17.5 mM phosphate buffer. The slight decrease in affinity in 1× PBS could be attributed to the more salt ions attached to the protein as well as to the NPs, which shielded the NPs from BSA better. Additionally, the physiological condition of PBS could well reserve the structure of BSA and impede with its unfolding on the NP surface. Both effects reduced the nonspecific binding between BSA and NPs. Affinity variations observed in different buffers should be considered in an interaction study. If possible, similar buffer conditions, like the type

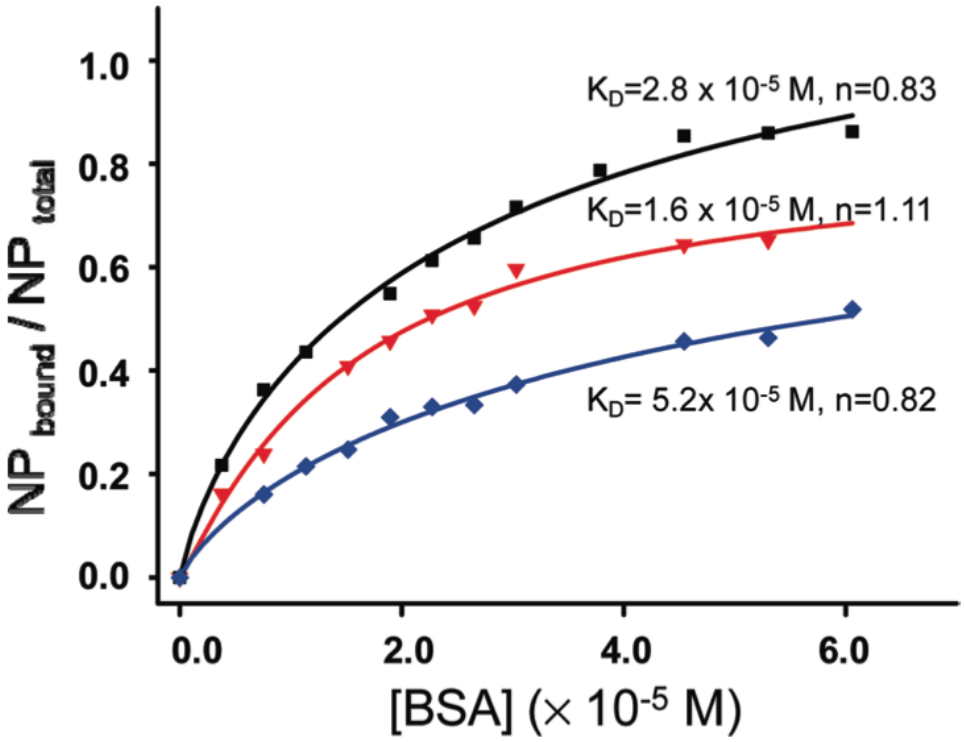

Figure 2.4 Salt and pH effects from preincubation buffer for interaction between BSA and 8 nm PAA-Fe_3O_4 NPs. ■: in 17.5 mM phosphate buffer; ▼: in 10 mM borate buffer;♦: in 1× PBS buffer.

of buffer components, pH, and salt level, should be maintained. The phosphate buffer and the PBS exhibited around a 1.8-fold change in the affinities, with identical n values. Thus, affinities measured in the phosphate buffer without NaCl added could be used to approximate the situation in PBS, simplifying the CE study.

2.3.5 Understanding the Interaction from K_D and n

The K_D and n values for the interaction of BSA with four types of NPs were calculated by the Hill equation and listed in Table 1. Size and surface functionalization define the surface curvature, the formation of electrical double layer, and the geometrical accommodation of proteins and are probably the most determinant factors for binding affinity and cooperativity. Our results pointed out that relatively strong interactions existed between BSA and the investigated NPs, with K_D values in the range between 10 and 0.01 μM (including those shown in Figure 2.4). The affinity increased with the size of NPs: the 8 nm Fe_3O_4 NPs yielded a K_D value 40 times larger than the 10 nm ones and the 5 nm Au had a 2-fold higher K_D than the 10 nm Au NPs. The affinity scale and its dependence on the size of NPs matched with values reported on Au NPs in the literature which were measured with spectroscopic methods[14,36], but no systematic study of BSA with the Fe_3O_4 NPs was found. The reduction in affinity for the smaller NPs might be related to the higher space hindrance to accommodate the relatively large BSA molecule around the NPs (in neutral solutions, the crystal structure of BSA was found to have a heart-shaped structure with dimensions of 8.4 nm × 8.4 nm × 8.4 nm × 3.15

nm).[37] The sharper curvature of the smaller NPs may also impede the refolding of the BSA molecule on the surface.

Within the scope of our study, Au NPs displayed an average higher affinity to BSA than the Fe_3O_4 NPs. The difference in surface coating may be one of the driving forces for the relative strength in affinity. The electrostatic repulsion from negatively charged BSA and NPs did not prevent the relatively strong interaction between them. The high structure flexibility of BSA probably allowed easy refolding of the BSA molecule to adapt to the surface. A conformational change in BSA upon its adsorption onto the 2D surface or NPs has been well documented.[14,16,38-41] The Au NPs were coated with citrate, and the Fe_3O_4 NPs were stabilized with PAA.[42] The longer chain of PAA than the citrate groups on the Au surface may extend the thickness of the diffusion layer and prevent the BSA molecules to get closer to the Fe_3O_4 NPs surface. Indeed, hydration size measurement indicated that the 5 and 10 nm Au NPs had hydrodynamic sizes of 22.6 and 37.7 nm, respectively, both smaller than the 47.5 nm hydrated Fe_3O_4 NPs. Furthermore, the polymer layer provided adequate shielding of the iron oxide core[43] that may prevent the coordination between the metal oxide core and the functional groups on BSA. A difference in surface coating may also exist within the Fe_3O_4 NPs, even though they were both coated with PAA. The Au NPs were produced by a modified tannic acid/citrate method44 with different amounts of reducing tannic acid added to the reaction. However, the synthesis procedures for the 8 and 10 nm iron oxide NPs were significantly different after the seeds had formed. The 8 nm NPs went through a 12 h pyrolysis process and may

have a considerably higher amount of PAA on the surface that contributed to the 40 fold affinity reduction.[30] The exact contribution from the core or surface coating needs to be further explored with the preparation of a series of NPs with only one physicochemical property being changed at a time. The could-be-tedious, systematic comparison of a large number of different NPs is simplified with the straightforward but effective CE platform and will reveal more information about the driving forces for the interaction.

The dependence of interaction cooperativeness on the physicochemical properties of NPs is also evaluated.[33] Interaction between BSA and the Au NPs were cooperative, with $n > 1$. This result is contradictory to that reported previously when the Au NPs and proteins were viewed as ligands and receptors[14], respectively, opposite to our model. Our model reflects the accommodation of proteins on the NP surface. Since the surface ligands are dynamically bound to the surface through coordination with the surface metal, they may reorganize upon the binding of the first BSA molecule to expose more sites for interaction with the subsequent BSA, showing positive cooperativeness. In addition, for NPs with the same core material, e.g., Au NPs, the larger NPs showed weaker cooperativity (smaller n). The same trend was observed in the previous study using fluorescence quenching spectroscopy.[14] The larger surface area available for binding may lead to only local reorganization of the surface groups and, thus, less impact on the subsequent binding.

Interactions of BSA with the iron oxide NPs in water (Table 2.1) showed positive cooperativity, i.e., n > 1, while those in buffers (2.) were noncooperative. This again could be related to the more rigid structure of BSA in the buffered solutions than in water, reducing the influence from peer BSA molecules coadsorbed onto the same NP. The noncooperativity of the 8 nm iron oxide NPs measured in the phosphate buffer is significantly different than the situation for Au NPs in the same buffer. The larger hydration size and thicker polymer layers, i.e., more flexible structure and less stringency on reorganization, on the iron oxide particles could both contribute to such a variation. The cooperativity also deceased with the size of the Fe_3O_4 NPs.

Table 2.1 Model Fitting Parameters for Interaction between BSA and PAA-Fe_3O_4 NP, Au NP*a*

NPs interacted with BSA	K_D (M)	n	R^2
8 nm PAA−Fe_3O_4 NP	$7.9 \times 10^{-6} \pm 2.1 \times 10^{-7}$	3.3 ± 0.3	0.988
10 nm PAA−Fe_3O_4 NP	$1.9 \times 10^{-7} \pm 7.3 \times 10^{-9}$	2.4 ± 0.3	0.996
5 nm Au NP	$2.3 \times 10^{-7} \pm 1.9 \times 10^{-8}$	2.3 ± 0.4	0.979
10 nm Au NP	$9.5 \times 10^{-8} \pm 6.8 \times 10^{-9}$	1.2 ± 0.1	0.997

[a] In triplicate.

2.4 Conclusions

We demonstrated here that CE can be employed for quantitative study of the interaction between protein and NPs. Interaction systems with slow dissociation rates relative to CE speed can be analyzed by CZE where the bound and free NPs can be separated and quantified. Systems with fast dissociation rates can be analyzed by ACE, monitoring the mobility shift of NPs. The interaction endures minimal disturbance in the open separation channel of CE compared to the packed column chromatography. The fast separation speed significantly improves the study efficiency. The separation-based platform will permit study of the more complicated systems which involve multiple interactive components.

The investigated systems are relatively simple for CE study, with both the proteins and NPs carrying negative charges and in buffers having low ionic strength. Future development should focus on interactions under physiological conditions and expand the investigation to proteins with high pI values and nanoparticles carrying positive charges. It is convenient to switch incubation buffers for a stable NP-protein complex, but it is difficult to employ saline buffers in ACE due to the peak dispersion with increased running current. Therefore, ultrafast CE, such as microsecond CE[45,46], can be developed to separate the transient NP-protein complex from the free NPs. A coated capillary will be considered to minimize the adsorption of the positively charged proteins and NPs on the capillary wall. Fluorescence detection can be employed to lower the

protein and NP concentrations and avoid side effects accompanied with high protein concentrations in the running buffer in ACE, such as EOF alteration, peak distortion, and low peak intensity. Adsorption of multiple protein layers on NPs and the possible disturbance to the NP-protein complex by the strong electric field of CE should be paid attention to as well in future studies.

2.5 References

[1] Nel, A. E.; Ma¨dler, L.; Velegol, D.; Xia, T.; Hoek, E. M. V.; Somasundaran, P.; Klaessig, F.; Castranova, V.; Thompson, M. *Nat. Mater.* **2009**, *8*, 543– 557.

[2] Cedervall, T.; Lynch, I.; Lindman, S.; Berggard, T.; Thulin, E.; Nilsson, H.; Dawson, K. A.; Linse, S. *Proc. Natl. Acad. Sci. U.S.A.* **2007**, *104*, 2050– 2055.

[3] Deguchi, S.; Yamazaki, T.; Mukai, S.; Usami, R.; Horikoshi, K. *Chem. Res. Toxicol.* **2007**, *20*, 854–858.

[4] Samanta, B.; Yan, H.; Fischer, N. O.; Shi, J.; Jerry, D. J.; Rotello, V. M. *J. Mater. Chem.* **2008**, *18*, 1204–1208.

[5] Lynch,I.;Cedervall,T.;Lundqvist,M.;Cabaleiro-Lago,C.;Linse,S.;Dawson, K. A. *Adv. Colloid Interface Sci.* **2007**, *134-135*, 167–174.

[6] Aggarwal, P.; Hall, J. B.; McLeland, C. B.; Dobrovolskaia, M. A.; McNeil, S. E. *Adv. Drug Delivery Rev.* **2009**, *61*, 428–437.

[7] Zhang,D.;Neumann,O.;Wang,H.;Yuwono,V.M.;Barhoumi,A.;Perham, M.; Hartgerink, J. D.; Wittung-Stafshede, P.; Halas, N. J. *Nano Lett.* **2009**, *9*, 666–671.

[8] You, C. C.; De, M.; Han, G.; Rotello, V. M. *J. Am. Chem. Soc.* **2005**, *127*, 12873–12881.

[9] Bayraktar, H.; Ghosh, P. S.; Rotello, V. M.; Knapp, M. J. *Chem. Commun.* **2006**, *2006*, 1390–1392.

[10] De, M.; You, C. C.; Srivastava, S.; Rotello, V. M. *J. Am. Chem. Soc.* **2007**, *129*, 10747.

[11] Lundqvist, M.; Sethson, I.; Jonsson, B. H. *Langmuir* **2004**, *20*, 10639– 10647.

[13] Roecker, C.; Poetzl, M.; Zhang, F.; Parak, W. J.; Nienhaus, G. U. *Nat. Nanotechnol.* **2009**, *4*, 577–580.

[14] DePaoliLacerda, S. H.; Park, J.-J.; Meuse, C.; Pristinski, D.; Becker, M. L.; Karim, A.; Douglas, J. F. *ACS Nano* **2010**, *4*, 365–379.

[15] Bayraktar, H.; Ghosh, P. S.; Rotello, V. M.; Knapp, M. J. *Chem. Commun.* **2006**, *2006*, 1390–1392.

[16] Chen, Y.; Flowers, K.; Calizo, M.; Bishnoi, S. W. *Colloids Surf., B* **2010**, *76*, 241–247.

[17] Kim, H. R.;Andrieux,K.;Delomenie,C.;Chacun,H.;Appel,M.;Desmae˙le, D.; Taran, F.; Georgin, D.; Couvreur, P.; Taverna, M. *Electrophoresis* **2007**, *28*, 2252–2261.

[18] Li, L.; Mu, Q.; Zhang, B.; Yan, B. *Analyst* **2010**, *135*, 1519–1530.

[19] d'Orlye, F.; Varenne, A.; Georgelin, T.; Siaugue, J.-M.; Teste, B.; Descroix, S.; Gareil, P. *Electrophoresis* **2009**, *30*, 2572–2582.

[20] Pyell, U. *Electrophoresis* **2008**, *29*, 576–589.

[21] Vicente, G.; Colon, L. A. *Anal. Chem.* **2008**, *80*, 1988–1994.

[22] Nilssona, C.; Birnbaumb, S.; Nilsson, S. *J. Chromatogr., A.* **2007**, *1168*, 212–224.

[23] Nilsson, C.; Nilsson, S. *Electrophoresis* **2006**.

[24] Luong, J. H. T.; Bouvrette, P.; Liu, Y.; Yang, D.-Q.; Sacher, E. *J. Chromatogr., A* **2005**, *1074*, 187–194.

[25] Huang, M.-F.; Kuo, Y.-C.; Huang, C.-C.; Chang, H.-T. *Anal. Chem.* **2004**, *76*, 192–196.

[26] Stathakis, C.; Arriaga, E. A.; Dovichi, N. J. *J. Chromatogr., A* **1998**, *817*, 233–238.

[27] Nilsson, C.; Becker, K.; Harwigsson, I.; Blow, L.; Birnbaum, S.; Nilsson, S. *Anal. Chem.* **2009**, *81*, 315–321.

[28] Heegaard, N. H. H. *J. Chromatogr., A* **1994**, *680*, 405–412.

[29] Heegaard, N. H. H. *Electrophoresis* **2009**, *30*, S229–S230.

[30] Ge, J.; Hu, Y.; Biasini, M.; Dong, C.; Guo, J.; Beyermann, W. P.; Yin, Y. *Chem.sEur. J.* **2007**, *13*, 7153–7161.

[31] Dobrovolskaia, M. A.; Patri, A. K.; Zheng, J.; Clogston, J. D.; Ayub, N.; Aggarwal, P.; Neun, B. W.; Hall, J. B.; McNeil, S. E. *Nanomed. Nanotechnol.* **2009**, *5*, 106–117.

[32] Hill, A. V. *J. Physiol.* **1910**, *40*, iv–vii.

[33] Weiss, J. N. *FASEB J.* **1997**, *11*, 835–841.

[34] Chu, Y. H.; Lees, W. J.; Stassinopoulos, A.; Walsh, C. T. *Biochemistry* **1994**, *33*, 10616–10621.

[35] Schnabel, U.; Fischer, C. H.; Kenndler, E. *J. Microcolumn Sep.* **1997**, *9*, 529–534.

[36] Brewer, S. H.; Glomm, W. R.; Johnson, M. C.; Knag, M. K.; Fransen, S. *Langmuir* **2005**, *21*, 9303–9307.

[37] Ferrer, M. L.; Duchowicz, R.; Carrasco, B.; de la Torre, J. G.; Acun˜a, A. U. *Biophys. J.* **2001**, *80*, 2422–2430.

[38] Turci, F.; Ghibaudi, E.; Colonna, M.; Boscolo, B.; Fenoglio, I.; Fubini, B. *Langmuir* **2010**, *26*, 8336–8346.

[39] Gray, J. J. *Curr. Opin. Struct. Biol.* **2004**, *14*, 110–115.

[40] Latour, R. A. *J. Biomed. Mater. Res., A* **2006**, *78A*, 843–854.

[41] Lu, J. R. *Neutron Scattering Biol.* **2006**, 265–282.

[42] Buchholz, F. L. *Ullmann's Encyclopedia of Industrial Chemistry*; VCH: Weinheim, 1992.

[43] Baigorri,R.;Garcia-Mina,J.M.;Gonzalez-Gaitano,G.*ColloidsSurf., A***2007**, *292*, 212-216.

[44] Slot, J. W.; Geuze Hans, J. *Eur. J. Cell Biol.* **1985**, *38*, 87–93.

[45] Plenert, M. L.; Shear, J. B. *Proc. Natl. Acad. Sci. U.S.A.* **2003**, *100*, 3853.

[46] Ritschdorff, E. T.; Plenert, M. L.; Shear, J. B. *Anal. Chem.* **2009**, 11860–11864.

2.6 Supporting Information

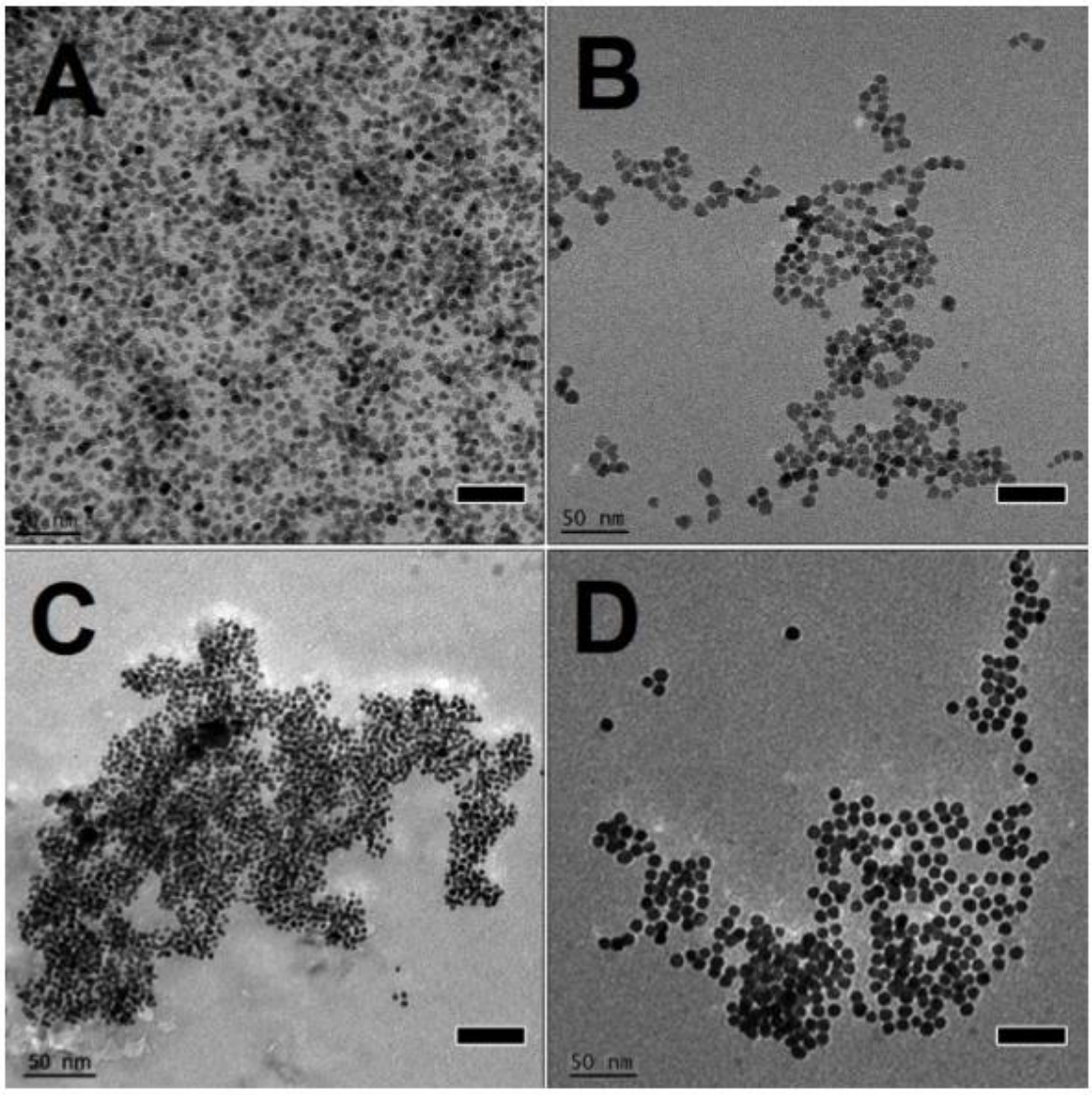

Figure S2.1. TEM images for PAA-Fe_3O_4 NPs (A: 8 nm, B: 10 nm) and Au NPs (C: 5 nm, D: 10 nm) with 50 nm.

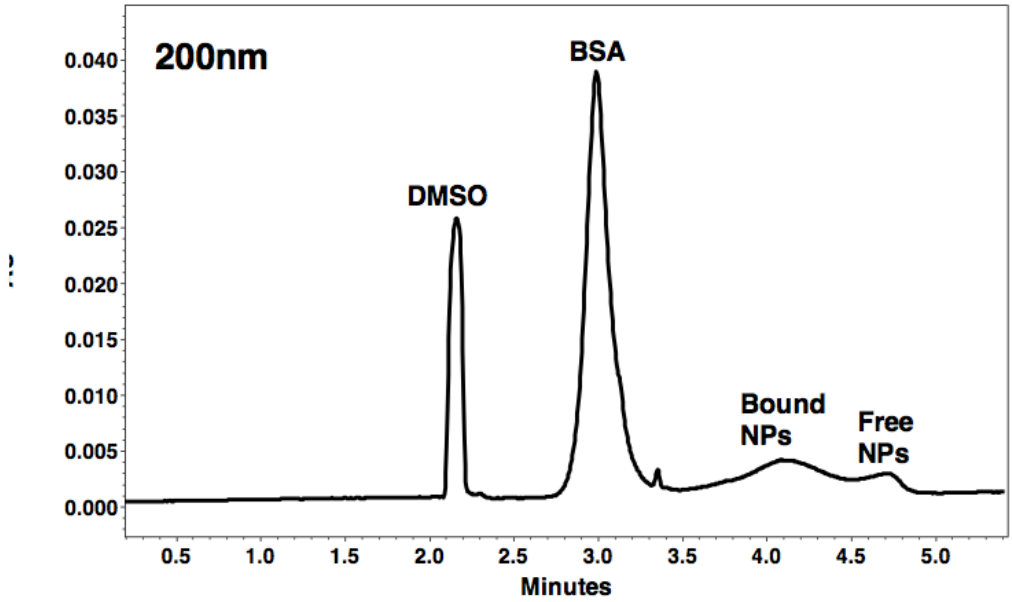

Figure S2.2. Electropherogram at 200nm for pre-incubated mixture of BSA and 8nm PAA-Fe_3O_4 (molar ratio 58.3:1).

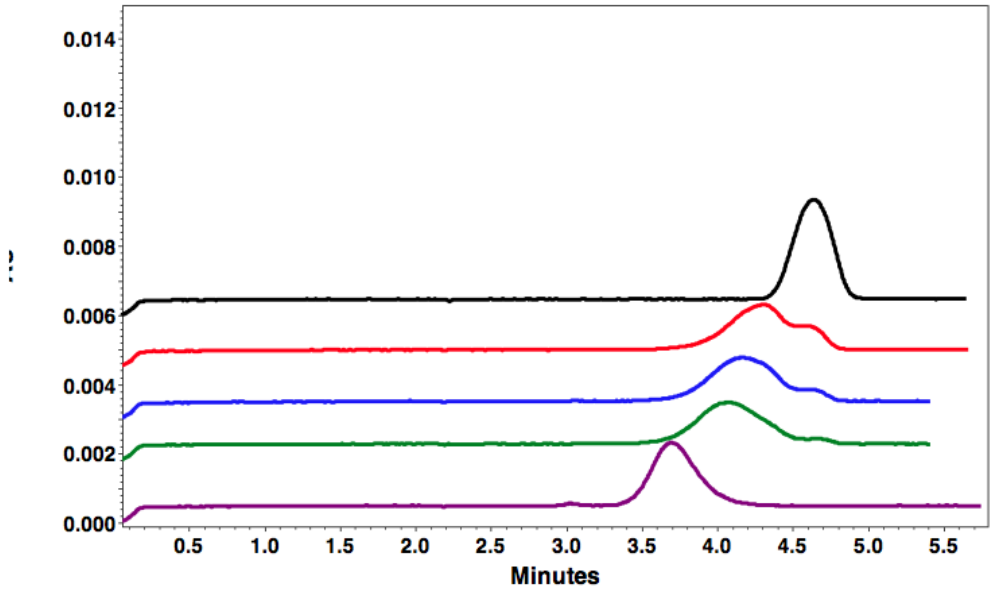

Figure S2.3. Representative electropherograms at 288nm for interaction study between BSA and 10 nm PAA-Fe_3O_4 NPs (1.08×10^{-7} M) at different molar ratio (from top to bottom: 0:1, 2.8:1, 4.2:1, 5.6:1 and 17.5:1) by CZE.

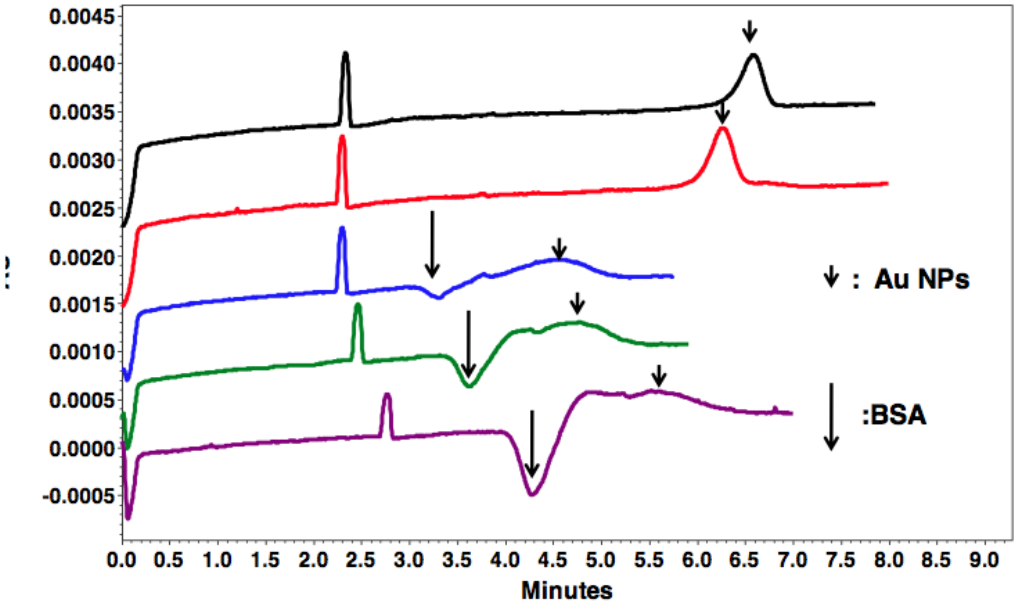

Figure S2.4. Representative electropherogram at 235nm for interaction study between BSA and 5nm Au NPs (1.91×10^{-8} M) at different molar ratios (from top to bottom: 0:1, 2.0:1, 15.9:1, 39.7:1, 79.3:1) by ACE.

Chapter 3

Protein binding for detection of small changes on a nanoparticle surface

3.1 Introduction

Nanoparticles (NPs) have been replacing bulk materials for application in diverse areas. With increasing exposure of humans to NPs, much research attention has been drawn to the interactions between NPs and biomolecules,[1–3] which could affect the behaviors of NPs in biosystems. Protein adsorption has been found to be strongly influenced by the surface properties of NPs.[4–9] Some adsorption behaviors are governed by the overall surface charge and hydrophobicity, similar to those observed on a flat surface made by bulk materials.[10] However, the comparable dimensions of NPs and proteins suggest that protein–NP interactions could mimic protein–protein interactions, and the NP surface ligands may target particular domains on proteins via particular functional groups.[11–13] This feature suggests that protein adsorption could be very sensitive to changes in the surface properties of NPs.

One possible change in the NP surface properties is alteration of the ligand structure during particle preparation, which could be induced by slight variations in synthesis conditions or use of alternative methods. For example, high-quality nanocrystals, including the II–VI binary semiconductors and metal oxides, which possess unique

optical, electrical, and magnetic properties, are typically prepared by pyrolysis reactions or solvothermal processes. All these approaches involve conditions such as high temperature, high pressure, and/or elongated reaction duration to achieve tight size control and/or high crystallinity.[14–18] Nevertheless, these harsh synthetic conditions may lead to structural changes in the capping agents that are used to stabilize the nanocrystals. Additionally, ligand exchange and surface modification are common in preparing watersoluble NPs for biomedical research and applications. Varied ligand exchange efficiency may lead to different surface coverage with the hydrophilic ligands on NPs; and chemical modification often requires multiple treatments that may lead to unexpected structural alteration to the surface ligands as well.[19] In many cases changes in ligand density and its structure could be subtle enough to not affect ligand binding to the NP surface and dispersion of NPs in solution. However, they could lead to variation in the surface properties of these ligand-capped nanocrystals, and ultimately affect the performance of NPs as biosensors, drug carriers, and in other targeted applications. Thus, such changes should be detected before the deployment of NPs. Though, detailed study of the surface properties of NPs could be challenging because most of the NP core could strongly interfere with many spectroscopic measurements, such as FT-IR spectroscopy, NMR, and MS.[20–23] Commonly, the ligands are removed from the NP surface by exchange reaction or chemical cleavage[24,25] and are studied in the absence of NPs. In addition, the NP core could be digested by strong acids and the surface ligands purified extensively after tedious procedures before structure analysis.

In the present study, we investigated whether protein adsorption could reveal small changes in the surface ligand of NPs. Highly stable iron oxide NPs were coated with polyacrylic acid (PAA). Up to 20-fold difference in the dissociation constant of the protein–NP complex was detected on the NPs synthesized at different heating durations. Investigation of the PAA structures by NMR and MS confirmed that the heating duration could affect the head group of PAA. Computational work also verified that the subtle difference in the head-group structure was sufficient to alter the binding energy to a target protein. Our results support the finding that protein adsorption could be a quick and simple way to evaluate particle surfaces and assess small variations in surface ligands, before detailed characterization was performed by more sophisticated techniques. Such assessments are highly important for particles intended for biomedical applications or with biosafety concerns.

3.2 Experiment Section

3.2.1 Synthesis of PAA–Fe_3O_4 NPs

The highly water-soluble superparamagnetic iron oxide (Fe_3O_4) NPs coated with PAA (average Mw: 1.8 kDa) were used in our study. The reagents for synthesis were purchased from Sigma-Aldrich Corporation. A NaOH–diethylene glycol (DEG) stock solution was prepared by dissolving 50 mmol of NaOH in 20 mL of DEG. The synthesis approach used in this study followed the procedure previously reported by the Yin group.15 In brief, a mixture of PAA (4 mmol), $FeCl_3$ (2 mmol), and DEG (15 mL) was

heated up to 220 °C under a nitrogen atmosphere with stirring. Upon a rapid injection of the NaOH–DEG stock solution (4.5 mL), the mixture was further heated for 10 min or 12 h at 220 °C to yield the magnetite nanoparticles. The excess PAA or its possible byproducts and other reagents were removed by centrifugation-assisted washing several times using a mixture of deionized water and ethanol. Finally, the Fe_3O_4 NPs were suspended in 10 mL of water to form the stock solutions.

3.2.2 Capillary electrophoresis

Capillary electrophoresis (CE) separation for K_D measurement was reported in our previous work.26 Briefly, a 50 cm fused-silica capillary (75 mm id, 365 mm od; Polymicro Technologies, AZ, USA) with an effective length of 40 cm was sequentially rinsed at 30 psi with 0.1 M NaOH (2 min), deionized water (1 min), and the separation buffer (6 min) prior to injection. All CE separations were done at 25 kV at room temperature. Capillary zone electrophoresis (CZE) was performed using a 10 mM borate buffer at pH 8.3 as the separation buffer, in which the samples were pre-incubated in a 17.5 mM phosphate buffer (pH: 7.5). In affinity capillary electrophoresis (ACE) experiments, no pre-incubation of protein and NPs was needed, and the separation buffer was 17.5 mM sodium phosphate (pH: 7.5).

3.2.3 Characterization of NPs

A Philips Tecnai 12 transmission electron microscope was used to investigate the morphology of NPs. Inductively coupled plasma atomic emission spectroscopy (ICP-

AES) tests were performed on a Perkin-Elmer Optima 2000 DV optical emission spectrometer to measure the concentration of the Fe element in NPs. With the average diameter of the spherical iron oxide NPs measured under transmission electron microscopy (TEM) and the element content obtained by ICP-AES, molar concentration of the NP stock solution was obtained. Dynamic light scattering (DLS) was performed on a Beckman Coulter Delsa Nano C particle analyser at 25 °C. Zeta potential was calculated from the mobility of NPs during CZE.[27]

3.2.4 Characterization of PAA structures

The structure of PAA was analyzed using mass spectroscopy (MS) and NMR spectroscopy. The PAA underwent the same hydrolysis procedure as that in synthesis of NPs but without the addition of $FeCl_3$. Once dissolved in DEG, the PAA solution was heated to 220 °C under N_2 followed by injection of NaOH–DEG. The PAA structures obtained at different hydrolysis durations, such as 10 min, 1 h, 2 h, and 12 h, were tested by sampling 1 mL of the reaction mixture at the corresponding time point.

MS measurement was done by a Thermo-Fisher Electrospray Ionization LTQ Mass Spectrometer (ESI-LTQ-MS) in the negative ionization mode. Ten mL of the resulting PAA solution was mixed with 190 mL water and 200 mL HPLC grade acetonitrile. The ESI conditions used were as follows: spray voltage = 1.5 kV, capillary temperature = 200 °C, capillary voltage = 38 V, tube lens voltage = 100 V.

A combination of one- and two-dimensional (2D) ^{1}H and ^{13}C nuclear magnetic resonance (NMR) spectroscopy was performed on the Varian Inova 500 NMR instrument (Varian Inc., Palo Alto, CA). The 2D NMR included correlation spectroscopy (COSY) and heteronuclear single-quantum correlation spectroscopy (HSQC). The COSY experiment correlates bond coupling interactions between protons. The diagonal peaks correspond to the peaks in a 1D-NMR experiment, while the off diagonal cross peaks indicate coupling between pairs of nuclei. The ^{1}H–^{13}C HSQC provides correlation between a proton and the carbon it is directly bonded to.

3.2.5 Computational details for calculating PAA–protein interaction energy

The 3-dimensional (3D) experimental structure of CaM was extracted from the Protein Data Bank with PDB code 1CFD.[28] We created the 3D structures of the dimeric acrylic acid fragment with two head groups, head group A (HGA) (γ-lactone) and HGB (–$C(OH)(CH_3)_2$), using the VegaZZ program.[29] The Vconf program[30] was used to carry out conformational search to obtain the lowest energy state as the starting molecules for the following docking. Ligand–protein docking was performed by the Autodock[31] program with the Lamarckian genetic algorithm, which fixed the protein and allowed the polymer fragment to move around in the docking box. Autodock tools 1.5.4[32] was used to assign Gasteiger[33] charges to the PAAs. The Autodock scoring function is a subset of the AMBER force field that treats molecules using the United Atom model. We focused docking simulations on six potential binding sites: spots near Gln8, Asp24, Thr79, Glu84, Glu114 and the center of the CaM. For each binding site,

Autogrid version 4.0 was used to create affinity grids with 0.375 Å spacing. The cubic grid box with a dimension of 2.25 nm was assigned centering six different locations on CaM for each docking simulation. The final docking result was obtained by 10 runs of simulation with one million rounds of energy evaluation in each run. Each round of energy evaluation was for one possible orientation of the head group structure at the docking site. Ligand conformations with negative computed binding free energies were further analyzed.

3.3 Results and Discussion

3.3.1 IONPs synthesized at different heating durations carried PAA capped with different head groups

To test whether protein adsorption is sensitive enough to reveal small variations in the NP surface ligands, we prepared two batches of the superparamagnetic Fe_3O_4 NPs coated with PAA (average Mw: 1.8 kDa). We picked this type of NPs because they have been widely used in biomedical research and practice for examining molecule or cell isolation, cancer treatment, drug delivery, and MRI.[34–38] Additionally, polyelectrolytes have gained great popularity as surface ligands on NPs owing to their exceptional capability of stabilizing a NP suspension, assisting NP assembly, enhancing drug loading capacity, and controlling protein resistance or attraction.[39–42] In particular, PAA allows easy protein immobilization and promotes high particle stability in aqueous solutions.[43–46] The highly simple NP preparation strategy we used involves solution-phase hydrolysis at a

high temperature, of 220 °C, in DEG.[15] The particles prepared by this method are Fe_3O_4 as confirmed by X-ray absorption spectroscopy in the previous report from the Yin group.[15] Hydrolysis at elevated temperature is a common approach in preparation of nanomaterials, and hydrolysis duration is often tuned to improve the formation and crystallinity of NPs. Because PAA can undergo thermal degradation at temperature >160 °C[47,48], we postulated that if we prepared the NPs at two very distinct hydrolysis durations, the PAA structure might be altered, resulting in NPs having the same chemical compositions and close physical properties, but carrying surface ligands with small variations.

Indeed, NPs prepared by 10 min and 12 h hydrolysis shared good similarity in particle shape (spherical), diameters measured by TEM (Figure 3.1) and DLS, as well as zeta potential (inserted table in Figure 3.1c). To be more specific, the difference in the particle diameter obtained from the TEM images was only 5%. Although 12 h hydrolyzed NPs had relatively large (17%) hydrodynamic diameters, the surface charge densities were similar, which was reflected by the 5% difference in zeta potentials. The particles were highly stable in water, with no precipitation even after several months' storage. Additionally, when analyzed by capillary electrophoresis (Figure S3.1), both particles gave out sharp and close to symmetrical peak shape. Both facts support the finding that the particles were stably covered by PAA and had quite uniform charge to size ratio.

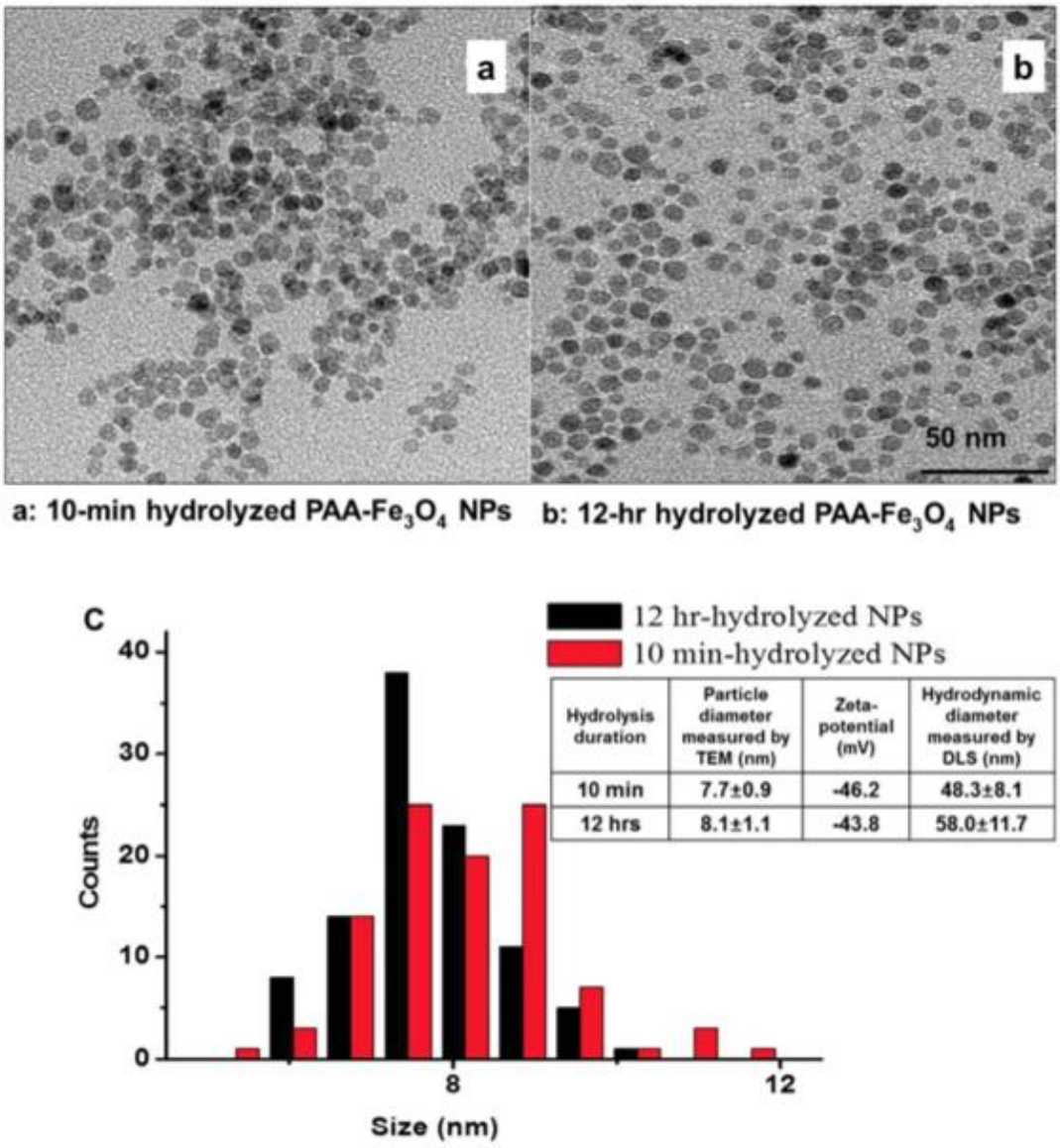

Hydrolysis duration	Particle diameter measured by TEM (nm)	Zeta-potential (mV)	Hydrodynamic diameter measured by DLS (nm)
10 min	7.7±0.9	-46.2	48.3±8.1
12 hrs	8.1±1.1	-43.8	58.0±11.7

Figure 3.1 TEM images of the PAA-Fe_3O_4 NPs prepared by 10 min (a) or 12 h (b) hydrolysis. The two TEM images share the same scale bar. (c) Distribution profiles of the particle diameters measured in the TEM images for 100 particles. The inserted table shows the average particle diameters measured by TEM and DLS; and zeta-potentials calculated from mobility during capillary electrophoresis (Figure S3.1).

To confirm that the PAA structures were different when hydrolyzed for 10 min or 12 h, we measured the purchased PAA before and after hydrolysis by ESI-MS. Before hydrolysis, the PAA contained two types of the –($CH_2CH(COOH)$)– polymer chains (Figure S3.2).[48] One type of the PAA chains was capped with a head-group of –C(OH)(CH3)2 (HGB), and with a molecular weight (Mw) pattern of 72n + 60. This type is called the B series PAA (bPAA) in the following text. The other type of PAA was capped with a γ-lactone (HGA) and had a Mw pattern of 72(n - 1) + 114. We referred this type as the A series (aPAA), which should be produced after the bPAA went through an esterification reaction between the –OH group and the –COOH group of the adjacent acrylic monomer. The peak intensities for both types of PAA chains were comparable before hydrolysis. However, after the PAA was hydrolyzed at 220 °C in NaOH–DEG for 10 minutes, most of the MS peaks observed belonged to the B series (Figure 3.2a); whereas the A series was the dominant species in samples heated for 12 h (Figure 3.2b). The intensities of peaks belonging to the A series gradually increased with longer heating duration compared to that of the B series peaks and reached saturation after 4 h (Figure S3.3).

NMR experiments also verified the structure change in the PAA head group at different hydrolysis durations. The result of one-dimensional 1H NMR spectroscopy is displayed in Figure 3.3, aPAA series. Due to the different environments above and below the plane of the ring, these two methyl groups have different chemical shifts. The peak labeled as "b" corresponds to the two methyl groups in HGB of the bPAA series. These two methyl

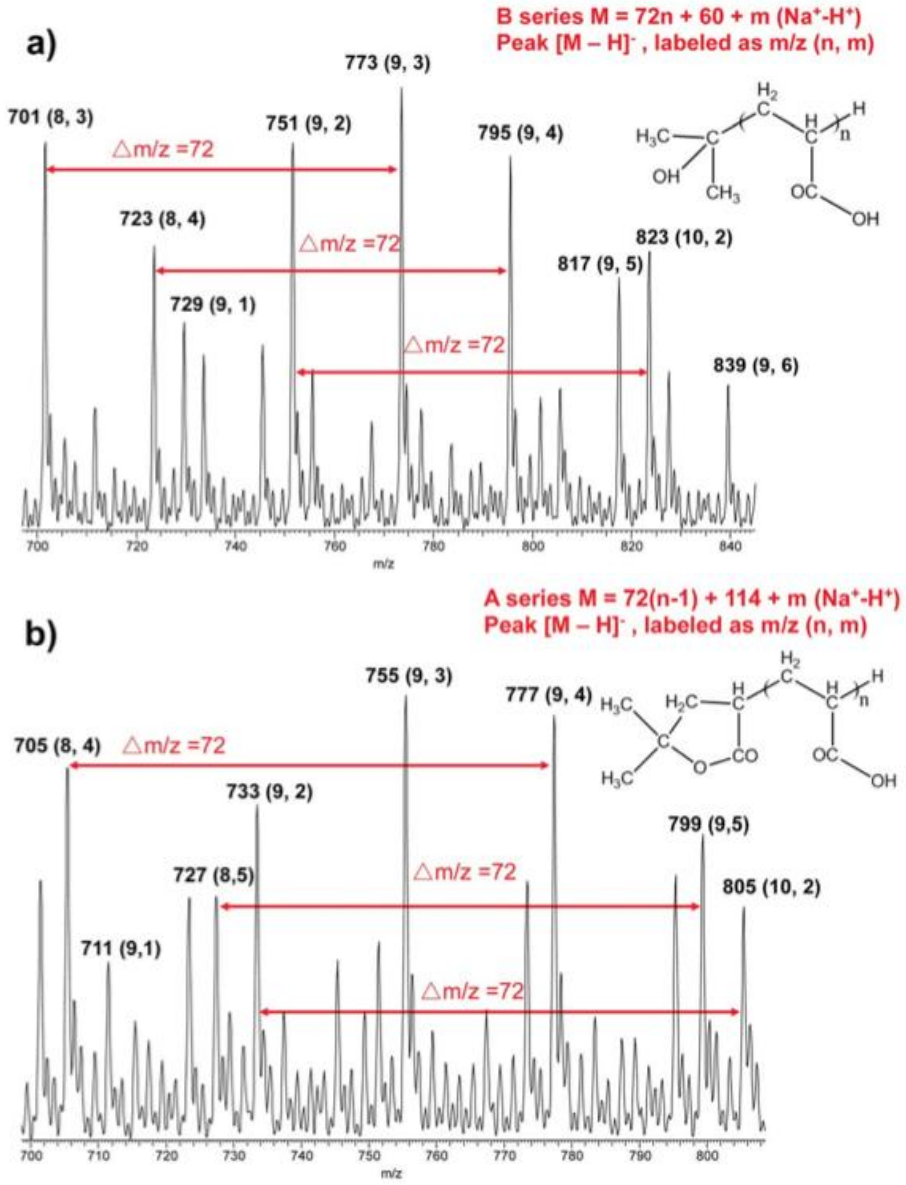

Figure 3.2 Mass spectrum of (a) B series PAA obtained by 10 min thermal treatment and (b) A series PAA by 12 hours' heating treatment in the range of m/z 680–850. The quasimolecular ions of $(M–H)^-$ were formed in the negative ionization mode, with M losing one H^+. Both MS uniformly showed $\Delta m/z = 72$, the exact mass of the acrylic acid monomer; and the peaks were all sodium adducts due to the presence of NaOH: among "n" numbers of monomers on each PAA chain, various numbers (dictated as "m" in Fig. 2) of monomers carried $–COO^-Na^+$ instead of $–COO^-H^+$. The molecular weight difference after H^+ being replaced by Na^+ is +22.

groups are chemically identical and have the same chemical shift. Because PAA is a mixture of polymer chains with different lengths, it would be expected to have line broadening and chemical shift effects associated with the different polymer chain lengths and head-group interactions, which can be seen in the asymmetrical peak shapes of all the methyl resonances, and is more pronounced in peak b. The area ratio of peaks “a” and “b” also showed gradual change with the hydrolysis duration. In the standard PAA, the ratio of peak “a” : “b” was 1.6 : 1. In the 10 min hydrolyzed PAA, peak “b” did not change much, while peak “a” decreased in intensity, which indicates that bPAA was the dominant species when hydrolyzed for 10 min. However, after 2 h of hydrolysis, the situation has reversed, and the ratio of peak “a” to “b” increased to 4.9 : 1, meaning that more aPAA was present. Unfortunately, neither peak “a” nor “b” was found in the 12 h hydrolyzed PAA sample, and probably was masked by the debris from PAA fragmentation over the long heating event (Figure S3.4a). Still, the trend of change in the relative abundance of the aPAA and bPAA series with hydrolysis duration agreed with that observed by MS.

3.3.2 The head-group change in PAA on a NP surface could be detected by protein adsorption

Because the hydrolysis durations of 10 min and 12 h should have yielded the PAA with HGB and HGA, the NPs synthesized by 10 min hydrolysis should be coated with bPAA and those produced by 12 h hydrolysis should be coated with aPAA. The aPAA seemed to yield a hydrodynamic size of the NPs 17% larger than the bPAA, although the core

sizes of the NPs measured by TEM differed by only 5%. To determine whether protein adsorption is sensitive enough to detect such a small difference in the surface PAA structure, despite the highly comparable physical and chemical properties of these NPs, we evaluated the adsorption of a series of proteins on these NPs. We selected human serum albumin (HSA), β-casein, calmodulin (CaM), myoglobin, and cytochrome c (Cyt c) because they possess relatively strong affinity to a large variety of flat surfaces or NPs,[49–52] have varied Mw and isoelectric point (pI) values, and differ in structure rigidity. Three of them are acidic proteins, all with pI < 5: CaM, β-casein, and HSA, with Mw increasing from CaM to HSA (Table 3.1). CaM, myoglobin, and Cyt c have comparable Mw, but carry negative, zero, and positive charges, respectively, at pH 7. CaM (no Ca^{2+} bound) and β-casein are considered highly flexible proteins, while HSA, myoglobin and Cyt c are globular proteins with relatively rigid structures.

We measured affinity by a method developed by our group. The molar fraction of the protein-bound NPs, θ, was obtained with capillary electrophoresis (CE), and the data were fitted to the Hill equation[53]:

$$\theta = [\text{protein}]^n/(K_D{}^n + [\text{protein}]^n),$$

where K_D is the microscopic dissociation constant of the NP–protein complex and n is the binding cooperativeness. "n" < 1 represents strong repulsion between proteins, which prevents adsorption of more than one protein on the same NP, and "n" > 1 but <2 often corresponds to a 1 : 1 binding ratio.[53,54] The K_D and n values for interactions of the

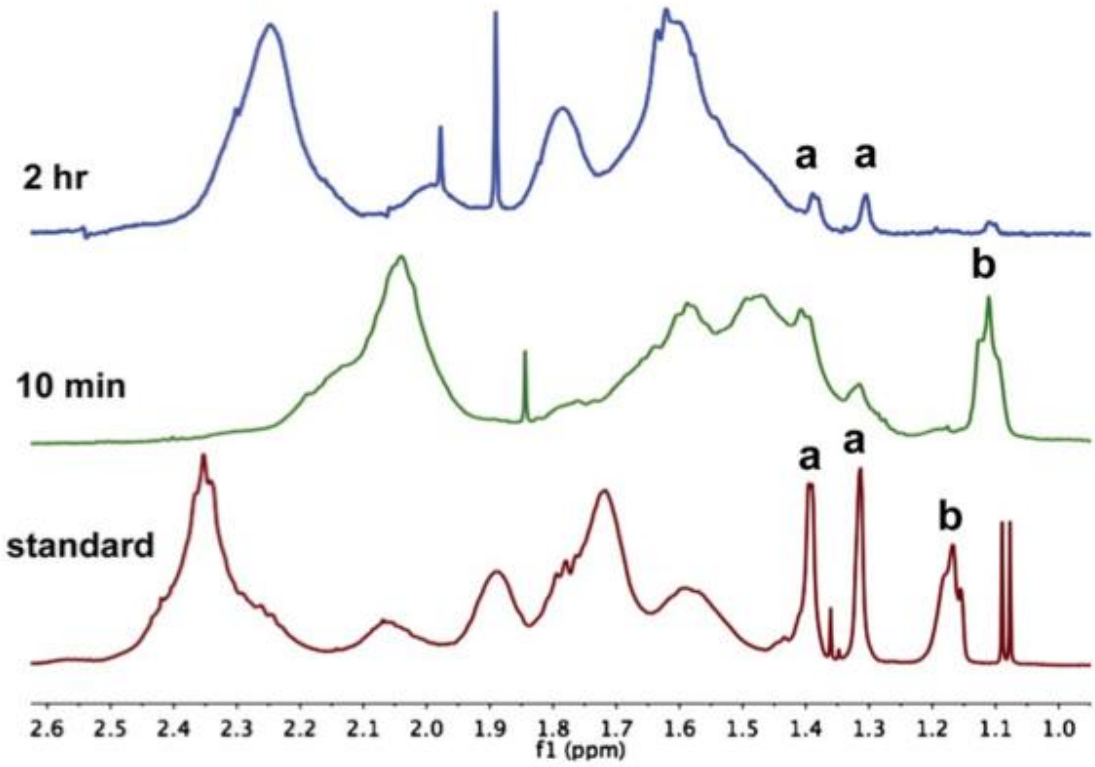

Figure 3.3 ^{1}H NMR spectra for standard PAA and PAA heated for 10 min and 2 h.

selected proteins and the two batches of NPs are shown in Table 1 (CE spectra and the affinity fitting curve shown in Figure S3.5).

We detected significant affinity differences, ranging from 2- to 20-fold, between the NPs produced at varied hydrolysis durations in all proteins. The NPs obtained from 10 min hydrolysis interacted more strongly with HSA, β-casein, and myoglobin, with K_D differing by 3.6-, 20-, and 2.2-fold, respectively, whereas the NPs prepared by 12 h hydrolysis had stronger interaction with CaM (the Ca^{2+} free form) and Cyt c, with 20- and 6-fold difference in K_D values. The n values for the two highly flexible proteins, β-casein and CaM, were quite different as well. β-casein bound to the NPs was heated for 10 min with an *n* of 2.7 but to the other type with an *n* of 1.3. A high *n* suggests high cooperativity during binding and high possibility of having two β-casein molecules on the NPs with 10 min hydrolysis. In contrast, we found an n of 0.4 for CaM binding to the NPs heated for 10 min. Such a small n indicates high repulsion between the protein molecules bound to the same NP and thus low possibility of having more than one protein on the same particle. In agreement with the findings of protein adsorption onto PAA-coated flat surfaces[55], the binding affinity seemed to be irrelevant to the net charge of the protein: the positively charged Cyt c did not show higher affinity to the negatively charged PAA-coated NPs than the acidic proteins. Instead, the highly flexible proteins, CaM and b-casein, had the smallest K_D values. Easier adaptation to the NP surface curvature may have generated more interaction points to strengthen the binding.

Table 3.1 Affinity measurement of the PAA-Fe_3O_4 NPs towards selected proteins

Proteins	Hydrolysis duration of NPs	K_D (μM)	n	Dissociation kinetics
HSA: 66 kDa, pI: 4.8	10 min	1.4 ± 0.11	1.0	Fast
	12 h	5.1 ± 0.18	1.1	Slow
β-casein: 24 kDa, pI: 4.6	10 min	0.23 ± 0.0085	2.7	Fast
	12 h	4.6 ± 0.093	1.3	Slow
Calmodulin: 17 kDa, pI: 3.9	10 min	0.28 ± 0.024	0.4	Fast
	12 h	0.015 ± 0.00063	2.1	Fast
Myoglobin: 17 kDa, pI: 6.8	10 min	1.8 ± 0.11	1.3	Fast/medium
	12 h	4.0 ± 0.27	1.4	Slow
Cytochrome C: 12 kDa, pI: 10.7	10 min	18 ± 4.8	1.9	Fast/medium
	12 h	2.9 ± 0.091	1.1	Slow

3.3.3 Calculation of the interaction energy between CaM and PAA head groups

To better understand the high sensitivity of protein adsorption over a tiny structural change on the surface of NPs, we calculated the interaction energy between the protein and the PAA head groups. Moreover, we illustrated atomistic details of the binding modes of a PAA head group and protein to provide insights into how the binding was established. We chose CaM for this calculation because it showed the largest K_D difference in the two sets of NPs and its experimental 3D structure was available.[28] Our studies showed that the computed trends of binding affinities between different PAA head groups were insensitive to use of a dimer or a trimer of an acrylic acid. From the cavity size of the ligand binding site, we linked the head group to a dimer of the acrylic acid to mimic the freely movable PAA head on the NP surface to save computation time

in our calculation. In addition to exploring intermolecular interactions, we examined the orientation of the complex structures with the lowest binding free energy and evaluated the difference between the polymer fragments with HGA and HGB.

Our docking results showed that both HGA and HGB could successfully fit into the binding cavity within the docking boxes, and the HGA–CaM complex generally had more negative binding free energy than the HGB–CaM complex (Table 3.2). This trend agrees well with our experimental observation that the NPs coated by aPAA bound to CaM stronger than that coated by bPAA. The measured affinity difference between these two complexes corresponded to a DG difference of 1.8 kcal/mol (difference in $\Delta G = -RT \ln(K_{AaPAA}) - (-RT \ln(K_{AbPAA})) = RT \ln(K_{DaPAA})/(K_{DbPAA}) \approx 1.8$ kcal/mol; K_A is the association constant, equal to $1/K_D$), which fell within the calculated energy difference of 0.57–2.75 kcal/mol.

The binding of HGA and HGB to the cavity between the N- and C-terminal domains is shown in Figure 3.4a as a representative of the simulated complex structure. HGA and HGB face the protein and interact with residue Thr5, Glu7, Glu114 and Lys115 (Figure 3.4b and c). The orientation of the head groups agrees with the established concept that the carboxylate groups on the PAA side chains strongly coordinate to the iron cations on the NP surface to form a robust coating, whereas the head groups extend into the aqueous solution and play an important role in NP interaction with proteins. Among the overall free energy change, the non-polar van der Waals (vdw) energy between HGA and CaM

(−6.34 kcal/mol) is more favorable than that of HGB and CaM (−3.59 kcal/mol) (Table S3.1). The binding mode of HGA illustrates that the bulky head group can fit nicely into

Table 3.2 Calculated binding energy values of HGA and HGB to the binding cavity defined by the docking box with the listed amino acid as the center

Center of docking box	Interaction energy (kcal mol^{-1})		Energy difference (kcal mol^{-1})
	Head group A	Head group B	
Default center	−3.79	−1.52	−2.75
Thr79	−5.05	−3.33	−1.72
Gln8	−3.39	−1.77	−1.62
Glu114	−3.04	−1.87	−1.17
Glu84	−2.83	−1.81	−1.02
Asp24	−4.09	−3.52	−0.57

the binding cavity, as compared with that formed by HGB, which also agrees with the energy calculations. The electrostatic energy described here is a broader category, which includes conventional electrostatic interactions, hydrogen bonding and salt bridge. HGB shows favorable electrostatic energy (−0.02 kcal/mol) when binding with CaM as compared with HGA (+0.76 kcal/mol) (Table S3.1) because of the hydrogen bonding formed among the Glu114, Lys115 and the hydroxyl group of HGB (Figure S4.4c). However, this hydrogen bonding still cannot result in strong attraction for HGB. Taken together, the overall binding free energy between HGA (−3.79 kcal/mol) and CaM was

more negative than with HGB (−1.52 kcal/mol), with the vdw attractions contributing more to determine the interactions.

The calculations did not account for potential ligand-induced protein conformation changes.[7,9,56,57] However, the insignificant spatial difference in the two head groups is unlikely to result in considerably different complex conformations in the PAA bound state. The scoring function in Autodock approximated the solvent effect and desolvation, and entropic penalty. Because both aPAA and bPAA have the same acrylic acid backbone, which contributes mainly to solvent effect and PAA flexibility, the backbone may not contribute to the affinity differences.[45,46] Additionally, these two types of NPs had comparable size and surface curvature, and CaM has a highly flexible structure without Ca^{2+} binding. Both features suggest comparable CaM conformational changes on binding to these two types of NPs.

The same computer simulation was also performed with the other proteins having an available 3D structure, including HSA (only to drug-binding site 2 because of the large size of HSA; site 2 was identified as the binding site of PAA-NP on HSA13), myoglobin and Cyt c (Table S3.2). Like CaM, Cyt c simulation results agreed with the protein-particle affinity trend: HGA showed stronger binding energy than HGB to Cyt c. However, for HSA and myoglobin, HGA showed more binding free energy than did HGB, which was opposite to the K_D value trend.

Nevertheless, the simulation results suggest that both good fitting into the protein binding cavity by the NP surface ligand and large overall interaction energy established between the protein amino acid side chains and the ligand are required for stable protein

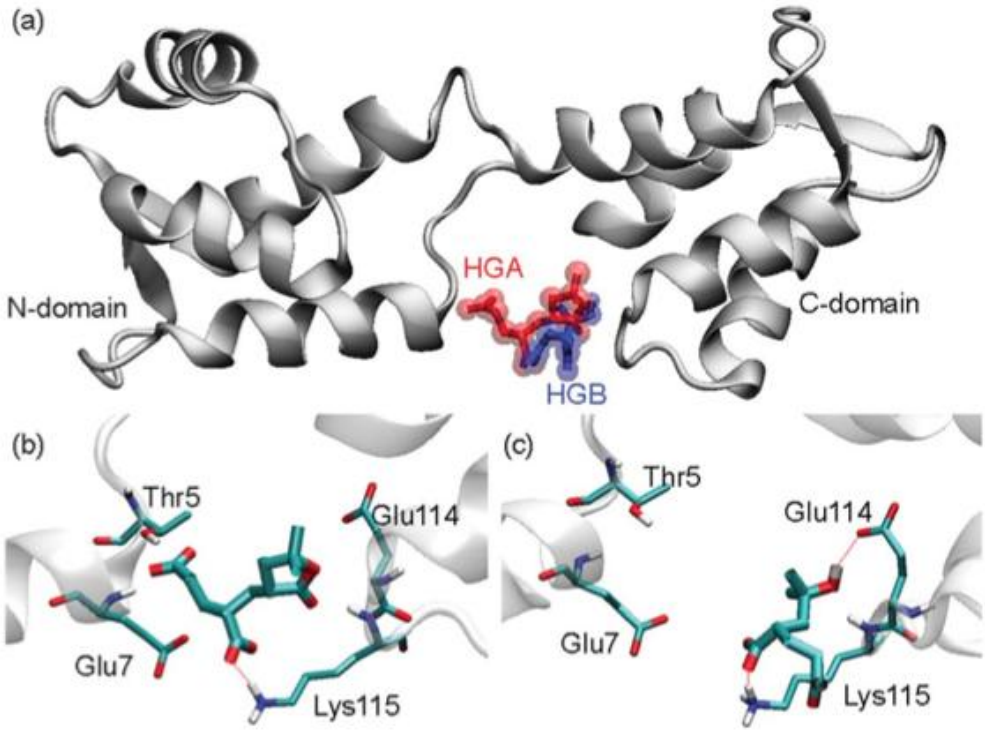

Figure 3.4 (a) Overview of docking the head groups (HGA in red and HGB in blue) to the default center of CaM that is located between the N- and C-domains, in which the head group faces CaM and the dimeric acrylic acid part of the structure is pointed away from CaM. The zoom-in view of detailed interactions of amino acid side chains with (b) HGA and (c) HGB. The red dotted lines represent the H-bonds.

adsorption on NPs. These two requirements determine that protein adsorption would be strongly affected by subtle structural changes on the ligand, especially when the change happens to the portion of the ligand molecule that directly faces the protein.

3.3.4 Protein adsorption for assessment of NP surface properties after ligand exchange

In the above study, variation in the structure of the surface ligand was introduced owing to small changes in the condition of particle synthesis. We also prepared two batches of NPs that were particularly coated with ligands having small structural difference and tested if that could be detected by protein adsorption. The Au NPs originally carried the Ni–nitrolotriacetic acid (NTA) chelate on the surface; and the ligands were two types of polyhistidine (6 His)-peptides, one carrying a free –COOH group (P2) at the C-terminus and the other having the C-terminus blocked by $–CONH_2$ (P1). The 6 His peptides were conjugated to the Au NPs via their high affinity with Ni– NTA. This is a common approach to couple His-tagged biomolecules on NPs for biomedical applications. During preparation, P1 and P2 were incubated with the Ni–NTA–Au NPs at the ratios of 0:100 or 5:95. After removal of the free P1 and P2 by the 10 kDa Amicon filter, the obtained Au NPs, named Au-100P2 and Au-95P2, respectively, showed the same color in solution, which indicated no change in particle diameter; and the same mobility in CE, meaning comparable zeta-potential (Figure S4.6a). Despite the high similarity in their physicochemical properties, they bound to β-casein quite differently. More protein–NP

complexes were formed with the Au–95P2 particles than with the Au–100P2 ones when incubated with the same concentration of β-casein (Figure S4.6b). The measured affinity was about 5-fold higher for the Au-95P2, even though only 5% of the surface ligands were different between these two batches of particles. Increase in the neutral P1 percentage may reduce electrostatic repulsion between the $–COO^-$ end of 6 His peptide and acidic β-casein, leading to stronger protein–NP interactions.

3.4 Conclusions

The PAA ligand has an average molecular weight of 1.8 kDa; thus the head group structure is only a small portion of the entire molecule. The hydrodynamic diameter of the NPs carrying PAA with HGA was 17% larger than that with HGB, although the core sizes of NPs differed by only 5%. More importantly, they induced big variations in the NPs' affinity to proteins. The high sensitivity of protein adsorption to the head group structure is mainly because, as pointed out by computer simulation, the head group of PAA is located at the binding interface with the protein. In order for stable binding to be formed, part of the NP surface ligand should fit well onto certain binding pockets on the protein surface. Even slight structural change in this part could alter the fitting and change the binding energy, ultimately varying the affinity to the protein.

Overall, our results support the fact that screening interactions between NPs and judiciously selected proteins could be an effective way to quick and initial evaluation of

the particle surface of NPs. Such screening will be useful for rapid assessment of the surface properties of NPs produced in different batches or with varied preparation procedures, which is particularly important for quality control of NPs made for biomedical purposes. It is even possible that, by analyzing the interaction change with proteins of distinct properties, such as pI value, shape, hydrodynamic size, and surface hydrophobicity, more information about the kind of changes occurring in the NP surface ligand could be revealed.

3.5 References

[1] D. W. Grainger and D. G. Castner, *Adv. Mater.*, **2008**, *20*, 867.

[2] K. Riehemann, S. W. Schneider, T. A. Luger, B. Godin, M. Ferrari and H. Fuchs, *Angew. Chem., Int. Ed.*, **2009,** *48*, 872.

[3] W. R. Sanhai, J. H. Sakamoto, R. Canady and M. Ferrari, *Nat. Nanotechnol.*, **2008**, *3*, 242.

[4] S. H. De Paoli Lacerda, J.-J. Park, C. Meuse, D. Pristinski, M. L. Becker, A. Karim and J. F. Douglas, *ACS Nano*, **2010**, *4*, 365.

[5] K. Lind, M. Kresse and R. H. Muller, *Electrophoresis*, **2001**, *22*, 3514.

[6] M. Lundqvist, J. Stigler, G. Elia, I. Lynch, T. Cedervall and K. A. Dawson, *Proc. Natl. Acad. Sci. USA*, **2008**, *105*, 14265.

[7] D. F. Moyano and V. M. Rotello, *Langmuir*, **2011**, *27*, 10376.

[8] H. Bayraktar, C.-C. You, V. M. Rotello and M. J. Knapp, *J. Am. Chem. Soc.*, **2007**, *129*, 2732.

[9] C.-C. You, R. R. Arvizo and V. M. Rotello, *Chem. Commun.*, **2006**, 2905.

[10] M. De, C.-C. You, S. Srivastava and V. M. Rotello, *J. Am. Chem. Soc.*, **2007**, *129*, 10747.

[11] L. Calzolai, F. Franchini, D. Gilliland and F. Rossi, *Nano Lett.*, **2010**, *10*, 3101.

[12] S. Ghosh, S. Jana and N. Guchhait, *J. Phys. Chem. B*, **2012**, *116*, 1155.

[13] N. Li, S. Zeng, L. He and W. Zhong, *Anal. Chem.*, **2011**, *83*, 6929.

[14] M. F. Casula, Y.-w. Jun, D. J. Zaziski, E. M. Chan, A. Corrias and A. P. Alivisatos, *J. Am. Chem.Soc.*, **2006**, *128*, 1675.

[15] J. Ge, Y. Hu, M. Biasini, C. Dong, J. Guo, W. P. Beyermann and Y. Yin, *Chem.–A Eur. J.*, **2007**, *13*, 7153.

[16] C. N. R. Rao, V. V. Agrawal, K. Biswas, U. K. Gautam, M. Ghosh, A. Govindaraj, G. U. Kulkarni, K. P. Kalyanikutty, K. Sardar and S. R. C. Vivekchand, *Pure Applied Chem.*, **2006**, *78*, 1619.

[17] S. Si, C. Li, X. Wang, D. Yu, Q. Peng and Y. Li, *Cryst. Growth Des.*, **2005**, *5*, 391.

[18] Z.-G. Yan and C.-H. J. Yan, *Mat. Chem.*, **2008**, *18*, 5046.

[19] J. N. Waddell, D. G. Mullen, B. G. Orr, M. M. Banaszak Holl and L. M. Sander, *Phys. Rev. E*, **2010**, *82*, 108.

[20] C. Morasso, P. Verderio, M. Colombo and D. Prosperi, *ACS Sym. Ser.*, **2011**, *69*, 1091.

[21] J. D. Padmos and P. Zhang, *J. Phys. Chem. C*, **2012**, *116*, 23094.

[22] L. Polito, M. Colombo, D. Monti, S. Melato, E. Caneva and D. Prosperi, *J. Am. Chem. Soc.*, **2008**, *130*, 12712.

[23] H. Zhou, F. Du, X. Li, B. Zhang, W. Li and B. Yan, *J. Phys. Chem. C*, **2008**, *112*, 19360.

[24] H. Zhou, X. Li, A. Lemoff, B. Zhang and B. Yan, *Analyst*, **2010**, *135*, 1210.

[25] J. Chen, S. Chen, X. Zhao, L. V. Kuznetsova, S. S. Wong and I. Ojima, *J. Am. Chem. Soc.*, **2008**, *130*, 16778.

[26] N. Li, S. Zeng, H. Le and W. Zhong, *Anal. Chem.*, **2010**, *82*, 7460.

[27] U. Schnabel, C.-H. Fischer and E. Kenndler, *J. Microcolumn Sep*., **1997**, *9*, 529.

[28] H. Kuboniwa, N. Tjandra, S. Grzesiek, H. Ren, C. B. Klee and A. Bax, *Nat. Struct. Biol.*, **1995**, *2*, 768.

[29] A. Pedretti, L. Villa and G. J. Vistoli, *Computer-Aided Mol. Design*, **2004**, *18*, 167.

[30] C.-E. Chang and M. K. J. Gilson, *Computational Chem*., **2003**, *24*, 1987.

[31] G. M. J. Morris, *Comput.Chem*., **1998**, *19*, 1639.

[32] G. M. Morris, R. Huey, W. Lindstrom, M. F. Sanner, R. K. Belew, D. S. Goodsell and A. J. Olson, *J. Computational Chem.*, **2009**, *30*, 2785.

[33] J. Gasteiger and M. Marsili, *Tetrahedron*, **1980**, *36*, 3219.

[34] H. Ai, Adv. *Drug Delivery Rev*., **2011**, *63*, 772.

[35] M. Yang, J. Chen, F. Su, B. Yu, F. Su, L. Lin, Y. Liu, J.-D. Huang and E. Song, *Mol. Cancer*, **2011**, *10*, 117.

[36] F. M. Kievit and M. Zhang, *Acc. Chem. Res.*, **2011**, *44*, 853.

[37] F. Liu, S. Laurent, H. Fattahi, L. Vander Elst and R. N. Muller, *Nanomedicine*, **2011**, *6*, 519.

[38] C. Tassa, S. Y. Shaw and R. Weissleder, *Acc. Chem. Res*., **2011**, *44*, 842.

[39] M. Rabe, D. Verdes and S. Seeger, *Adv. Colloid Interface Sci*., **2011**, *162*, 87.

[40] K. G. Neoh and E. T. Kang, *Polymer Chem.*, **2011**, *2*, 747.

[41] T. Chen, M. Yang, X. Wang, L. H. Tan and H. Chen, *J. Am. Chem. Soc.*, **2008**, *130*, 11858.

[42] L. H. Tan, S. Xing, T. Chen, G. Chen, X. Huang, H. Zhang and H. Chen, *ACS Nano*, **2009**, *3*, 3469.

[43] J. Dai, Z. Bao, L. Sun, S. U. Hong, G. L. Baker and M. L. Bruening, *Langmuir*, **2006**, *22*, 4274.

[44] O. Hollmann and C. Czeslik, *Langmuir*, **2006**, *22*, 3300.

[45] A. Wittemann and M. Ballauff, *Phys. Chem. Chem. Phys*., **2006**, *8*, 5269.

[46] A. Wittemann, B. Haupt and M. Ballauff, *Phys. Chem. Chem. Phys*., **2003**, *5*, 1671.

[47] F. X. Roux, R. Audebert and C. Quivoron, *Eur. Polym. J*., **1973**, *9*, 815.

[48] R. P. Lattimer, *J. Anal. Appl. Pyrolysis*, **2003**, *3*, 68.

[49] V. Hlady and J. Buijs, *Curr. Opin. Biotechnol.*, **1996**, *7*, 72.

[50] B. Milthorpe, Protein Adsorption to Surfaces and Interfaces, in Surface and Interfaces for Biomaterials, ed. P. Vadgama, Woodhead Publishing Ltd., **2005**, pp. 763–781.

[51] D. R. Schmidt, H. Waldeck and W. J. Kao in Biological Interactions on Materials Surfaces, ed. Puleo, D. A. and Bizios, R., Springer Science + Business Media, LLC, **2009**, p. 1.

[52] P. M. Claesson, E. Blomberg, J. C. Froberg, T. Nylander and T. Arnebrant, *Adv. Colloid Interface Sci*., **1995**, *57*, 161.

[53] J. N. Weiss, FASEB J., **1997**, *11*, 835.

[54] H. Abeliovich, *Biophys. J.*, **2005**, *89*, 76.

[55] C. Czeslik, R. Jansen, M. Ballauff, A. Wittemann, C. A. Royer, E. Gratton and T. Hazlett, *Phys. Rev. E*, **2004**, *69*, 021401.

[56] R. U. Lemieux, *Acc. Chem. Res*., **1996**, *29*, 373.

[57] C.-C. You, S. S. Agasti and V. M. Rotello, *Chem.–A Eur. J*., **2008**, *14*, 143.

3.6 Supporting Information

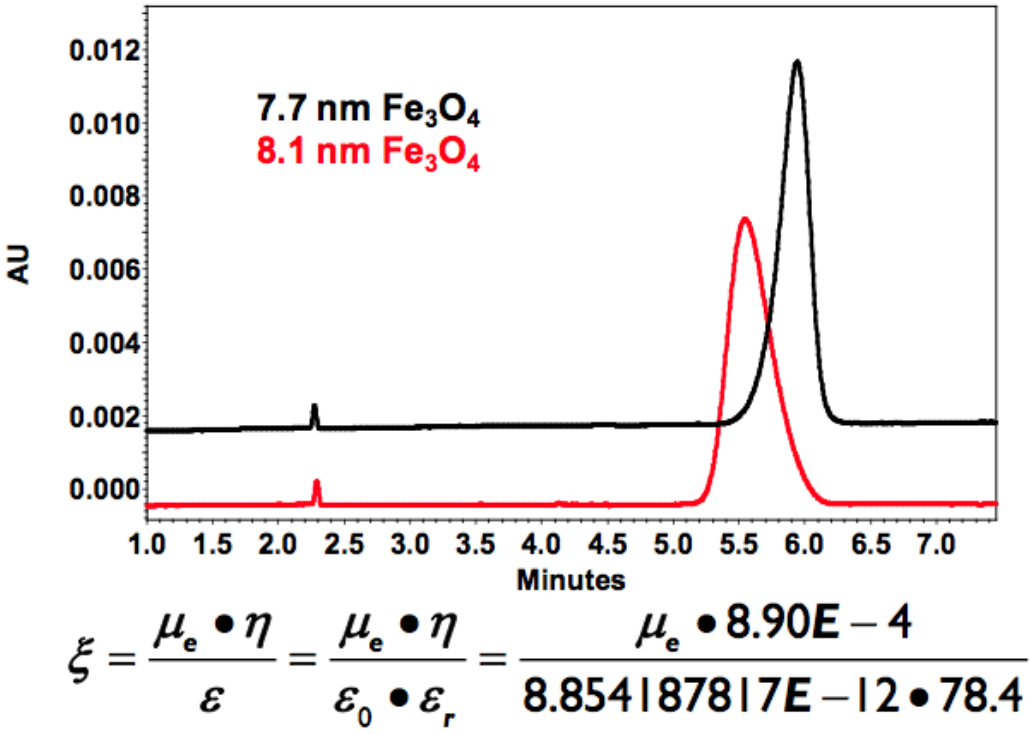

$$\xi = \frac{\mu_e \bullet \eta}{\varepsilon} = \frac{\mu_e \bullet \eta}{\varepsilon_0 \bullet \varepsilon_r} = \frac{\mu_e \bullet 8.90E-4}{8.854187817E-12 \bullet 78.4}$$

Figure S3.1 The electropherograms of PAA-Fe_3O_4 nanoparticles for zeta-potential measurement and calculation.

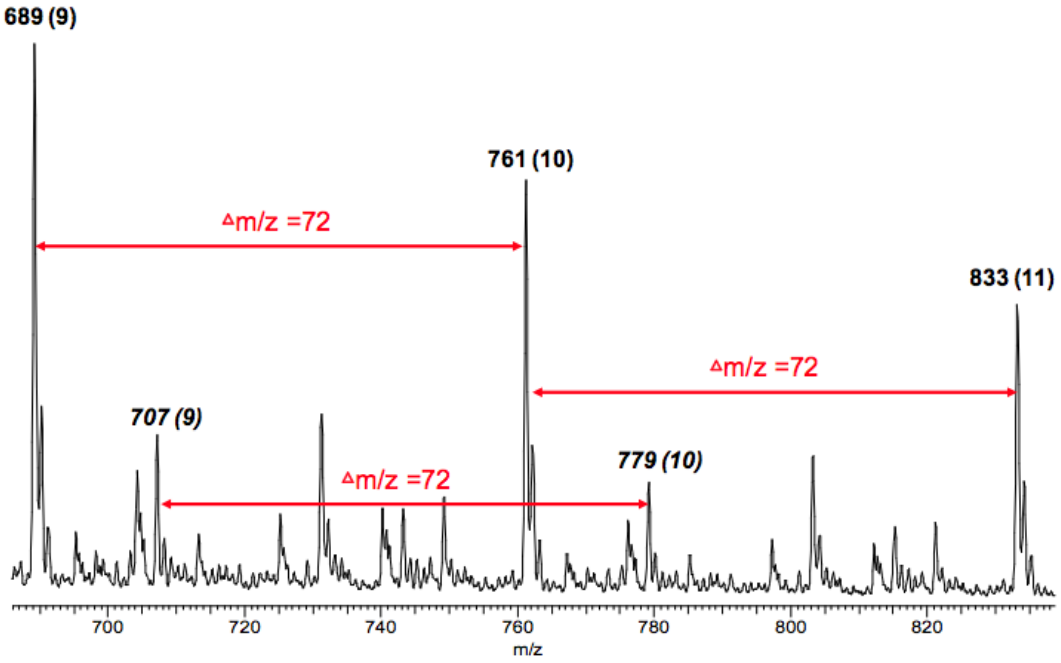

Figure S3.2 The mass spectrum of standard PAA obtained by ESI-LTQ-MS. The A series PAA is shown in regular front, while the B series PAA is in italic. The m/z range 680-850 is selectively shown to display details.

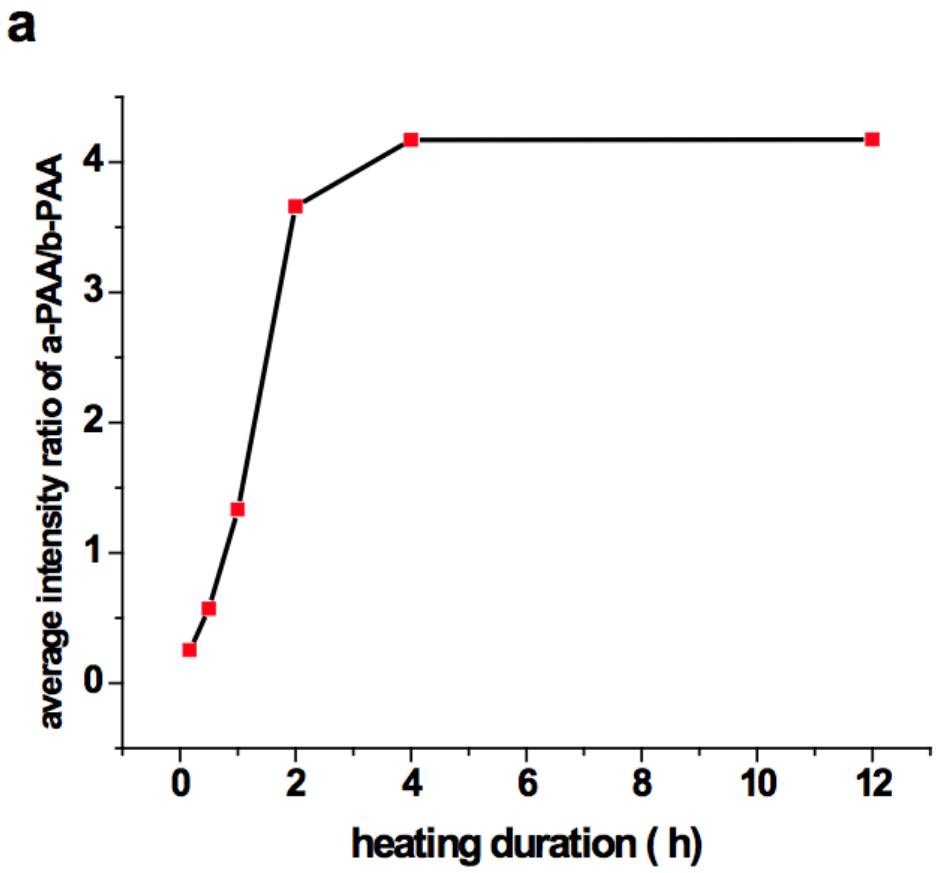

Figure S3.3 a) The intensity ratio of PAA series (a/b) measured on an Agilent 6210 multi-mode liquid chromatography-time of flight-mass spectrometer (LC-TOF-MS). Sample ionization was performed under the conditions of ESI and atmospheric-pressure chemical ionization. The ratio changes with heating duration;

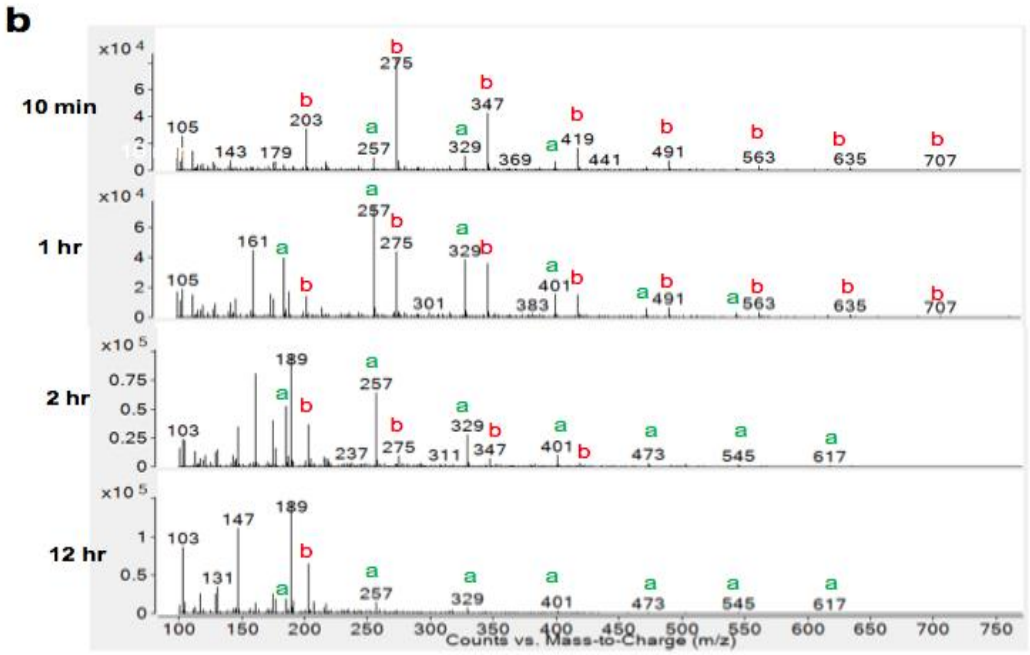

Figure S3.3 b) the mass spectra for hydrolyzed PAA obtained by ESI-TOF- MS. Four time points are selectively shown to demonstrate the trend.

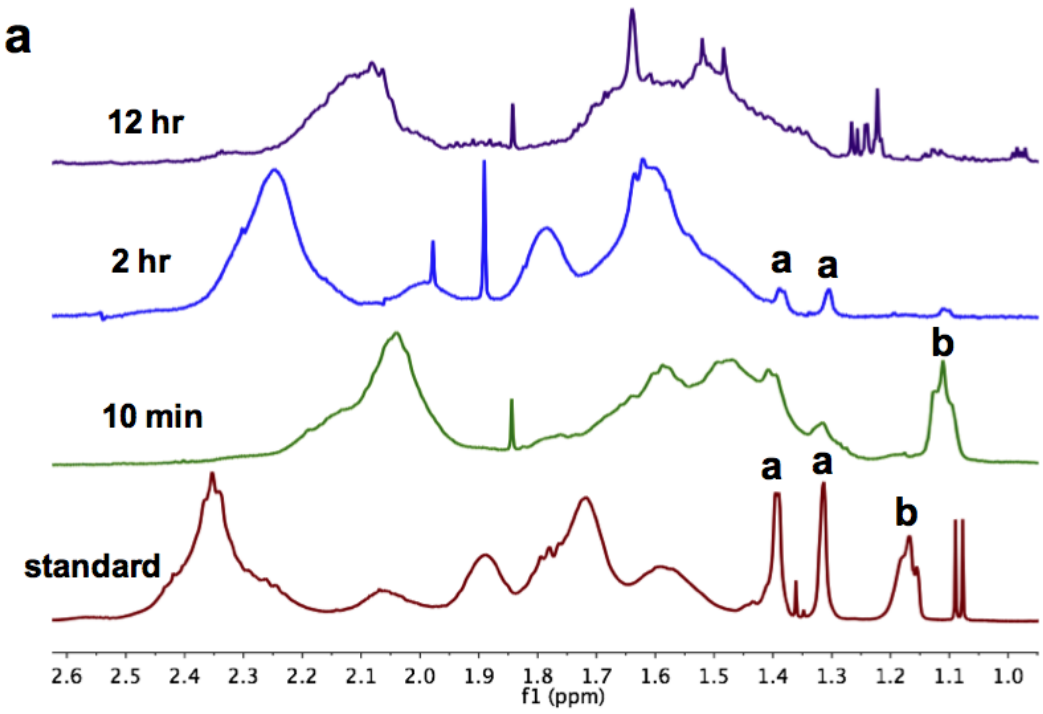

Figure S3.4. a) ^{1}H NMR spectra for standard and hydrolyzed PAA.

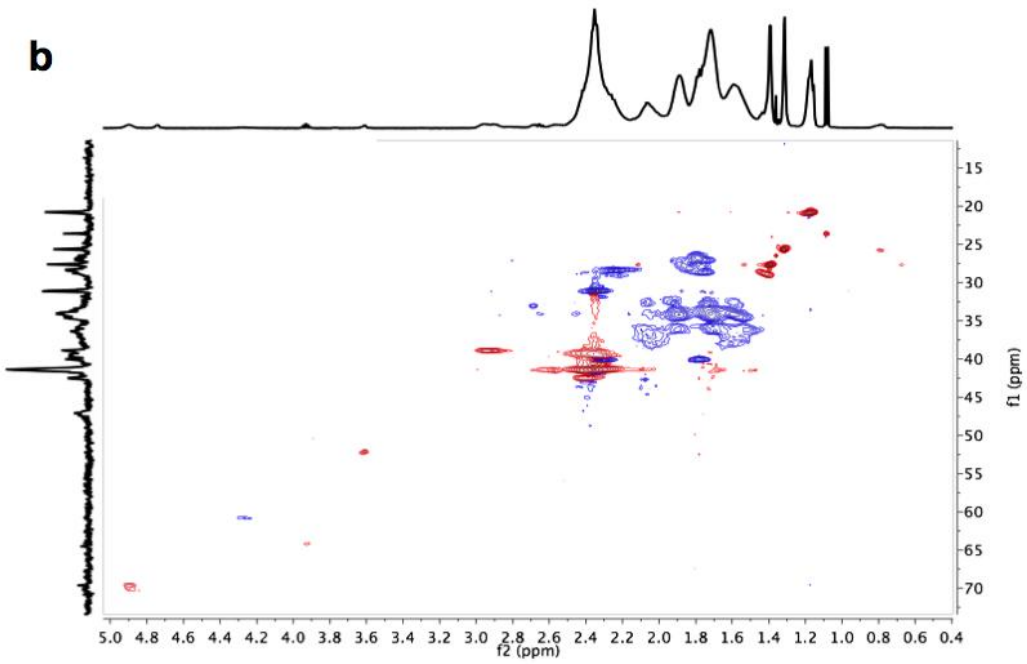

Figure S3.4. b) HSQC NMR spectra for standard PAA.

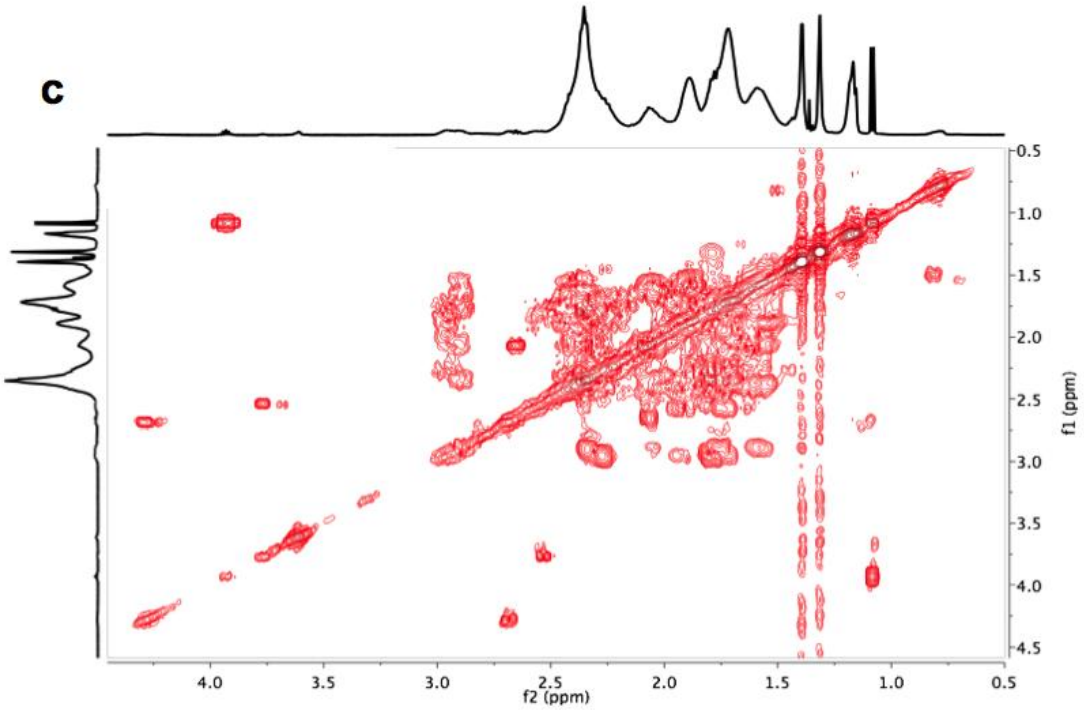

Figure S3.4. c) COSY NMR spectra for standard PAA.

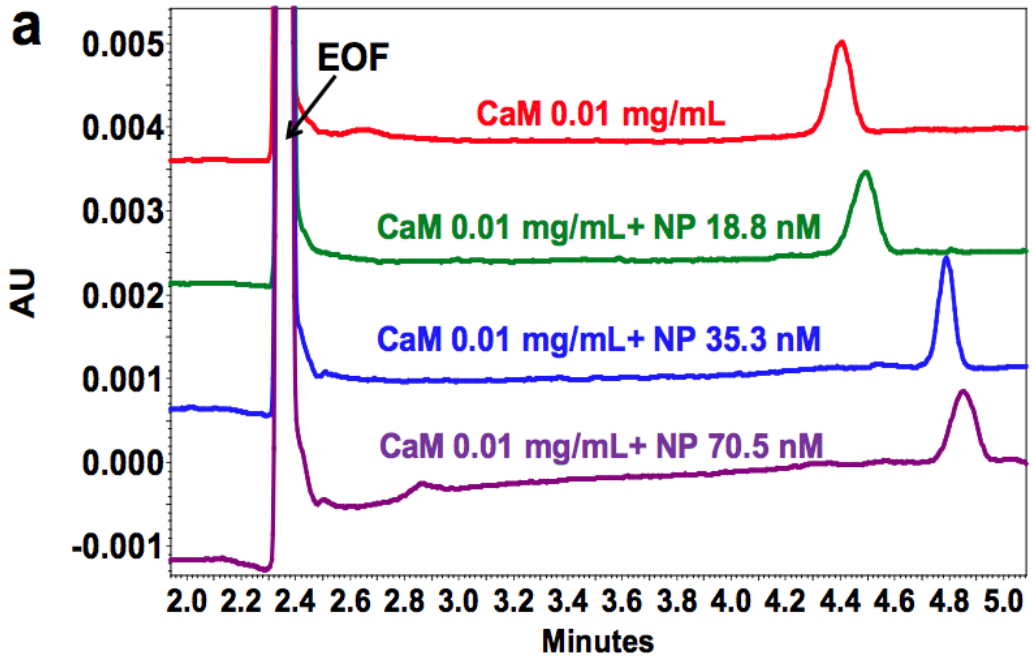

Figure S3.5 a) The eletropherograms for the interaction between calmodulin (CaM) and 7.7 nm PAA-Fe_3O_4 NPs measured by affinity capillary electrophoresis in 17.5 mM phosphate buffer.

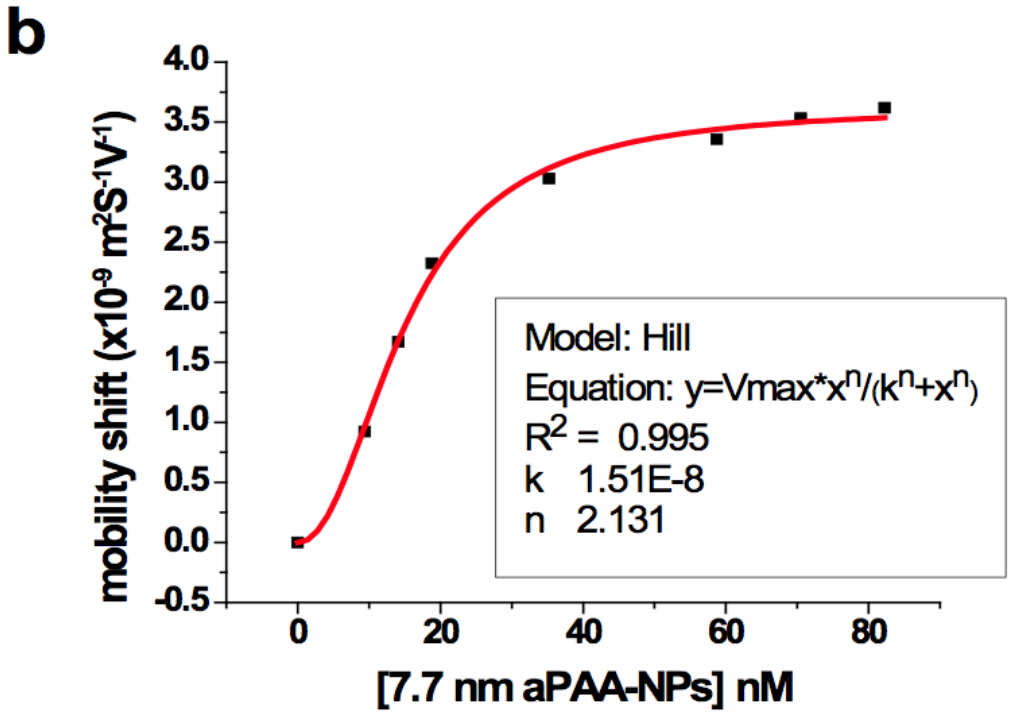

Figure S3.5 b) the affinity curve fitted by Hill equation for the interaction between calmodulin (CaM) and 7.7 nm PAA-Fe_3O_4 NPs measured by affinity capillary electrophoresis in 17.5 mM phosphate buffer.

Table S3.1 Calculated energy of HGA and HGB to the default binding cavity of calmodulin.

polymer fragment	binding free energy (kcal/mol)	vdw energy (kcal/mol)	electrostatic energy (kcal/mol)
Head group A	-3.79	-6.34	+0.76
Head group B	-1.52	-3.59	-0.02

Chapter 4

Exploration of Possible Binding Sites of Nanoparticles on Protein by Cross-Linking Chemistry Coupled with Mass Spectrometry

4.1 Introduction

Finding out the possible binding sites of nanoparticles (NPs) on proteins can benefit both the study of nanotoxicity and the preparation of functional bionanomaterials, helping to promote safer and more effective implementation of nanotechnology. The layer of adsorbed proteins on the surface of nanomaterials entering the biosystems is believed to serve as the biosignature of nanomaterials and impact their uptake[1], distribution, and excretion.[2−4] The adsorption may also alter protein conformation and function,[5,6] causing adverse health effects. By exploring where the NPs would bind on proteins, we can predict the biological consequence of protein adsorption and thus the potential toxicity. On the other hand, nanobio hybrid materials are prepared by attaching proteins to nanomaterials for energy production[7], sensing[8], separation[9], biomedical imaging[10], drug delivery[11], etc. The locations of nanomaterials on proteins could be strategically controlled to prevent any interference to protein function, to allow efficient energy[12] or electron transfer[13] between the proteins and the supporting materials, or to permit natural molecule recognition.[14,15] Tactical coupling of nanomaterials to

proteins calls for more knowledge about the dependence of binding epitope on nanomaterial properties.

Few attempts have explored the binding interface of nanoparticles and proteins at the amino acid level, employing hydrogen/deuterium (H/D) exchange-mass spectrometry (MS)[16] and nuclear magnetic resonance (NMR).[17] These methods are technically demanding and require delicate treatment of proteins.[18,19] Alternatively, chemical cross-linking in combination with MS has been used to reveal the topology of protein complexes.[20−23] The reaction is rapid, and a large variety of cross-linking reagents have been developed to target a wide range of functional groups. This method could be a facile solution to identification of the binding interface of the NP-protein complex. The judgment is based on two considerations: (1) the involvement of NPs could simplify peptide identification by providing a solid support for easy isolation and cleanup of the cross-linked peptides before MS analysis; (2) most of the functional bionanomaterials are pre- pared by covalent attachment to gain long-term stability.[24] Hence, this proof-of-principle study was devoted to test the hypothesis of whether the cross-linking chemistry was suitable for exploration of the possible binding sites of the poly(acrylic acid) (PAA)-coated Fe_3O_4 NPs on human serum albumin (HSA). Three peptides were consistently identified to be close to the surface of NPs during protein adsorption, and they belong to the drug binding site 2 of HSA. Competition for this binding site between ibuprofen and NPs was observed to confirm the identification. These results demonstrated that cross-linking chemistry coupled with MS could be a quick approach to reveal peptides near the NPs when protein adsorption occurs, which will be beneficial to the study of interaction

between nanoparticles and proteins for gaining more understanding on nanotoxicity and imposing better guidance to the design of biofunctional nanostructures.

4.2 Experiment Section

4.2.1 Synthesis and Characterization of PAA- Fe_3O_4 NPs

The reagents for NP synthesis were obtained from Sigma-Aldrich Corporation (St. Louis, MO, USA). A NaOH/diethylene glycol (DEG) stock solution was prepared by dissolving 50 mmol of NaOH in 20 mL of DEG. In a typical synthesis, a mixture of PAA (4 mmol, Mw = 1.8 kDa), $FeCl_3$ (2 mmol), and DEG (15 mL) was heated up to 220 °C in a nitrogen atmosphere with stirring. A NaOH/DEG stock solution (4.5 mL) was then injected rapidly into the above hot mixture. The NPs with an average diameter around 8 nm were obtained by continuously heating the mixture for 12 h at 220 °C. An excess amount of PAA and other reagents in the reaction mixture were removed by centrifugation-assisted washing several times with a mixture of deionized water and ethanol. Finally, the PAA-Fe_3O_4 NPs were suspended in 10 mL of water to form the stock solution.

Characterization of the obtained NPs was carried out, and the results were displayed in Figure S4.1 in the Supporting Information. A Philips Tecnai 12 transmission electron microscope (TEM) was used to investigate the morphology of NPs. Inductively coupled plasma atomic emission spectroscopy (ICP-AES) tests were performed on a Perkin-Elmer

Optima 2000 DV optical emission spectrometer to measure the concentration of Fe element in NPs. With the size measured under TEM and the element content obtained from ICP-AES, the molar concentration of the NP stock solutions was obtained. Hydrodynamic size was measured with a ZetaPALS system (Brookhaven, Holtsville, NY) at 25 °C, which was equipped with a 660 nm laser and a build-in precision Peltier temperature controller.

4.2.2 Incubation, Cross-Linking, and Protein Digestion

Trypsin from porcine pancreas (Type IX-S, lyophilized powder, 13 000_ 20 000 BAEE units/mg) and albumin from human serum (lyophilized powder, ≥97%) were attained from Sigma-Aldrich Corporation (St. Louis, MO, USA). The 1-(3-dimethylaminopropyl)-3-ethyl- carbodiimide hydrochloride (EDC) (≥98%) was purchased from Fisher Scientific (Fairlawn, NJ). HSA (7.5 μg) was incubated with the PAA-Fe_3O_4 NPs (1.37 10_10 mol; the molar ratio of protein to NPs was about 1: 1) in the deionized water (Milli-Q water purification system, Billerica, MA) overnight with a total volume of 20 μL. Eighty microliters of 2-(N-morpholino)-ethanesulfonic acid (MES) buffer (50 mM, pH 6.2) and the freshly prepared EDC solution (1 μL 100 mg/mL) were added into the above mixture to allow cross-linking for 4 h at room temperature. We particularly skipped the denaturing step during the tryptic digestion, aiming to remove only the peptides far away from the NP surface but keep those belonging to the binding site on the NPs. Excess EDC and salts were removed with an Amicon 30 kDa filter (Millipore, Billerica, MA) by spinning it at 14 krcf for 10 min. The sample mixture was recovered by spinning the filter

reversely in another clean centrifuge tube at 1 krcf for 2 min. Afterward, 0.15 μg of trypsin was incubated with the recovered NP-HSA mixture in NH4HCO3 buffer (50 mM, pH 8.0) with a final reaction volume of 100 μL at 37 °C overnight. Another centrifugation (16.1 krcf 30 min) in a 1.5 mL centrifuge tube helped to precipitate and remove the NPs. The supernatant containing the free peptides was collected, dried in a Savant SpeedVac concentrator (Bridgepath Scientific, MD), and redissolved in 0.1% trifluoroacetic acid (TFA). After removing the NH_4HCO_3 with a C18 ziptip (Millipore), the peptides were re- covered into 50% acetonitrile (ACN, HPLC grade, 99.9%, Fisher Scientific) containing 0.05% TFA and ready for matrix-assisted laser desorption/ionization-time-of-flight-mass spectrometry (MALDI-TOF-MS) or MALDI-quadrupole (Q)-TOF MS/MS. Supernatant analysis was repeated 10 times.

4.2.3 Peptide Removal from the NPs after Cross-Linking and Trypsin Digestion

After trypsin digestion, the NPs recovered by centrifugation were washed sequentially with 0.09% sodium dodecyl sulfate (SDS) and deionized water to remove all the possibly adsorbed peptides. During the washes, the NPs were retained by the Amicon 30 kDa filter while the filter was spun at 14 krcf for 10 min to allow the adsorbed but not cross-linked peptides to go through. Then, the NPs were treated with 10 μL of a mixture solution containing 40% dimethylamine (DMA, from Sigma-Aldrich), concentrated hydrochloride (12 N, Fisher Scientific), and acetonitrile at a volume ratio of 7:1:24 (final pH of 10) for 4 h at room temperature. Amicon 30 kDa filters were used to remove the NPs from the above mixtures at 14 krcf for 10 min. The solution containing the released peptides was

collected and subject for MS analysis. Peptide removal by DMA after cross-linking was repeated 5 times.

4.2.4 MALDI-TOF-MS and MALDI-Q-TOF-MS/MS

The MALDI- TOF-MS experiment was carried out on a Voyager-DE STR MALDI-TOF mass spectrometer (Applied Biosystems, Framingham, MA, USA) operating in positive reflective mode. The spectrometer is equipped with a pulsed nitrogen laser operated at 337 nm with 3 ns pulses. MS spectra were acquired as an average of 100 laser shots. Mass resolution is greater than 10 000. All the chemicals used for MS analysis are highly pure. The HPLC-grade α-cyano-4-hydroxycinnamic acid (CHCA) from Sigma-Aldrich is >99% pure, and the biochemistry-grade trifluoroacetic acid (TFA) from Acros Organics has a purity of 99.5%. Peptide samples were cleaned up using the C18 ziptips. For sample spotting, in brief, 0.5 μL of the saturated CHCA in 50% ACN and 0.05% TFA and 0.5 μL of the clean peptide solution were sequentially spotted on a MALDI plate. Adequate time was allowed for solvent evaporation. The sequences of the concerned peptides of m/z 961, m/z 1640, and m/z 2045 were verified by the Applied Biosystems Q-STAR XL oMALDI MS/MS (Carlsbad, CA), and the data were analyzed using Mascot.

4.2.5 Drug Inhibition on NP-HSA Interaction

Ibuprofen (>98%) and fusidic acid were from Sigma-Aldrich. The drug was dis- solved in 50% ethanol (HPLC grade, Fisher Scientific) to make a series of stock solutions with concentrations from 4.84×10^{-5} M to 2.42×10^{-3} M. Two microliters of the drug stock

solution at different concentrations were mixed with 160 μg of HSA in a total volume of 18 μL (final HSA concentration was 1.19×10^{-4} M) and incubated at room temperature for 30 min. Then, 9.4×10^{-12} mol NPs were introduced into the HSA-drug mixture. The final mixture contained 5% ethanol with a final volume of 20 μL. After overnight incubation, these samples were analyzed by capillary electrophoresis in the Beckman Coulter P/ACE MDQ system. A 50 cm fused-silica capillary (75 μm id, 365 μm od; Polymicro Technologies, Phoenix, AZ, USA) with an effective length of 40 cm was sequentially rinsed at 30 psi with 0.1 M NaOH (2 min), deionized water (1 min), and the running buffer (6 min) prior to injection. All CE separations were done at 25 kV at room temperature. A borate buffer (10 mM, pH 8.3) was used as the separation buffer. The areas of the complex and the free NPs peaks were calculated by the 32 Karat Version 8.0 accompanied with the Beckman system. Normalization was performed by dividing the complex peak areas measured at the presence of ibuprofen with that obtained without ibuprofen.

4.3 Results and Discussion

HSA is the most abundant protein in human serum with a well-studied crystal structure[25], and it can bind to various types of NPs, including iron oxides.[2] Superparamagnetic Fe_3O_4 NPs have demonstrated great potential for biomedical applications, but their health impacts are not well understood so as the mechanisms of their transportation within circulation systems and delivery to tissues or cells.[11,26,27]

Study the binding of the Fe_3O_4 NPs to HSA and their locations on HSA may shed some lights on these mechanisms, since HSA has been known to be the carrier for a wide range of xenobiotic chemicals crossing the membranous structures.[28] The PAA-coated Fe_3O_4 NPs prepared as reported by Ge et al.[29] possess high water solubility that can be attributed to the strong coordination of carboxylate groups with surface iron cations and the multiple anchor points for every single polymer chain. It has been demonstrated that a large amount of carboxylate groups remained on the surface of nanocrystals after synthesis and extensive washing.[29] The average size of these NPs was 8.02 ± 1.26 nm, with a hydration size in water of 40.0 ± 3.9 nm and a zeta potential of -44.03 ± 0.08 mV (Supporting Information Figure S4.1b). These NPs interact with various proteins in aqueous solutions (Supporting Information Figure S4.1c), including HSA. The dissociation constant (K_D) of the NP- HSA complex in water was $5.1 \times 10^{-6} \pm 1.8 \times 10^{-7}$ M and that in 1 PBS was $6.3 \times 10^{-6} \pm 5.3 \times 10^{-7}$ M, measured by our reported method.[30]

Chemical cross-linking was performed after the stable HSA adsorption on NPs (at a 1:1 protein to NPs ratio) was obtained from overnight incubation. Water was chosen as the incubation environment in the present study to enhance the total amount of the NP-bound HSA and facilitate MS analysis. The carboxyl groups on the PAA coating were coupled to the free amines on HSA by a zero-length, amine-reactive cross-linker, EDC.[31] Then, we digested the protein by trypsin, leaving the cross-linked peptides on particle surface and those far away from the binding site of NPs in supernatant (Figure 4.1). The cross-linked peptides were isolated together with the NPs by centrifugation, cleaned thoroughly

with several rounds of sequential wash to remove the passively adsorbed fragments, and finally cleaved off the particle surface by the base-assisted hydrolysis. Both the cleaved peptides, i.e., interfacial peptides, and those remaining in the supernatant, i.e., peripheral peptides, were analyzed by MALDI-TOF-MS.

The typical MS result on peptides cross-linked to the NPs and then released by hydrolysis was shown in Figure 4.2a. Only one peptide with an m/z value of 1640 was found in this sample. Its sequence was confirmed to be (K) KVPQVSTPTLVEVSR (414-428, sequence numbers adopted from PDB ID: 2VUF) by MALDI-Q-TOF-MS/MS (Supporting Information Figure S4.2). (Note: The sequence numbers for peptides used here were adopted from PDB, because we used the crystal structure downloaded from PDB to map out the location of these peptides. These numbers were 24 residues different than those reported in UniProtKB/Swiss-Prot, protein ID P02768. For example, using UniProtKB sequence number, m/z 1640 should be 438-452.) No peptide was recovered from the NPs if no cross-linking reaction took place (Figure 4.2b), meaning that the nonspecifically adsorbed peptides were completely washed off. Agreeing with theseresults, supernatant analysis revealed that the peak intensity of m/z 1640 dropped significantly in the cross-linking sample (Figure 4.2c) but not in the not-cross-linked sample (Figure 4.2d). A total of 13 peptides were identified under our digestion and analysis conditions (Supporting Information Figure S4.3). Among them, three were

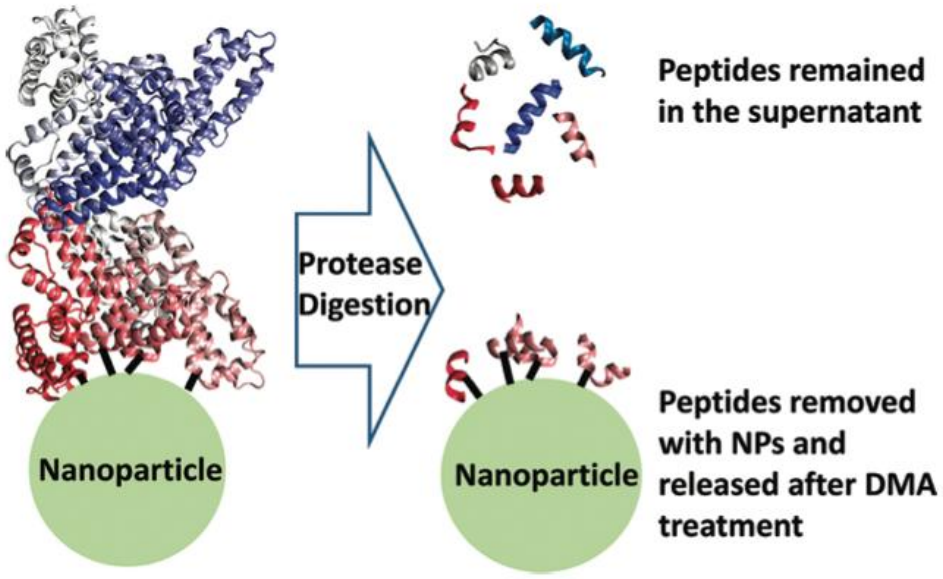

Figure 4.1 Identification of peptides associated with nanoparticle−protein interaction by cross-linking and MS.

consistently found with much reduced peak intensity in the supernatant samples (Figure 4.2c), including m/z 1640. The other two are m/z 961 (K)FQNALLVR (403-410) and m/z 2045 (K)VFDEFKPLVEEPQNLIK (373-389).

Because the circular dichroism (CD) spectra (Supporting Information Figure S4.4) showed negligible change to the secondary structure of HSA after being adsorbed to the NPs, we mapped these three peptides on the crystal structure of HSA (PDB ID: 2VUF). Interestingly, they all belong to the subdomain IIIA of HSA and locate quite close to each other.25 Therefore, they could be near the NP surface during protein adsorption and have all been cross-linked to the NPs. It is unknown at this point why only m/z 1640 was released by hydrolysis. We hypothesized it may be related to its consecutive lysine residues, K413 and K414. K413 was the tryptic digestion site on this fragment, and K414 could be the cross-linking site which was also the N-terminal of this fragment. This location possibly makes the amide bond formed between the lysine side chain K413 and the PAA quite easily be attacked by the amine during hydrolysis. Obviously, more investigation is needed to test this possibility and detailed method development is required to improve the peptide release efficiency. Nevertheless, the persistent identification of particular pep- tides in our cross-linking experiment strongly supports that those peptides, especially peptide KVPQVSTPTLVEVSR (414-428) with an m/z value of 1640, should be part of the binding site of the PAA-coated Fe_3O_4 NPs on HSA, and their approach to the NPs surface was not a random event. We examined the solvent

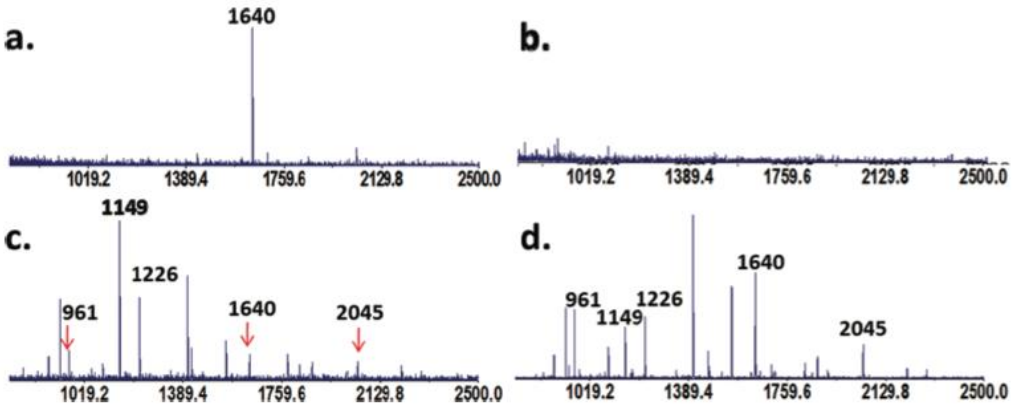

Figure 4.2 MALDI-MS spectra of released peptides when HSA was (a) cross-linked and (b) only adsorbed to the PAA-Fe3O4 NPs. Analysis of supernatant from the cross-linking and noncross-linking samples was shown in (c) and (d), respectively.

accessible surface areas of all lysine residues on HSA using the online tool of Getarea (http://curie.utmb.edu/getarea.html). This software obtains a percentage value to represent the solvent accessibility of individual residue. Residues are considered to be solvent exposed if the Getarea value exceeds 50% and to be buried if it is less than 20%. It turns out that the digestion sites for m/z 961 and m/z 2045, K402 and K372, both have the calculated percentages over 55%, and are considered to be exposed to the solvent but that of K413 and K414 was only 23.9% and 8.0%, respectively. Therefore, K413 and K414 in fact have very limited solvent accessible areas. They could be cross-linked to the NPs solely because they are located near the NP surface during NP-protein interaction but not because they were more exposed than other lysine residues.

The subdomain IIIA is a putative binding site, the so-called drug-binding site 2, for drugs with acidic or electronegative features like ibuprofen and naproxen (Figure 4.3).[28] Ibuprofen binds to the site 2 on HSA with an equilibrium constant around 10^6 M^{-1}.[32,33] The binding can improve the solubility of the drug in serum and help its transportation in the circulation system, affecting the pharmacokinetics of the drug.[28,34] Because of the colocalization of the binding sites of ibuprofen and the PAA-coated Fe_3O_4 NPs on HSA, competitive binding between the NPs and ibuprofen was expected. To verify this possibility, we incubated 1.19×10^{-4} M HSA with ibuprofen at concentrations starting from 4.84×10^{-5} M for 30 min and then added a constant amount of NPs to the HSA-ibuprofen mixture. The HSA concentration was selected so that a large portion of NPs

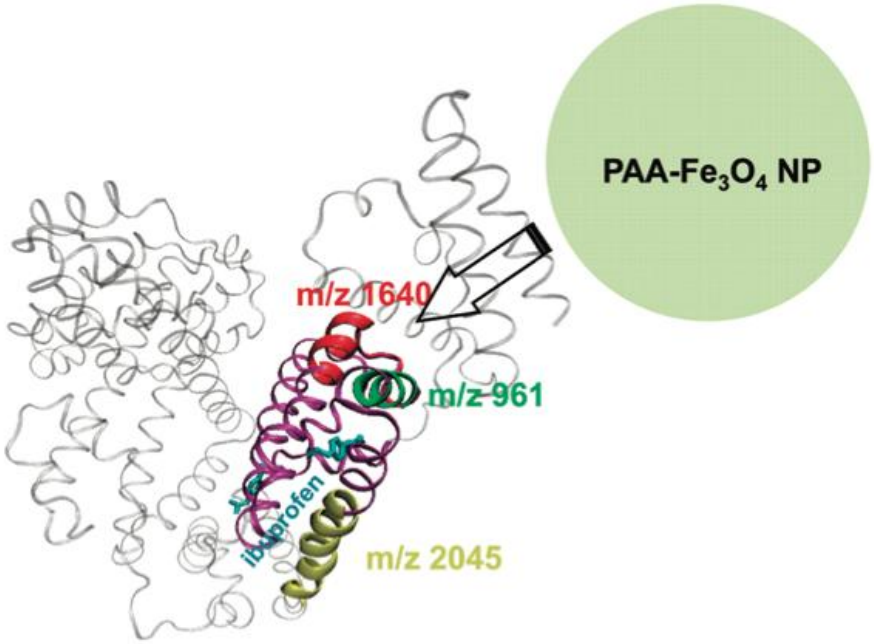

Figure 4.3 Crystal structure of HSA with ibuprofen bound (PDB ID: 2BXG), with the peptides of interest highlighted in red, green, and yellow, respectively.

was bound to HSA with the complex peak well observed under the experimental conditions. The drug concentration range was chosen to gradually saturate the binding site 2 of HSA, until ibuprofen became in large excess. The mixture was analyzed with capillary electrophoresis (CE) after another round of incubation with the NPs present at room temperature overnight. Since the NP-HSA complexes could be well separated from the free HSA and NPs,[30] the fraction of protein-bound NPs, θ, obtained from the peak area ratio of the protein-bound and free NPs, was used to judge the NP-HSA interaction strength: a smaller θ representing weaker binding. The selected electropherograms and the plot of the normalized θ (θ obtained with no drug present was seen as 1 in normalization) vs drug concentration were shown in Figure 4.4. A decrease in θ was observed with increasing ibuprofen concentration, and the reduction reached a maximum of 28% at 3×10^{-4} M ibuprofen. Since binding of ibuprofen induces very little conformational change in HSA[28], inhibition of NP-HSA interaction by ibuprofen could not be due to the exposure of new epitopes on HSA upon drug binding but rather from the occupation of ibuprofen in site 2. We also confirmed that there was no interaction between the drug and the NPs by the same CE method (Supporting Information Figure S4.5a). However, when the drug concentration increased further, θ started to increase back but the complex peak shifted slightly toward the injection peak in CE. At even higher drug concentrations (Supporting Information Figure S4.5b), the free NP peak disappeared, and the complex peak profile changed completely with a much earlier migration time. It is possible that, ibuprofen might bind to HSA at sites other than the drug binding site 2 and increase the hydrophobicity of the protein, which in turn enhances

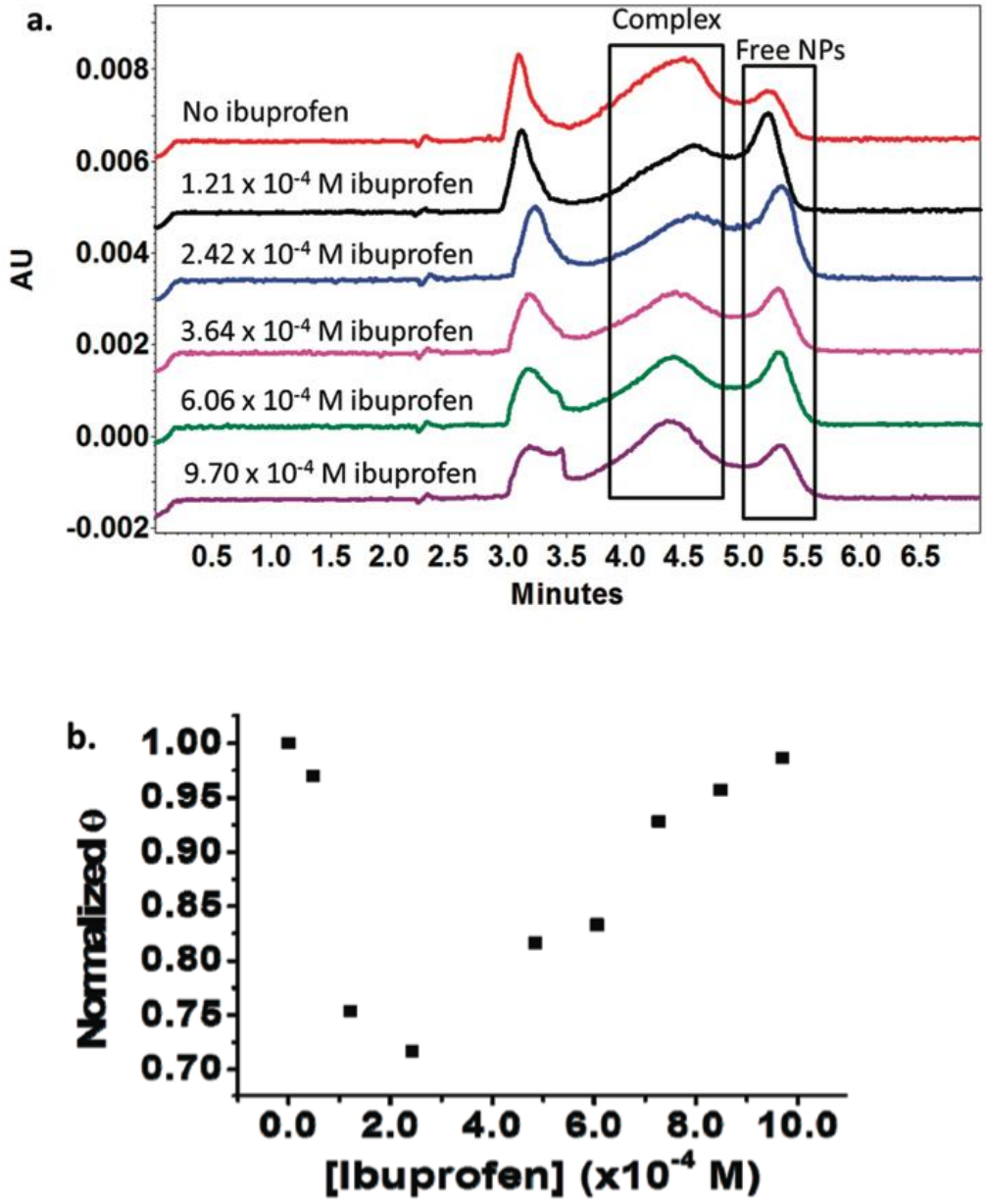

Figure 4.4 (a) Representative electropherograms attained at 288 nm for the study of competitive binding to HSA between ibuprofen and PAA-Fe3O4 NPs. HSA peak appeared at 3.2 min, and the free ibuprofen showed up at around 3.4 min. (b) Normalized θ (the fraction of protein-bound NPs) was plotted against the drug concentration.

the binding between the protein and the NPs and forms a three-party complex with both the drug and the NP binding simultaneously on HSA. Certainly, more exploration is needed to find out thereason for the observed results. On the contrary, a drug, fusidic acid, that binds further away from the subdomain IIIA[35] (PDB ID: 2VUF), exhibited no effect on the NP-HSA interaction (Supporting Information Figure S4.5c, d).

The particular binding of the PAA-coated Fe_3O_4 NPs toward the drug binding site 2 could be determined by the carboxyl groups of the PAA coating. It has been known that the drug binding site 2 has a preformed hydrophobic cavity with distinct polar features and a single main polar patch at the pocket entrance.[28] Distribution of basic and polar residues on the largely hydrophobic interior walls attracts the electronegative drugs, attributed to this binding pocket.[28] For example, ibuprofen has a carboxyl side chain (Supporting Information Figure S4.6). The carboxyl group could be attracted toward site 2, helping the aromatic rings be adapted into the hydrophobic pocket. Similarly, the PAA molecules on the NPs surface carried a large number of carboxyl groups that could be pulled close to the basic residues of R410, Y411, and K414. However, it is unclear at this point if the Fe_3O_4 surface was exposed and contributed to the interaction with HSA.

4.4 Conclusions

Identification of the binding sites of NPs on proteins can help us predict the possible biological consequences after the attachment. The specific binding of the PAA-coated

NPs to the drug binding site 2 on HSA may be closely related to the biodistribution and cell internalization of the NPs, which should be explored further in future studies. The present work demonstrated that cross-linking chemistry coupled with MS was a convenient approach to probe the possible binding sites of NPs on proteins. Still, it is not clear if this was the only binding site, and only one peptide was discovered. Further development is needed to increase coverage of all binding sites and to mimic interaction under physiological conditions. For example, different proteases and cross-linking chemistry can be employed to target functional groups other than lysine. Moreover, complementary peptide identification methods like LC-MS/MS can be used to target smaller peptides, and different release methods can be explored to improve the release efficiency. All of these are currently under investigation in our lab.

4.5 References

[1] Mu, Q.; Li, Z.; Li, X.; Mishra, S. R.; Zhang, B.; Si, Z.; Yang, L.; Jiang, W.; Yan, B. J. *Phys. Chem. C* **2009**, *113*, 5390–5395.

[2] Aggarwal, P.; Hall, J. B.; McLeland, C. B.; Dobrovolskaia, M. A.; McNeil, S. E. *Adv. Drug Delivery Rev.* **2009**, *61*, 428–437.

[3] Lynch, I.; Cedervall, T.; Lundqvist, M.; Cabaleiro-Lago, C.; Linse, S.; Dawson, K. A. Adv. *Colloid Interface Sci.* **2007**, *134–135*, 167–174.

[4] Zhu, Z.-J.; Carboni, R.; Quercio, J. M. J.; Yan, B.; Miranda, O. R.; Anderton, D. L.; Arcaro, K. F.; Rotello, V. M.; Vachet, R. W. *Small* **2010**, *6*, 2261–2265.

[5] Lundqvist, M.; Sethson, I.; Jonsson, B.-H. *Langmuir* **2004**, *20*, 10639–10647.

[6] Shang, W.; Nuffer, J. H.; Muniz-Papandrea, V. A.; Colon, W.; Siegel, R. W.; Dordick, J. S. *Small* **2009**, *5*, 470–476.

[7] Kim, J.; Jia, H. F.; Wang, P. *Biotechnol.Adv*.**2006**, *24*, 296–308.

[8] De, M.; Rana, S.; Akpinar, H.; Miranda, O. R.; Arvizo, R. R.; Bunz, U. H. F.; Rotello, V. M. *Nat. Chem*. **2009**, 1 (461–465), S461/ 461–S461/426.

[9] Long, M. S.; Keating, C. D. *Anal. Chem*. **2006**, *78*, 379–386.

[10] Corot, C.; Robert, P.; Idee, J.-M.; Port, M. *Adv. Drug Delivery Rev*. **2006**, *58*, 1471–1504.

[11] Neuberger, T.; Schoepf, B.; Hofmann, H.; Hofmann, M.; Von, R. B. *J. Magn. Magn. Mater*. **2005**, *293*, 483–496.

[12] Oh, E.; Lee, D.; Kim, Y.-P.; Cha, S. Y.; Oh, D.-B.; Kang, H. A.; Kim, J.; Kim, H.-S. *Angew. Chem., Int. Ed.* **2006**, *45*, 7959–7963.

[13] Delfino, I.; Cannistraro, S. *Biophys.Chem*. **2009**, *139*, 1–7.

[14] De, M.; You, C.-C.; Srivastava, S.; Rotello, V. M. *J. Am. Chem. Soc*. **2007**, *129*, 10747–10753.

[15] Cliffel, D. E.; Turner, B. N.; Huffman, B. J. *Wiley Interdisciplinary Rev.: Nanomed. Nanobiotechnol*. **2009**, *1*, 47–59.

[16] Bayraktar, H.; You, C.-C.; Rotello, V. M.; Knapp, M. J. *J. Am. Chem. Soc*. **2007**, *129*, 2732–2733.

[17] Calzolai, L.; Franchini, F.; Gilliland, D.; Rossi, F. *Nano Lett*. **2010**, *10*, 3101–3105.

[18] Atzrodt, J.; Derdau,V.; Fey, T.; Zimmermann, J. *Angew.Chem., Int. Ed*. **2007**, *46*, 7744–7765.

[19] Tsutsui, Y.; Wintrode, P. L. *Curr. Med Chem.* **2007**, *14*, 2344–2358.

[20] Bennett, K. L.; Matthiesen, T.; Roepstorff, P. *MethodsMol.Biol*. **2000**, *146*, 113–131.

[21] Chakravarti, B.; Lewis, S. J.; Chakravarti, D. N.; Raval, A. *Curr. Proteomics* **2006**, *3*, 1–21.

[22] Leitner, A.; Walzthoeni, T.; Kahraman, A.; Herzog, F.; Rinner, O.; Beck, M.; Aebersold, R. *Mol. Cell. Proteomics* **2010**, *9*, 1634–1649.

[23] Miernyk, J. A.; Thelen, J. J. *Plant J.* **2008**, *53*, 597–609.

[24] Rana, S.; Yeh, Y.-C.; Rotello, V. M. *Curr. Opin. Chem. Biol.* **2010**, *14*, 828–834.

[25] Sugio, S.; Kashima, A.; Mochizuki, S.; Noda, M.; Kobayashi, K. *Protein Eng.* **1999**, *12*, 439–446.

[26] Singha, N.; Jenkinsa, G. J. S.; Asadib, R.; Doaka, S. H. *NanoRev*. **2010**, 1, DOI: 10.3402/nano.v3401i3400.5358.

[27] Liu, S. J.; Han, Y. C.; Qiao, R. R.; Zeng, J. F.; Jia, Q. J.; Wang, Y. L.; Gao, M. Y. J. *Phys.Chem. C* **2010**, *114*, 21270–21276.

[28] Ghuman, J.; Zunszain, P. A.; Petitpas, I.; Bhattacharya, A. A.; Otagiri, M.; Curry, S. *J. Mol. Biol.* **2005**, *353*, 38–52.

[29] Ge, J.; Hu, Y.; Biasini, M.; Dong, C.; Guo, J.; Beyermann, W. P.; Yin, Y. *Chem.—Eur. J*. **2007**, *13*, 7153–7161.

[30] Li, N.; Zeng, S.; He, L.; Zhong, W. *Anal. Chem*. **2010**, *82*, 7460–7466.

[31] Hermanson, G. T. BioconjugationTechniques; 2nded.; Academic Press: New York, **2008**.

[32] Jin, L.; Choi, D. Y.; Liu, H.; Row, K. H. Bull. *Korean Chem. Soc.* **2005**, *26*, 136–138.

[33] Yamasaki, K.; Rahman, M. H.; Tsutsumi, Y.; Maruyama, T.; Ahmed, S.; Kragh-Hansen, U.; Otagiri, M. AAPS PharmSciTech **2000**, 1, DOI: 10.1007/BF02830527.

[34] Ascenzi, P.; Fasano, *M. Biophys. Chem*. **2010**, *148*, 16–22.

[35] Zunszain, P. A.; Ghuman, J.; McDonagh, A. F.; Curry, S. *J. Mol. Biol.* **2008**, *381*, 394–406.

4.6 Supporting Information

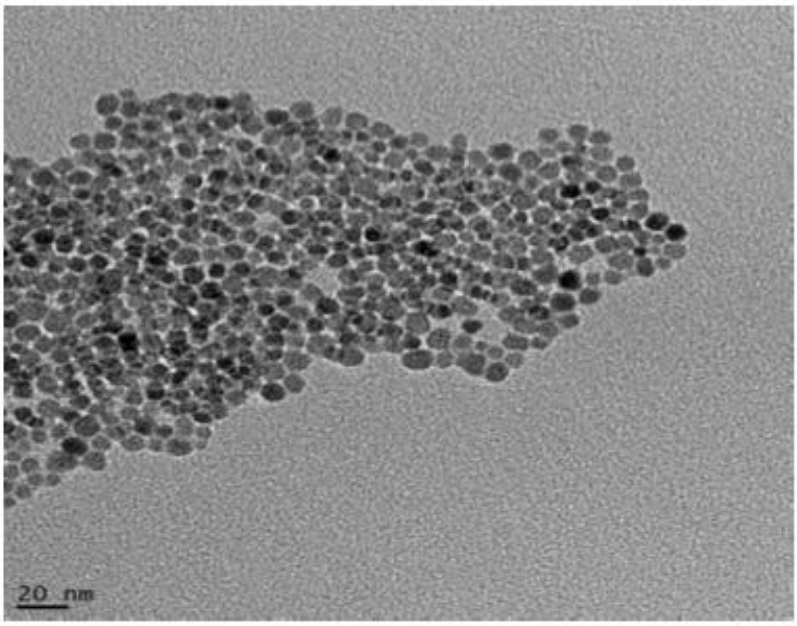

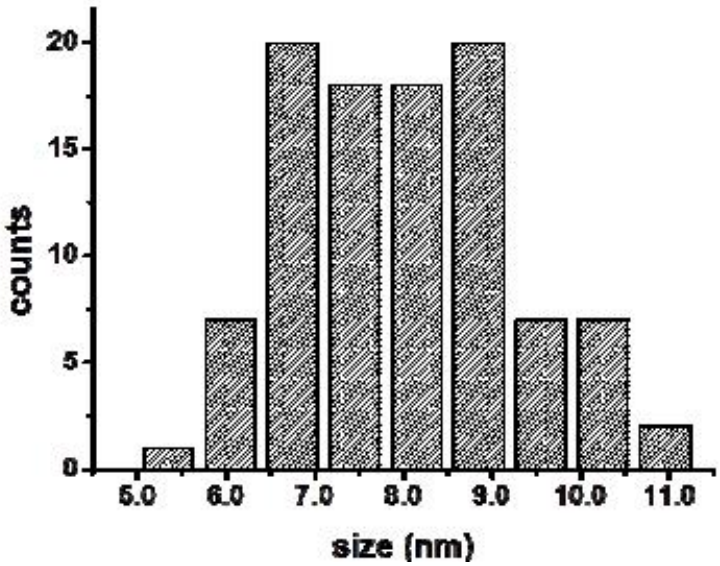

Figure S4.1a TEM image of the PAA-Fe_3O_4 NP (average diameter = 8.02 ± 1.26 nm (n = 100)).

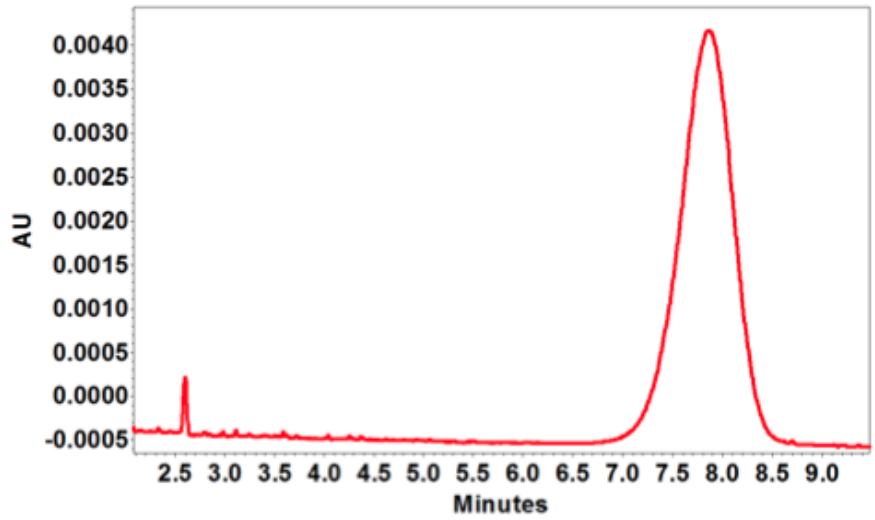

Fe_3O_4 NPs	Electrophoretic mobility ($m^2 V^{-1} S^{-1}$)	Zeta potential (mV)
8.02 nm	$-3.44 \times 10^{-8} \pm 4.01 \times 10^{-11}$	-44.03 ± 0.08

$$\xi = \frac{\mu_e \bullet \eta}{\varepsilon} = \frac{\mu_e \bullet \eta}{\varepsilon_0 \bullet \varepsilon_r} = \frac{\mu_e \bullet 8.90E-4}{8.854187817E-12 \bullet 78.4}$$

Figure S4.1b Zeta potential calculation from CE data. Top: Electropherogram of the 8.02-nm NPs; Bottom: Zeta potential calculated by the electrophoretic mobility of NPs from the equation[1] shown below the plot.

Reference:1. Schnabel, U.; Fischer, C.-H.; Kenndler, E. J. Microcolumn Sep. 1997, 9, 529-534.

Protein	Mw (kDa)	Dimension (nm)	n	K_D (M)
apo-calmodulin	17	2.1 × 2.1 × 5.8	2.1	1.51×10^{-8}
beta-casein	24		1.3	4.60×10^{-6}
bovine serum albumin	66	2.7 × 2.7 × 11.6	1.1	1.37×10^{-5}
gamma-globulin	60-70		1.0	3.36×10^{-7}
Superoxide dismutase	32.5	7.2 × 4.0 × 3.8	Too weak to measure	
Insulin	5.8	2.0 × 2.5 × 2.0	Too weak to measure	

Figure S4.1c K_D values for interaction of the PAA-Fe_3O_4 NPs with various proteins.

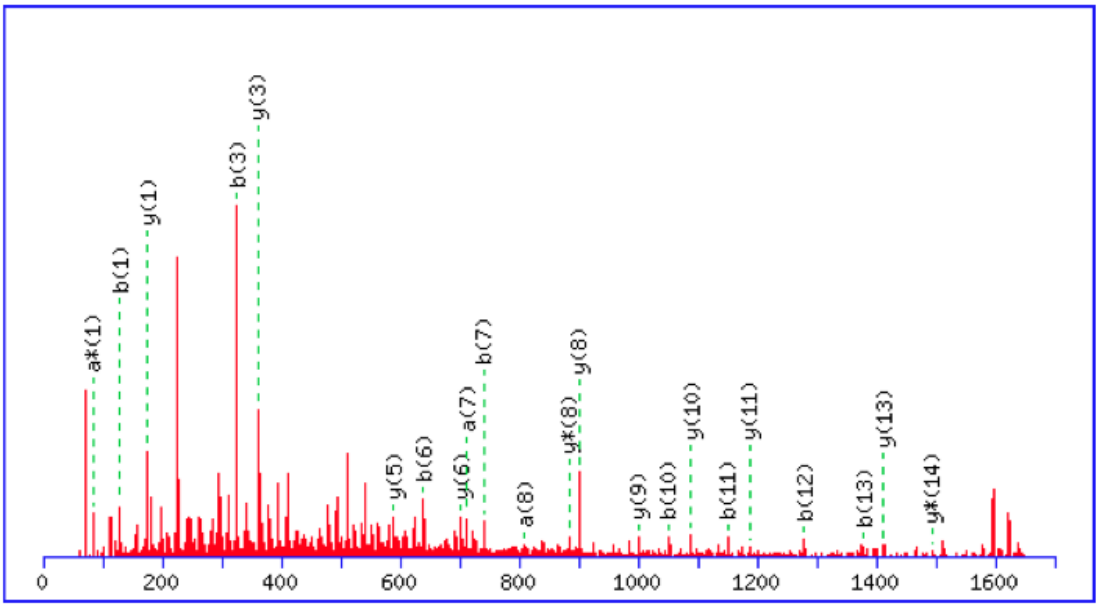

Figure S4.2 MALDI-Q-TOF MS/MS results for peptide peak at m/z 1640 KVPQVSTPTLVEVSR. Search result was obtained by MASCOT with an ions score of 44. There are 22 matches out of 84 fragment ions using 64 most intense peaks.

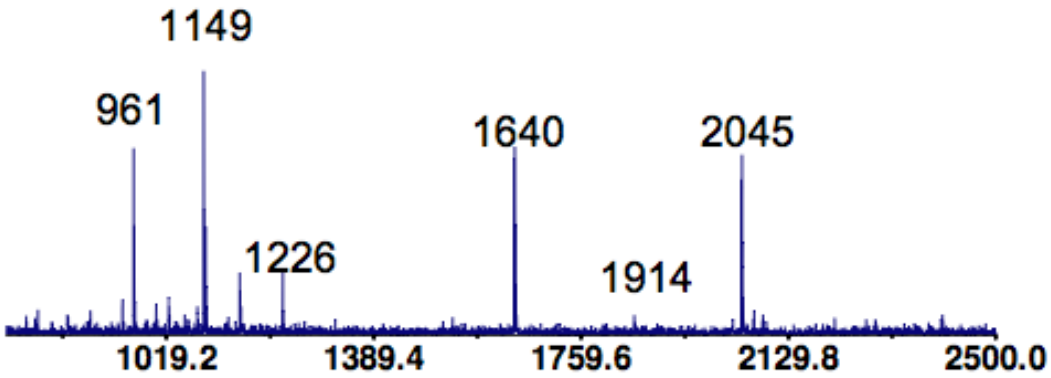

List of typical HSA peptides found in our samples:

m/z	Sequence
649	CASLQK
674	TPVSDR
715	AACLLPK
789	LVTDLTK
927	YLYEIAR
940	DDNPNLPR
961	FQNALLVR
1074	LDELRDEGK
1149	LVNEVTEFAK
1226	FKDLGEENFK
1386	YICENQDSISSK
1640	KVPQVSTPTLVEVSR
2045	VFDEFKPLVEEPQNLIK

Figure S4.3 MALDI-TOF-MS spectrum for the tryptic digestion of HSA. A total of 13 peptides were consistently identified and they are listed in the table.

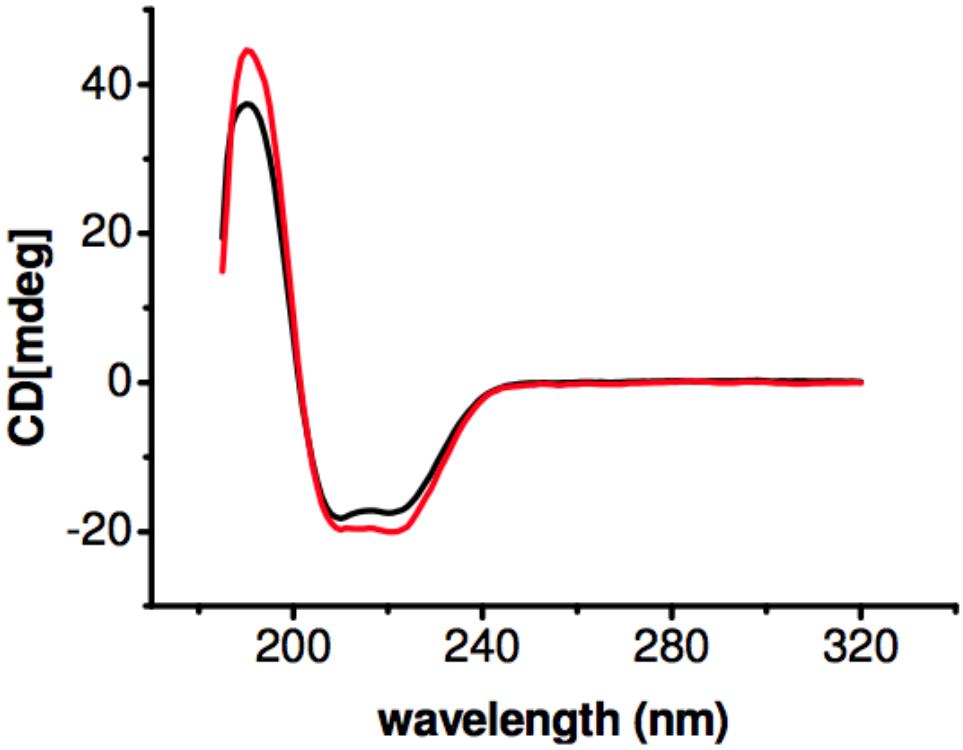

Figure S4.4 Circular dichroism spectra of 2.2×10^{-7} mol/L HSA (black) and 2.2×10^{-7} mol/L HSA with 2.4×10^{-8} mol/L PAA-Fe_3O_4 NPs (red).

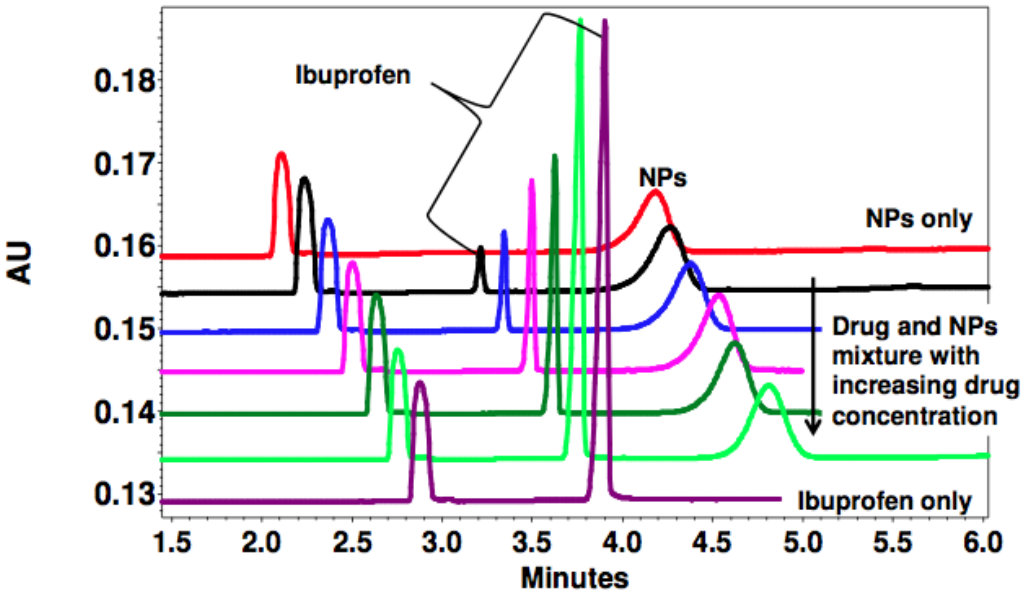

Figure S4.5a Electropherograms showing no interaction between ibuprofen and the PAA-coated Fe_3O_4 NPs. In this test, the ibuprofen was dissolved in 50% ethanol (HPLC grade, Fisher Scientific) to make a series of stock solutions with concentration from 4.84×10^{-4} M to 9.70×10^{-3} M. Two micro liters of the drug stock solution at different concentration was mixed with 9.4×10^{-12} mol NPs in a total volume of 20 μL which contained 5% ethanol. After overnight incubation, these samples were analyzed with capillary electrophoresis. No shift was observed in either the peak of NPs or that of ibuprofen, indicating no interaction occurring between these two. All traces were measured at 200 nm.

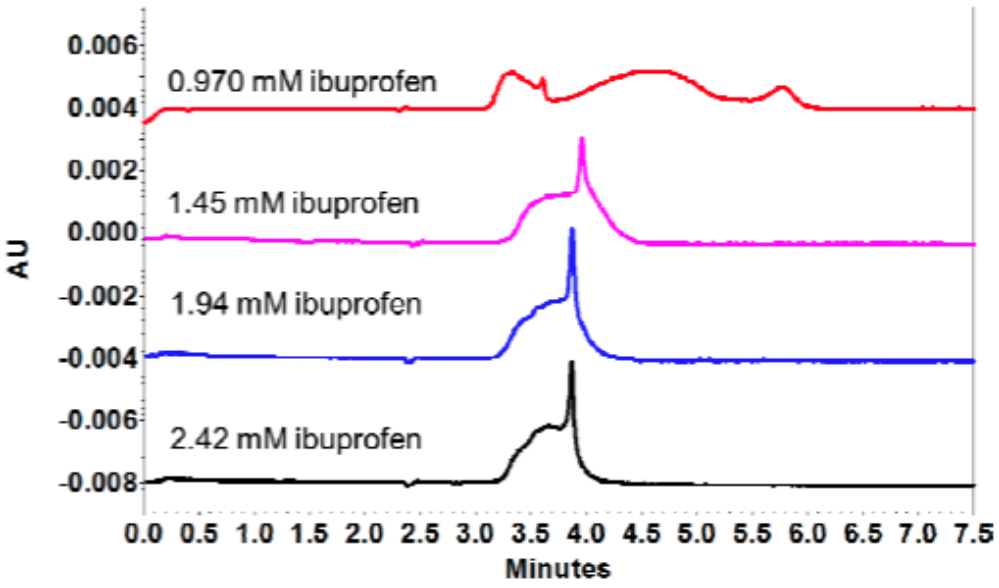

Figure S4.5b Electropherograms of incubation of HSA with NPs and ibuprofen at ibuprofen concentration equal to or larger than 9.70×10^{-4} M. Traces were measured at 288 nm.

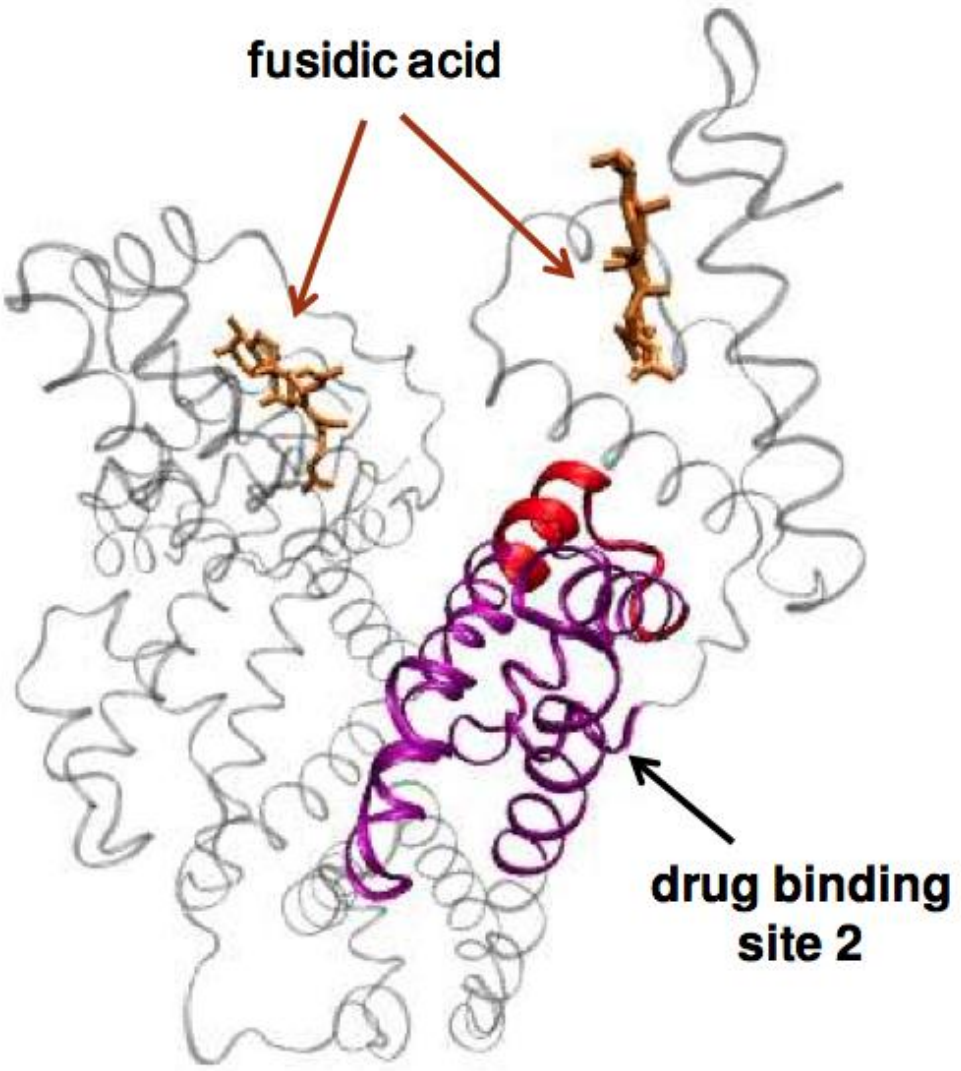

Figure S4.5c Crystal structure of HSA bound with fusidic acid (PDB ID: 2VUF)

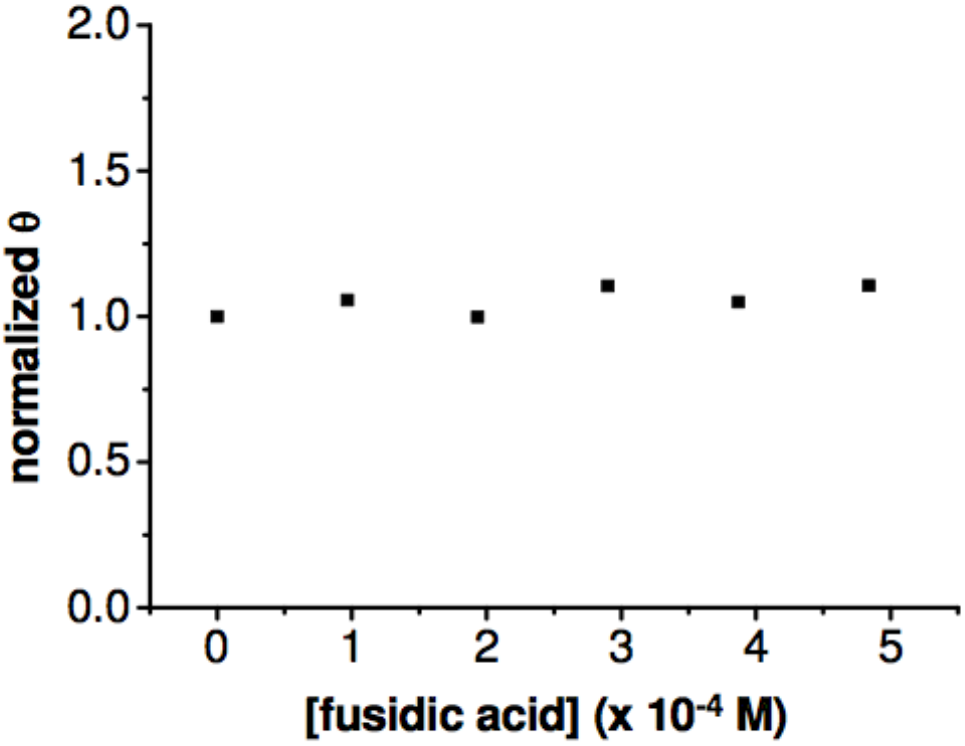

Figure S4.5d. Effect of fusidic acid on binding affinity between HSA and PAA-Fe_3O_4 NPs. The θ obtained with no fusidic acid was set as 1.0 for normalization.

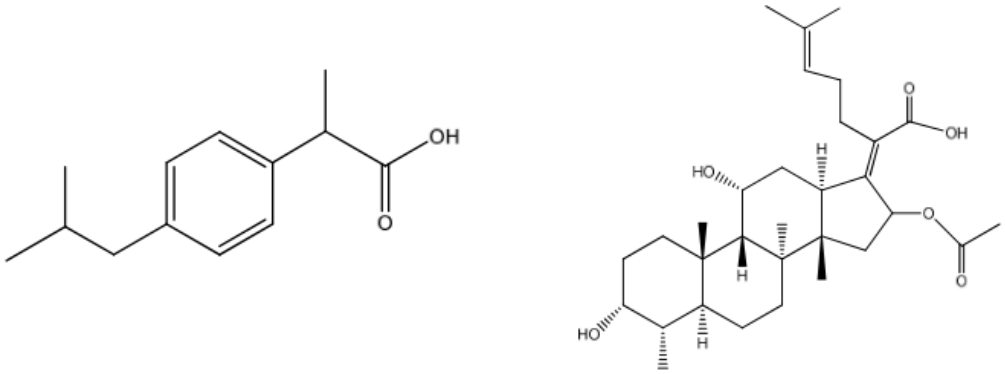

Figure S4.6. Molecular structures of ibuprofen and fusidic acid.

Chapter 5

Investigation on cellular protein perturbations upon nanotube-conjugated CpG immunotherapy in mouse macrophage cells

5.1 Introduction

Carbon nanotubes (CNTs) were firstly discovered by Iijima in 1991.[1] They have attracted huge attention since their discovery not only because of their own unique mechanical, electronic and optical properties[2-5], but also thanks to the development of their surface modification that brings in new useful properties.[6-16] For instance, when CNTs are modified through side-wall derivation with polymers or biological molecules, their solubility and biocompatibility are largely enhanced, which makes them potentially applicable for biomedical areas.[17-24] Single wall carbon nanotubes (SWCNTs) are proposed to be potential delivery vehicles because their large surface area and tube channel allows for high loading and efficient transportation of molecules.[25] Meanwhile, recent studies have shown that purified SWCNTs are not toxic to cells and are well tolerate *in vivo*.[26-28] Recently the peptide-functionalized SWCNTs were reported to be able to pass through cell membranes and accumulated in the cytoplasm of fibroblasts and phagocytic cells with no obvious sign of cell toxicity.[17] Similarly the functionalized SWCNTs was found to be able to help transport large attached groups into HL60 cells without showing any obvious cellular toxic effect[18]. These observations demonstrated that suitably modified SWCNTs would be useful as delivery vehicles for

cell therapy. Based on this concept, immunotherapy could be developed by conjugating immunity-activating biomolecules on to SWCNTs.

Oligodeoxynucleotides (OND) containing unmethylated CpG motifs (CpG) is one of the most promising classes of molecules for this type of immunotherapy. CpG is known to activate host defense mechanisms through recognition of toll-like receptor 9 (TLR9) and activation of nuclear factor-κB (NF-κB) binding activity leading to innate and acquired immune responses.[29] CpG was shown to enhance the cellular antitumor immune responses when used as an adjuvant in cancer vaccines.[30-32] It was recently found a single intratumoral injection of low-dose CpG conjugated SWCNT (collectively, SWCNT-CpG) into glioma-bearing mice[33] induced a much more effective anti-tumor immunity[34] than the therapy with high-dose of free CpG. The SWCNT-CpG was found accumulated in endosomes[35] and significantly boosted the efficacy of the CpG. For instance, a one-time injection of SWCNT-CpG resulted in 60% of treated mice eradicating intracranial gliomas in 3 months without any evidence of tumor residue.[36] Furthermore, when these tumor-cured mice were rechallenged with an intracranial injection of GL261 glioma cells, all the mice showed resistance to the cancer cells, indicating that systemic immunity had been developed. However, this effect was unique to the SWCNTs; similarly CpG conjugated gold, iron oxide or PLGA NPs were ineffective at activating NF-κB *in vitro* and had no additional *in vivo* anti-tumor efficacy over free CpG.

It remains unclear why SWCNT-CpG has such superior anti-tumor efficacy than free CpG and why other nanomaterials have not worked as well. Once the nanomaterials enter a living system, their large surface area would cause strong protein adsorption, forming protein corona masking the naked surface of the nanomaterials.[37-39] Protein corona has been found to strongly affect cellular uptake of various nanomaterials and modulate cellular response to the invasion of nanomaterials.[40-45] We hypothesize that, for nano-CpG to work effectively, an appropriate protein corona is needed to not only improve cell internalization, but also modulate the cellular response to the carrier itself, which may affect the efficacy of the carried drug. Thus, we conducted this pilot study to identify the composition of the protein coronas found on SWCNT-CpG, addressing the importance of the protein corona for the bioactivity of CpG-conjugated nanomaterial in immunotherapy.

5.2 Experiment Section

5.2.1 Reagents and Materials

The SWCNT coated with both lipid-PEG-CpG and lipid-PEG-NH_2 (referred to below as SWCNT-CpG), SWCNT coated with only lipid-PEG-NH_2 (referred to below as SWCNT-NH_2) and Raw Blue 264 mouse macrophage cells were generously provided by Dr. Berlin Jacob (the City of Hope). Dulbecco's Modified Eagle's Medium (DMEM), penicillin-streptomycin solution, fetal bovine serum (FBS) and trypsin-EDTA for cell culture were obtained from American Type Culture Collection (ATCC, Manassas, VA). The BCA kit was purchased from Pierce (Rockford, IL). The CelLytic™ M Cell Lysis

Reagent was purchased from Sigma-Aldrich (St. Louis, MO). The sodium phosphate monobasic, sodium phosphate dibasic, trifluoroacetic acid, ammonium bicarbonate, and dithiothreitol (DTT)) were purchased from Fisher Scientific (Pittsburgh, PA) except for iodoacetamide (IAA), which was from Sigma Aldrich (St. Louis, MO). The water and organic solvent used in this research were all HPLC grade from Fisher Scientific (Fair Lawn, NJ).

5.2.2 Cell Culture

Raw Blue 264 mouse macrophage cells were cultured in DMEM supplemented with 10% fetal bovine serum and 100 IU/mL penicillin-streptomycin. Cells were maintained in a humidified atmosphere with 5% CO_2 at 37 °C, with medium renewal at every 1–2 days depending on cell densities.

5.2.3 Cell Lysis

Raw blue 264 cells, cultured in 75 cm^2 flasks at a density of ~5 × 10^6 cells per flask in DMEM medium, were detached with trypsin-EDTA and harvested by centrifugation at 450 × *g* at 4 °C for 5 min, washed for three times with ice-cold 1× phosphate-buffered saline (PBS), and lysed with CelLytic^{TM} M Cell Lysis Reagent with protease inhibitor on ice with vortexing every other 5 min for a total of 30 min. The lysed cells were centrifuged at 15,000 × g for 15 minutes to pellet the cellular debris. The protein-containing supernatant (lysate) was transferred to a chilled centrifuge tube and stored at –70 °C for further analysis.

5.2.4 Protein Binding Capability on SWCNT-CpG

30 μg SWCNT-CpG or SWCNT-NH_2 was incubated with 64.5 μg cell lysate for 30 min and then centrifuged in 1.5 mL centrifuge tube at 12,000 × g for 10 min. The protein content in the supernatant was quantified with BCA kit (Pierce, Rockford, IL).

5.2.5 Stability of CpG Ligand on SWCNT in the Present of Protein Corona

The stability of CpG ligand on SWCNT in the present of protein corona during centrifugation was evaluated. 15 μg SWCNT-CpG was incubated with 45 μg cell lysate for 30 min, then pelleted in tube by centrifugation at 12,000 × g for 10 min. The supernatant containing free CpG ligands was measured at 260 nm for the absorbance. The samples containing only SWCNT-CpG or only cell lysate gone through the same treatment were served as controls.

5.2.6 Identification of Protein Corona on SWCNT-CpG *in vitro*

The SWCNT-CpG associated proteins were identified with the method described below. 50 μg SWCNT-CpG was incubated with 150 μg cell lysate for 30 min, then centrifuged at 12,000 × g for 10 min with supernatant discarded and washed with 1× PBS for three times. The proteins adsorbed on SWCNT-CpG were reduced with dithiothreitol (DTT) at 95 °C for 5 min and alkylated with iodoacetamide (IAA) at dark for 20 min. The processed proteins were subsequently digested with trypsin at 37 °C overnight.

5.2.7 Identification of Protein Corona on SWCNT-CpG *in vivo* with formaldehyde

Formaldehyde solution was obtained by dissolving 0.4% paraformaldehyde (Fisher Scientific) in PBS for 2 h at ~80 °C. The solution was filtered (0.22 μm), stored in the dark at RT. For *in vivo* cross-linking, the Raw Blue 264 mouse macrophage cells were detached with trypsin-EDTA from culture flask and collected into a 15 ml centrifuge tube and counted with hemocytometer under microscope. Cells were transferred into 96-well plates with density of 1×10^6 cells per well. Cells were cultured with 0.01 mg/mL SWCNT-CpG-NH_2, or 0.01 mg/mL CpG-NH2 ligand in cell culture medium for 30 min at 37 °C with 5% CO_2. Then the cell culture medium was removed. Cells were carefully rinsed with 1 × PBS and incubated with 0.4 % formaldehyde solution for 10 min at RT. The formaldehyde solution was removed and the reaction was quenched with ice-cold 1.25 M glycine/ PBS for 10 min. Cells were rinsed with 1 × PBS and lysed with CelLytic™ M cell lysis reagent and protease inhibitor on ice with vortexing every other 5 min for a total of 30 min. The lysed cells were transferred into 2mL centrifuge tube and centrifuged at 15,000 × g for 15 minutes to pellet the cellular debris. The protein-containing supernatant (lysate) was transferred to a 2 mL centrifuge tube and mixed with biotinylated CpG complementary strand at RT for 8 hrs followed by incubation with streptavidin resin at 4 °C overnight. After washing with 1 × PBS for 4 times, the biotinylated CpG double strand along with crosslinked proteins were eluted with 8 M guanidine solution. The 8 M guanidine was then removed by dialysis against Millipore water using 1 kDa Tube-O-DIALYZER (GBiosciences, St. Louis, MO). The dialyzed proteins were boiled at 90 °C to break up the formaldehyde crosslinking, followed by

trypsin digestion with DTT and IAA treatment as described above. Control cells were treated exactly the same way, except that they were not treated with formaldehyde solution.

5.2.8 Peptide Purification

The resulted protein digests were dried in a Savant SpeedVac concentrator (Bridgepath Scientific, MD) and redissolved in 0.1% trifluoroacetic acid (TFA). Peptide desalting and purification was done by using C18 ziptip (Millipore, Billerica, MA). The C18 ziptip tips were hydrated in CH_3CN and solvent discarded, followed by equilibration with 0.1% TFA. Thereafter, peptide samples were aspirated and dispensed into ziptip tip. After rinsing the tip with 0.1% TFA, bound peptides were eluted with CH_3CN/0.1% TFA (1:1, v/v). The resulting peptide solution was dried in the SpeedVac concentrator and stored at −20 °C until further analysis.

5.2.9 LC–MS/MS for Protein Identification

Online LC–MS/MS analyses were conducted on a LTQ linear ion-trap mass spectrometer (Thermo Fisher Scientific, San Jose, CA) equipped with a nano electrospray ionization (NSI) source. Full MS spectra were recorded over a 300-2000 m/z range followed by four sequential data-dependent MS/MS scans. Dynamic exclusion was implemented. The 200 nL/min nano flow was achieved by split flow from a 200 μL/min delivered by a Waters 2695 HPLC pump. The peptide separation was performed on a self-packed (packed 10 cm with 3 μm C18 beads, Dr. Maisch HPLC GmbH, Germany) PicoFrit column (75 μm

in tubing ID and 15 μm in tip ID, New Objective, Inc., Woburn, MA). Mobile phase A consisted of 0.01% TFA in water, and mobile phase B was acetonitrile. The gradient started at 2% B for 15 min of enrichment and then linearly increased to 80% B within 75 min. The mobile phase was kept at isocratic conditions (80% B) for 10 min and then returned to 2% B for 50 min.

5.2.10 Protein Searching with Protein Prospector

The identification and quantification of global proteome were achieved by searching the LC–MS/MS data using Protein Prospector. The maximum number of miss-cleavages for trypsin was set at two per peptide. Cysteine carbamidomethylation and methionine oxidation were included as fixed and variable modifications, respectively. The search was performed with the tolerances in mass accuracy of 2.5 Da and 0.8 Da for MS and MS/MS, respectively. In addition, only proteins with at least two distinct peptides being discovered from LC–MS/MS analysis were considered reliably identified.

5.2.11. Estimation on Protein Abundance

To compare the abundance of proteins, the Exponentially Modified Protein Abundance Index (emPAI)[46], calculated as $10^{(\text{observed peptides/observable peptides} -1)}$, was applied to measure the abundance of proteins in each sample.

The value of observed peptides was calculated using Trans Proteomic Pipeline (TPP) [47] version 4.6 rev.3. SpectraST (Spectra Search Tool)[48] included in TPP was used to

search spectral libraries and to identify peptide LC-MS/MS spectra we got from previous experiments. The spectral library we used was library of peptide fragmentation mass spectra of mouse, 05-20-2013, obtained from NIST (National Institute of Standards and Technology). All protein sequences in this library were included in one fasta file and obtained at the same time, which was further used for in sillico digestion. After spectral library searching, PeptideProphet and ProteinProphet, two softwares contained in TPP, were applied to assign probability to and validate peptides and proteins, respectively. Proteins with zero probability were viewed as false positive and discarded.

The value of theoretically observable peptides was calculated based on the results of in silico digestion (in house scripts) of all the protein sequences mentioned above. The mass range of peptides was 300-2000, and the ionized states were +1, +2, and +3. Besides, cysteine carbamidomethylation was chosen.

After we got the emPAI value for each protein, the protein abundance was compared via the molar fraction percentage described by:

Protein content (mol%) = emPAI/Σ(emPAI) *100 [46]

If the protein contents in different samples had more than 1.5 time difference, we concluded that the content of this protein changed between those two samples.

5.3 Results and Discussion

5.3.1 Protein Binding Capability of SWCNT-CpG

30 μg SWCNT-CpG or SWCNT-NH_2 were incubated with 64.5 μg cell lysate and then isolated by centrifugation. The amount of protein remained in the supernatant was tested with BAC kit. By subtracting the remained amount in the supernatant from the original amount, we could get the amount of the adsorbed proteins. The amount of protein remained in the supernatant when there was no SWCNT present was 63.2 μg which indicated the protein loss during centrifugation was negligible. Our results indicated 0.57 μg protein bound to per μg of SWCNT-NH_2 while 0.2 μg protein bound to per μg of SWCNT-CpG (Table 5.1). Almost 2 more fold of proteins could be retained by per μg of SWCNT-NH_2. It may be attributed to the bulky size of CpG ligand. The molecular weight of lipid-PEG-CpG is around 11.5 kDa. Comparing to the 2.7 kDa of lipid-CpG-NH_2, the much larger size of CpG may cause steric hindrance and prevents proteins from getting access to the SWCNT surface.

5.3.2 Protein Adsorption Improved the Stability of CpG Ligand on SWCNTs

When any type of nanomaterial enters a biological system, the very primary event is usually the formation of protein corona. Therefore, in our study, it is essential to evaluate how the protein corona would affect the stability of the CpG ligand on SWCNT surface in protein matrix. We used centrifugation to separate the free CpG from its SWCNT-conjugated form.

Table 5.1 Measurement on protein binding capability of conjugated SWCNT samples.

Sample name	Protein remained in supernatant (μg)	Protein bound to SWCNT sample (μg)
Cell lysate without SWCNT	63.2±0.01295	-
SWCNT-NH_2	46.1± 0.00819	17.1
SWCNT-CpG	57.1±0.00589	6.1

During centrifugation, SWCNTs along with bound CpG were pelleted while the free CpG remained in the supernatant. We recovered 94.5% free CpG when using pure CpG ligand as standard. We noticed 5.5% CpG was lost possibly due to the incomplete removal of the supernatant. The free CpG found in the supernatant of SWCNT-CpG was 91.5%, but only 67.0% when SWCNT-CpG was pre-incubated with cell lysate. It indicated that in the SWCNT-CpG sample, most of the CpG was in free form. However, 24.5% more CpG was retained on the SWCNT surface when protein corona was present (Table 5.2). It might be explained that the protein corona wrapped around the CpG-conjugated SWCNT and improved the stability of the CpG ligand by preventing them from detaching off the SWCNT surface.

5.3.3 CpG-bound Proteins Identified *in vitro*

In order to identify the composition of protein corona formed on SWCNT-CpG when it is introduced into macrophage cells, we conducted the following study. Raw Blue 264 macrophage cell lysate was used to mimic the cytoplasm environment. SWCNT-CpG

was firstly incubated with the cell lysate and then was isolated by centrifugation. The identity of proteins present in the protein corona was determined by performing trypsin digestion and analyzing the resulted peptides with LC-MSMS (Figure 5.1).

Table 5.2 Measurement of retained CpG on the surface of SWCNTs with and without protein corona

Sample name	Percentage of CpG remained in supernatant	Percentage CpG retained on SWCNT
CpG standard	94.5 ± 0.062	-
CpG from SWCNT-CpG w/o protein	91.5 ± 0.117	3.0
CpG from SWCNT-CpG with protein corona	67.0 ± 0.066	27.5

In the LC-MSMS analysis, we identified totally more than 500 proteins in the protein corona formed on SWCNT-CpG surface. The emPAI value and protein content of each protein in three repeated batches were calculated as described in the experiment section. The content of a protein in the SWCNT-CpG corona was compared to that in the control or in the SWCNT-NH_2 corona. The protein with protein content ratio larger than 1.5 was considered as enriched protein. We identified 17 proteins enriched from cell lysate.

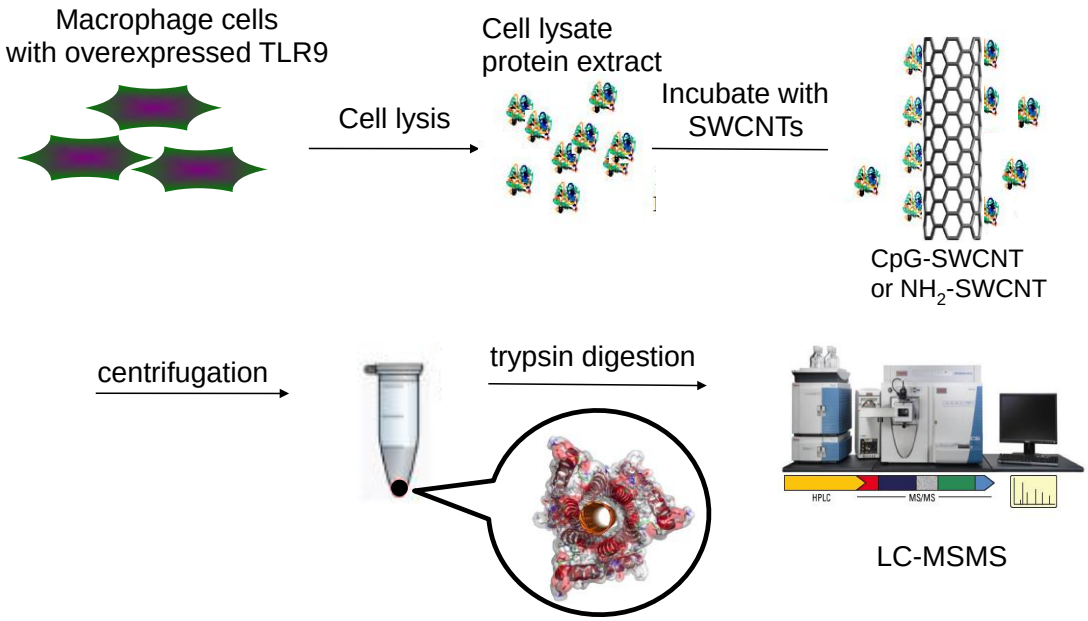

Figure 5.1 Scheme of protein corona identification.

Among these 17 proteins, 12 were solely found in the SWCNT-CpG sample but not in SWCNT-NH_2 sample indicating their high specificity towards CpG motif (referred as CpG-specific proteins from now). The other 5 of them were present in both SWCNT-CpG and SWCNT-NH_2 samples but with the protein content ratio larger than 1.5 (referred as CpG-enriched proteins).

To avoid any missing protein in the SpectraST searching during emPAI calculation, we also searched our peptides with Protein Prospector. There are 35 proteins enriched from cell lysate in the protein corona of SWCNT-CpG. Among the 35 proteins, 26 were found to be CpG-specific proteins. Three of these 26 CpG-specific proteins were overlapped with the emPAI analysis. Therefore, totally 35 CpG-specific proteins were identified after combining the emPAI analysis and protein prospector analysis (Table 5.3).

We further analyzed the properties of these 35 CpG-specific proteins (Figure 5.2). The isoelectric point of each protein was computed from the amino acid sequence on Uniprot website. The isoelectric points of these proteins distributed across 4 to 10. Totally 19 out of 35 proteins have pI values less than the physiological pH 7.4 while the other 16 proteins higher. It indicated the negatively charged SWCNT-CpG did not show much bias on the protein net charge, even though positively charged proteins were slightly more favorable than negatively charged ones.

Table 5.3 CpG-specific proteins identified by emPAI analysis and protein prospector

CpG-specific proteins identified by emPAI analysis	CpG-specific proteins identified by Protein Prospector
AP-2 complex	
Protein disulfide-isomerase	
Putative pre-mRNA-splicing factor ATP-dependent RNA helicase DHX15	
Aldehyde dehydrogenase	10 kDa heat shock protein
Calnexin	60S ribosomal protein
Cathepsin Z	Adenine phosphoribosyltransferase
Isoleucyl-tRNA synthetase	Adenylyl cyclase-associated protein
NADH-cytochrome b5 reductase	ADP-ribosylation
Peroxiredoxin	Alpha-enolase
Pyrroline-5-carboxylate reductase	Annexin
Sarcoplasmic/endoplasmic reticulum calcium ATPase	Aspartate aminotransferase
Stress-70 protein	Coronin
	Destrin
	Galectin
	GTP-binding nuclear protein Ran
	Heterogeneous nuclear ribonucleoprotein
	Macrophage-capping protein
	Microtubule-actin cross-linking
	Peptidyl-prolyl cis-trans isomerase
	Phosphoglycerate kinase
	Profilin
	S-formylglutathione hydrolase
	Succinyl-CoA:3-ketoacid-coenzyme A transferase
	T-complex protein
	Transaldolase
	Tyrosine-protein kinase BTK

From the location of these proteins inside the cell, it can be seen that cytoplasmic and membrane proteins were largely involved. The majority of proteins found in the crosslinked protein network was from cytoplasm, which was because SWCNT-CpG was always in contact with cytoplasm after transported into cells. The involving of membrane proteins could be explained by he membrane structure-mediated uptake and transportation of SWCNT-CpG. Meanwhile, nucleus, cytoskeleton, mitochondrion, secreted and lysosome proteins were also found in the protein corona.

When analyzing the ligand-binding properties of these proteins, we found most of these proteins bound to nucleotides-based molecules, including nucleotides, DNA, RNA, ATP or GTP. The CpG ligand is single-strand DNA oligonucleotide, which was expected to interact with these nucleotides-binding proteins. Metal ion (Ca, Mg, Zn, etc)-binding, actin-binding and lipid-binding proteins also had high affinity to CpG.

The function of proteins is further analyzed to explore the potential perturbation in cell function caused by SWCNT-CpG. We found 15 proteins belong to enzyme category such as transferase, isomerase, kinase, oxidoreductase and etc. The binding of these enzymatic proteins to SWCNT-CpG may inhibit their function by changing their confirmation or preventing them from binding to their substrate or cofactor. Other proteins such chaperone, regulatory protein, structure protein and transport proteins were also found in the protein corona.

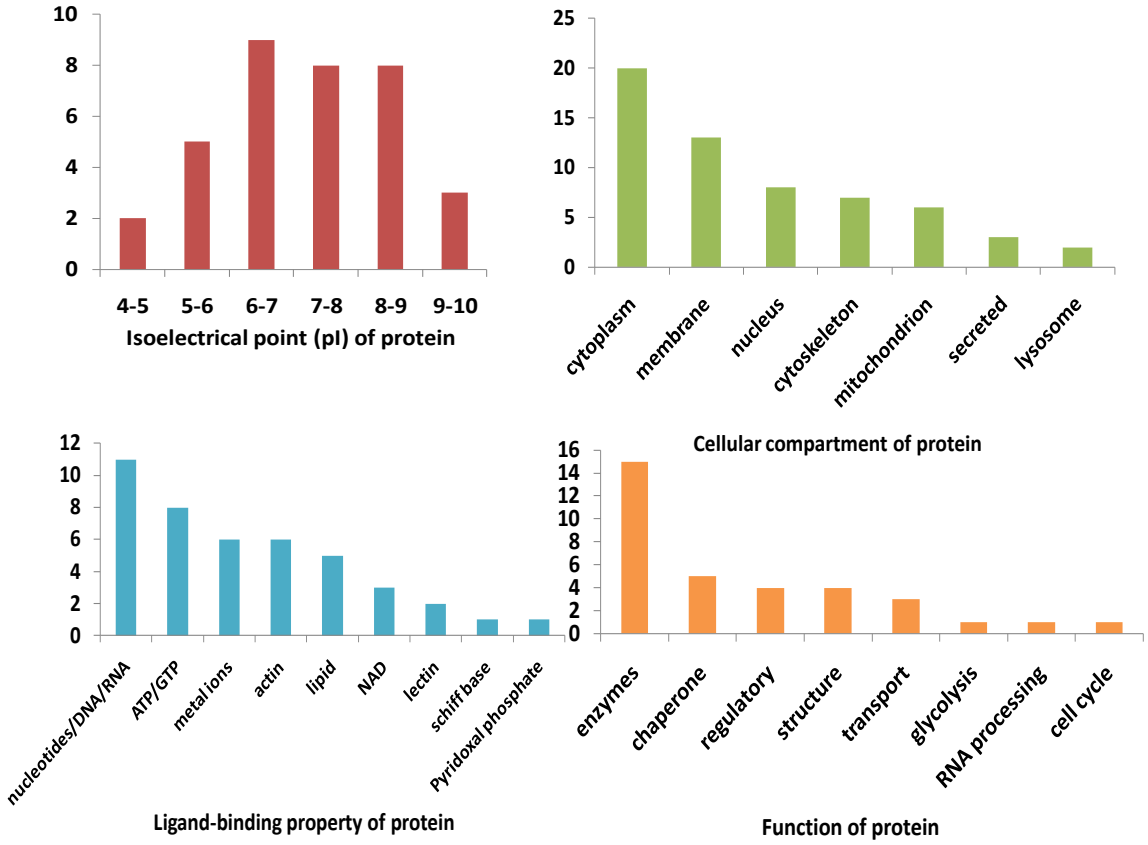

Figure 5.2 Distribution of CpG-specific proteins based on their properties. Red: isoelectrical point (pI) value; green: cellular compartment; blue: ligand-binding property; orange: function.

5.3.4 CpG-bound Proteins Identified with *in vivo* Crosslinking

In order to explore the instant protein network associated with CpG when SWCNT-CpG was delivered into cells, we utilized formaldehyde crosslinking strategy to fix the protein interactions and then isolated the CpG-bound proteins through DNA hybridization and biotin affinity purification. In this experiment, we used SWCNT-CpG-NH_2 in which the CpG motif was modified with an amine group at the terminal to provide a crosslinking site. Interestingly, we found the proteins bound to SWCNT-CpG-NH_2 were roughly identical to those bound to the free CpG-NH_2 ligand. Totally 12 proteins were isolated from the cells treated with SWCNT-CpG-NH_2 and 0.4% formaldehyde. Nine of them belong to the 13 proteins isolated from the cells treated with CpG-NH_2 ligand and 0.4% formaldehyde (Table 5.4). It indicates that CpG ligand is the main factor determining the identity of protein corona.

5.3.5 Important Proteins which may affect the cellular response to SWCNT-CpG

Among those proteins found in the protein corona of SWCNT-CpG *in vitro* and *in vivo*, some proteins were found deeply involved in the transport and processing of SWCNT-CpG.

AP-2 complex, a highly reliable CpG-specific protein identified by both emPAI analysis and protein prospector, is a multimeric protein that works on the plasma membrane and functions in cargo transport during endocytosis in different membrane traffic pathways.[49] The significant amount of AP-2 complex in the composition of protein

corona of SWCNT-CpG implies the transport of SWCNT-CpG is closely related to the AP-2 complex-mediated endocytosis. It was observed that SWCNT-CpG was rapidly uptaken and accumulated in the endosome, which increased the local concentration of CpG leading to an improved anti-tumor efficacy than free CpG.

Heat shock protein 90 (Hsp90), found in both protein corona of SWCNT *in vitro* and *in vivo*, is a chaperone protein functioning in the proper folding of some proteins, protecting cells against heat stress, and assisting protein degradation. Hsp90 could stabilize vascular endothelial growth factor (VEGF) and nitric oxide synthase (NOS).[50] Both of them play a key role in *de novo* angiogenesis required for tumor growth beyond limited diffusion distance of oxygen in tissues.[51] It is why Hsp90 inhibitors are investigated as anti-cancer drugs. Hsp90 also modulates tumor cell apoptosis through mediating the function of NF-κB, which is also the downstream target of CpG activation.[52] Therefore, the binding of HSP90 onto SWCNT-CpG may inhibit the function of HSP90 by occupying its binding site with other molecules or cause its conformational change, which may eliminate its stabilization of tumor-growth needed proteins. Another possibility is the local enrichment of HSP90 in the protein corona of SWCNT-CpG will assist the activation of NF-κB leading to enhanced anti-tumor efficacy of SWCNT-CpG.

Protein disulfide isomerase (PDI) is not only a highly reliable CpG-specfic protein, but also found in both protein corona of SWCNT-CpG in *vitro* and *in vivo*. PDI is an enzyme in the endoplasmic reticulum in eukaryotes that catalyzes the formation and breakage of

Table 5.4 Crosslinked proteins from CpG treated mouse macrophage cells with *in vivo* formaldehyde crosslinking strategy. The proteins with * are proteins that are also found in the protein corona *in vitro.* The proteins in red are uncommon proteins between two samples.

Proteins isolated from cells treated with SWCNT-CPG-NH_2 and formaldehyde	**Proteins isolated from cells treated with CPG-NH_2 ligand and formaldehyde**
Tubulin	
Clathrin	
Vimentin	
Prothymosin alpha	
Cofilin	
Heat shock protein HSP 90*	
Histone H2B*	
Protein disulfide-isomerase*	
60S ribosomal protein*	
ADP/ATP translocase	Galectin*
Poly(rC)-binding protein	Ribonuclease inhibitor
Cathepsin B*	ATP synthase
	Protein S100

disulfide bonds. The detection of PDI could be reached by using a fluorometric assay, in which the PDI could cleave the oxidized glutathione (GSSG) and recovered the originally quenched fluorescence.[53] In our study, the lipid-PEG-CpG contains a disulfide bond connecting the lipid-PEG portion with CpG motif. The enriched PDI in the protein corona may function in cleaving the disulfide bond and releasing the CpG motif into cytoplasm.

5.4 Conclusions

In this study, we demonstrated the identification of protein corona on CpG-conjugated SWCNT in the mouse macrophage cells. The SWCNT-CpG tended to tolerate less protein adsorption than the SWCNT-NH_2. When there was protein corona present, the stability of CpG ligand on SWCNT surface was improved significantly. In the protein corona composition analysis, we found 35 proteins were specifically enriched by CpG motif *in vitro*. These proteins did not show obvious trend in their isoelectrical point values, but more of them were cytoplasm and membrane proteins, nucleotides-binding proteins, and enzymatic proteins. When using formaldehyde to crosslink the CpG-interacting protein network, we found the protein corona composition of the SWCNT-CpG was almost identical to that of free CpG ligand indicating the CpG was the main factor determining the protein corona composition. AP-2 complex, protein disulfide isomerase and heat shock protein 90 were deeply involved in the transport or functioning of SWCNT-CpG. Further characterization of their function inhibition or conformational change upon binding to SWCNT-CpG needs to be carried out continuously.

5.5 References

[1] S. Iijima, *Nature,* **1991**, *354*, 586.

[2] Qiu X, Freitag M, Perebeinos V, Avouris P, *Nano Lett*, **2005**, *5*, 749.

[3] Ferrari M, *Nat Rev Cancer,* **2005**, *5*, 161.

[4] Ferriera L, Karp JM, Nobre L, Langer R, *Cell Stem Cell*, **2008**, *3*, 136

[5] Rivera GP, Oberdörster G, Elder A, Puntes V, Parak WJ, *ACS Nano,* **2010**, *4*, 5527

[6] Heller, D. A.; Mayrhofer, R. M.; Baik, S.; Grinkova, Y. V.; Usrey, M. L.; Strano, M. S. *J. Am. Chem. Soc.* **2004**, *126*, 14567.

[7] Lee, D. C.; Mikulec, F. V.; Korgel, B. A. *J. Am. Chem. Soc.* **2004**, *126*, 4952.

[8] Hudson, J. L.; Casavant, M. J.; Tour, J. M. *J. Am. Chem. Soc.* **2004**, *126*, 11158.

[9] Shim, M.; Kam, N. W. S.; Chen, R. J.; Li, Y.; Dai, H. *Nano Lett.* **2002**, *2*, 285.

[10] Besteman, K.; Lee, J. O.; Wiertz, F. G.; Heering, H. A.; Dekker, C. *Nano Lett.* **2003**, *3*, 727.

[11] Pantarotto, D.; Partidos, C. D.; Graff, R.; Hoebeke, J.; Briand, J.-P.; Prato, M.; Bianco, A. *J. Am. Chem. Soc.* **2003**, *125*, 6160.

[12] Pantarotto, D.; Partidos, C. D.; Hoebeke, J.; Brown, F.; Kramer, E.; Briand, J.-P.; Muller, S.; Prato, M.; Bianco, A. *Chem. Biol.* **2003**, *10*, 961.

[13] Bianco, A.; Prato, M. *Ad*V. *Mater.* **2003**, *15*, 1765.

[14] Williams, K. A.; Veenhuizen, P. T. M.; de la Torre, B. G.; Eritjia, R.; Dekker, C. *Nature* **2002**, *420*, 761.

[15] Bradford, J. T.; Adam, D. L.; Gary, D. W.; Aijun, Y.; Xu, J. M.; Shana, O. K. *J. Am. Chem. Soc.* **2004**, *126*, 12750.

[16] Jeong, S.-H.; Ko, J.-H.; Park, J.-B.; Park, W. *J. Am. Chem. Soc.* **2004**, *126*, 15982.

[17] Pantarotto, D.; Briand, J.-P.; Prato, M.; Bianco, A. *Chem. Commun.* **2004**, *1*, 16.

[18] Cherukuri, P.; Bachilo, S. M.; Litovsky, S. H.; Weisman, R. B. *J. Am. Chem. Soc.* **2004**, *126*, 15638.

[19] Kam, N. W. S.; Jessop, T. C.; Wender, P. A.; Dai, H. *J. Am. Chem Soc.* **2004**, *126*, 6850.

[20] Furtado, C. A.; Kim, U. J.; Gutierrez, H. R.; Pan, L.; Dickey, E. C.; Eklund, P. C. *J. Am. Chem. Soc.* **2004**, *126*, 6095.

[21] Hu, H.; Ni, Y.; Montana, V.; Haddon, R. C.; Parpura, V. *Nano Lett.* **2004**, *4*, 507-511.

[22] Georgakilas, V.; Tagmatarchis, N.; Pantarotto, D.; Bianco, A.; Briand, J.-P.; Prato, M. *Chem. Commun*. **2002**, *24*, 3050.

[23] Fu, K.; Li, H.; Zhou, B.; Kitaygorodskiy, A.; Allard, L. F.; Sun, Y.-P. *J. Am. Chem. Soc.* **2004**, *126*, 4669-4675.

[24] Georgakilas, V.; Kordatos, K.; Prato, M.; Guldi, D. M.; Holzinger, M.; Hirsch, A. *J. Am. Chem. Soc.* **2002**, *124*, 760.

[25] Kam, N. W.; Liu, Z.; Dai, H., *Angew Chem Int Ed Engl*, **2006,** *4*, 577.

[26] Liu, Z.; Davis, C.; Cai, W.; He, L.; Chen, X.; Dai, H., *Proc Natl Acad Sci USA* **2008,** *105* (5), 1410.

[27] Schipper, M. L.; Nakayama-Ratchford, N.; Davis, C. R.; Kam, N. W.; Chu, P.; Liu, Z.; Sun, X.; Dai, H.; Gambhir, S. S., *Nature nanotechnology* **2008,** *3*, 216.

[28] Kolosnjaj-Tabi, J.; Hartman, K. B.; Boudjemaa, S.; Ananta, J. S.; Morgant, G.; Szwarc, H.; Wilson, L. J.; Moussa, F., *ACS Nano* **2010,** *4*, 1481.

[29] McIntyre KW, Lombard-Gillooly K, Perez JR, Kunsch C, Sarmiento UM, Larigan JD, Landreth KT, Narayanan R. *Antisense Res. Dev.* **1993**, *3*, 309.

[30] Klinman, D. M., *Int Rev Immunol*, **2006,** *25*, 135.

[31] Goldstein, M. J.; Varghese, B.; Brody, J. D.; Rajapaksa, R.; Kohrt, H.; Czerwinski, D. K.; Levy, S.; Levy, R., *Blood* **2011,** *117*, 118.

[32] Baines, J.; Celis, E., *Clinical Cancer Research* **2003,** *9*, 2693.

[33] Carpentier, A. F.; Auf, G.; Delattre, J. Y., *Front Biosci* **2003,** *8*, 115.

[34] Alizadeh, D.; Zhang, L.; Brown, C. E.; Farrukh, O.; Jensen, M. C.; Badie, B., *Clinical cancer* **2010,** *16*, 3399.

[35] Kam, N. W.; Liu, Z.; Dai, H., *Angew Chem Int Ed Engl* **2006,** *45*, 577.

[36] Zhao, D.; Alizadeh, D.; Zhang, L.; Liu, W.; Farrukh, O.; Manuel, E.; Diamond, D. J.; Badie, B., *Clinical cancer research* **2011,** *17*, 771.

[37] Caracciolo, G.; Callipo, L.; Candeloro De Sanctis, S.; Cavaliere, C.; Pozzi, D.; Lagana, A., *Biochimica et Biophysica Acta, Biomembranes* **2010,** *1798*, 536.

[38] Lynch, I.; Cedervall, T.; Lundqvist, M.; Cabaleiro-Lago, C.; Linse, S.; Dawson, K. A., *Advances in Colloid and Interface Science* **2007,** *134*, 167.

[39] Mahmoudi, M.; Lynch, I.; Ejtehadi, M. R.; Monopoli, M. P.; Bombelli, F. B.; Laurent, S., *Chemical Reviews* **2011**, *111*, 5610.

[40] Monopoli, M. P.; Bombelli, F. B.; Dawson, K. A., *Nature Nanotechnology* **2011,** 6, 11.

[41] Lundqvist, M.; Stigler, J.; Elia, G.; Lynch, I.; Cedervall, T.; Dawson, K. A., *Proc Natl Acad Sci USA* **2008,** *105*, 14265.

[42] Maiorano, G.; Sabella, S.; Sorce, B.; Brunetti, V.; Malvindi, M. A.; Cingolani, R.; Pompa, P. P., *ACS Nano* **2010,** *4*, 7481.

[43] Monopoli, M. P.; Walczyk, D.; Campbell, A.; Elia, G.; Lynch, I.; Baldelli Bombelli, F.; Dawson, K. A., *J. Am. Chem. Soc* **2011,** *133*, 2525.

[44] Pozzi, D.; Caracciolo, G.; Marchini, C.; Montani, M.; Amici, A.; Callipo, L.; Capriotti, A. L.; Cavaliere, C.; Lagana, A., *Journal of Controlled Release* **2010,** *148*, 94.

[45] Safi, M.; Courtois, J.; Seigneuret, M.; Conjeaud, H.; Berret, J. F., *Biomaterials* **2011,** *32*, 9353.

[46] Ishihama, Y.; Oda, Y.; Tabata, T.; Sato, T.; Nagasu, T.; Rappsilber, J.; Mann, M., *Mol Cell Proteomics* **2005**, *4*, 1265.

[47] Deutsch, E. W.; Mendoza, L.; Shteynberg, D.; Farrah, T.; Lam, H.; Tasman, N.; Sun, Z.; Nilsson, E.; Pratt, B.; Prazen, B., *Proteomics* **2010**, *10*, 1150.

[48] Lam, H.; Deutsch, E. W.; Eddes, J. S.; Eng, J. K.; Stein, S. E.; Aebersold, R., *Nature methods* **2008**, *5*, 873.

[49] Pearse, BM, Smith, CJ, Owen, DJ. *Curr. Opin. Struct. Biol.* **2000**, *10*, 220.

[50] Fontana J, Fulton D, Chen Y, Fairchild TA, McCabe TJ, Fujita N, Tsuruo T, Sessa WC, *Circ. Res*. **2002**, *90*, 866.

[51] Calderwood SK, Khaleque MA, Sawyer DB, Ciocca DR, *Trends Biochem. Sci*. **2006**, *31*, 164.

[52] Whitesell L, Lindquist SL, Nat. Rev. Cancer **2005**, *5*, 761.

[53] Raturi A, Mutus B, *Free Radic. Biol. Med.* **2007**, *43*, 62.

Chapter 6

Conclusions

In summary, utilizing the modern analytical techniques, I developed novel methods to explore the interaction at nano-bio interface. I quantitatively measured the nanoparticle-protein interaction with capillary electrophoresis, revealed the influence of surface ligand on nanoparticle-protein interaction, determined the binding site of protein on nanoparticle surface, as well as investigated the identity of protein corona on CpG-functionalized single wall carbon nanotubes.

In chapter 2, we demonstrated here that capillary electrophoresis could be employed for quantitative study of the interaction between protein and nanoparticles. The separation-based platform will permit study of the more complicated systems which involve multiple interactive components. Future development should focus on interactions under physiological conditions and expand the investigation to proteins with high pI values and nanoparticles carrying positive charges. It is convenient to switch incubation buffers for a stable nanoparticle-protein complex, but it is difficult to employ saline buffers in affinity capillary electrophoresis due to the peak dispersion with increased running current. Therefore, ultrafast capillary electrophoresis, such as microsecond capillary electrophoresis, can be developed to separate the transient nanoparticle -protein complex

from the free nanoparticles. A coated capillary will be considered to minimize the adsorption of the positively charged proteins and nanoparticles on the capillary wall. Fluorescence detection can be employed to lower the protein and nanoparticle concentrations and avoid side effects accompanied with high protein concentrations in the running buffer in affinity capillary electrophoresis, such as electroosmotic flow alteration, peak distortion, and low peak intensity. Adsorption of multiple protein layers on nanoparticles and the possible disturbance to the nanoparticle-protein complex by the strong electric field of capillary electrophoresis should be paid attention to as well in future studies.

In chapter 3, the small structure change in polyacrylic acid head group induced big variations in the affinity of nanoparticle to proteins. The high sensitivity of protein adsorption to the head group structure is mainly because, as pointed out by computer simulation, the head group of polyacrylic acid is located at the binding interface with the protein. In order for stable binding to be formed, part of the nanoparticle surface ligand should fit well onto certain binding pockets on the protein surface. Even slight structural change in this part could alter the fitting and change the binding energy, ultimately varying the affinity to the protein. Overall, our results support the fact that screening interactions between nanoparticles and judiciously selected proteins could be an effective way to quick and initial evaluation of the particle surface of nanoparticles. Such screening will be useful for rapid assessment of the surface properties of nanoparticles produced in different batches or with varied preparation procedures, which is particularly

important for quality control of nanoparticles made for biomedical purposes. It is even possible that, by analyzing the interaction change with proteins of distinct properties, such as pI value, shape, hydrodynamic size, and surface hydrophobicity, more information about the kind of changes occurring in the nanoparticle surface ligand could be revealed.

In chapter 4, identification of the binding sites of NPs on proteins can help us predict the possible biological consequences after the attachment. The specific binding of nanoparticles to protein may be closely related to the biodistribution and cell internalization of the nanoparticles, which should be explored further in future studies. Our work demonstrated that cross-linking chemistry coupled with mass spectrometry was a convenient approach to probe the possible binding sites of nanoparticles on proteins. Further development is needed to increase coverage of all binding sites and to mimic interaction under physiological conditions. Moreover, complementary peptide identification methods like liquid chromatography-mass spectrometry/mass spectrometry can be used to target smaller peptides, and different release methods can be explored to improve the release efficiency. All of these are currently under investigation in our lab.

In chapter 5, we demonstrated the identification of protein corona on CpG-conjugated SWCNT in the mouse macrophage cells. The SWCNT-CpG tended to tolerate less protein adsorption than the SWCNT-NH_2. When there was protein corona present, the stability of CpG ligand on SWCNT surface was improved significantly. In the protein

corona composition analysis, we found 35 proteins were specifically enriched by CpG motif *in vitro*. These proteins did not show obvious trend in their isoelectrical point values, but more of them were cytoplasm and membrane proteins, nucleotides-binding proteins, and enzymatic proteins. When using formaldehyde to crosslink the CpG-interacting protein network in live cells, we found the protein corona composition of the SWCNT-CpG was almost identical to that of free CpG ligand indicating the CpG was the main factor determining the protein corona composition *in vivo*. AP-2 complex, protein disulfide isomerase and heat shock protein 90 were deeply involved in the transport or functioning of SWCNT-CpG. Further characterization of their function inhibition or conformational change upon binding to SWCNT-CpG needs to be carried out continuously.